12-2014

Determination of Area of Fire Origin through Examination of Structural Failure and Deformation

Andrew Thomas Tinsley
University of Tennessee - Knoxville, atinsle2@vols.utk.edu

To the Graduate Council:

I am submitting herewith a dissertation written by Andrew Thomas Tinsley entitled "Determination of Area of Fire Origin through Examination of Structural Failure and Deformation." I have examined the final electronic copy of this dissertation for form and content and recommend that it be accepted in partial fulfillment of the requirements for the degree of Doctor of Philosophy, with a major in Civil Engineering.

Edwin G. Burdette, Major Professor

We have read this dissertation and recommend its acceptance:

Harold J. Deatherage, David J. Icove, Richard M. Bennett

Accepted for the Council:

Carolyn R. Hodges

Vice Provost and Dean of the Graduate School

(Original signatures are on file with official student records.)

Determination of Area of Fire Origin through Examination of Structural Failure and Deformation

A Dissertation Presented for the

Doctor of Philosophy

Degree

The University of Tennessee, Knoxville

Andrew Thomas Tinsley

December 2014

DEDICATION

To my two fathers who left us too soon…..

Carl Thomas Tinsley

Willis LeRoy Freeman

ACKNOWLEDGEMENTS

There are way too many people to thank as I finish my work on my dissertation. I should start with my family. Thanks to my wife, Amanda, who has put up with the financial and time requirements of the completion of my degree and supported my decisions every step of the way. My mother, Denice, has provided constant support and motivation throughout my years to ensure that I actually did finish my degree. Thanks to my brother for constantly vowing to catch up to me even though he is eight years younger. Various other members of my family have also provided untold support for my academic career and I cannot thank them enough.

Within the University, there are a number of professors that have helped in my completion. Drs. Burdette and Deatherage have been involved in my graduate education from the first day. Thanks to both of them for allowing me to work as an assistant to them on a variety of projects. The trust you placed in me over the years has played a large role in my professional development. Thanks to Dr. Icove for taking me under his wing and providing me with the courage it took to pursue my Ph.D. Last, but not least, thanks to Dr. Bennett for continuing to serve on my doctoral committee.

It is also a necessity to thank Dr. Ian Burgess from the University of Sheffield and Vulcan Solutions, Ltd whose generous loaning of the Vulcan computer program allowed me to continue to eat reasonably well as I continued my work.

Professionally, I have to thank the Karns Volunteer Fire Department for providing me with the opportunity, knowledge, and desire to pursue a career within the fire service. Thanks to my colleagues at Eastern Kentucky University for serving as a sounding board throughout the research and presentation process.

My accomplishments would not have been possible without your support and motivation. Thank you for everything.

ABSTRACT

The effects of fire on steel have long been noted and studied. However, a scientific connection between the area of origin for a fire and the amount of steel deformation observed at the scene has never been established. The development and implementation of this type of analysis has the potential to decrease investigation times significantly as the types of structures to which this method would be applicable are typically large, expansive structures. In order to investigate the relationship between structural steel deformations and a fire's origin, a series of six tests were performed in a smaller size portal frame steel constructed building. The results from these tests were imported into a finite element program called "Vulcan" to investigate the possibility of recreating the conditions observed in the field using a structural modeling program with relative success. The research presented in this dissertation, directed as noted above, was successful in demonstrating the potential feasibility of using the pattern of structural deformations as an indicator of fire origin.

TABLE OF CONTENTS

LIST OF TABLES

LIST OF FIGURES

CHAPTER 1 - INTRODUCTION

1.1 Background

The National Fire Protection Association publication, NFPA 921 (2011) *Guide for Fire and Explosion Investigations*, states that the basic methodology of fire investigation should rely on the use of a systematic approach and attention to all relevant details. In order for a fire investigator to pay attention to all relevant details, it is imperative that they be able to recognize, record, and interpret all of the potentially useful details of a scene. There are many indicators of a fire's growth and travel left behind at most scenes. These indicators, when interpreted correctly, will typically lead the investigator to the true origin of a fire.

The effects of fire on steel have long been noted and studied. However, a scientific connection between the area of origin for a fire and the amount of steel deformation observed at the scene has never been established. The development and implementation of this type of analysis has the potential to decrease investigation times significantly as the types of structures to which this method would be applicable are typically large, expansive structures. While this type of analysis will not negate the need for collection of other types of data, it will provide investigators with another piece of evidence to create and test their hypothesis.

NFPA 921 (2011) points out that steel members such as beams, columns, studs, etc. can be deformed and distorted by exposure to heat generated by a fire. The effects of extreme temperatures on steel structures have been documented clearly in extensive research (FEMA 2002; Carden & Itani, 2007; Wang & Kodur, 2000). However, outside of an obscure mention in a fire investigation text or lecture, there has been very limited research into the use of structural deformations as an indicator of fire origin. In addition, the few mentions that deformations

provide little evidence to justify their being utilized in the field and are thus of little value until adequate research has been done to provide justification.

In addition to the use of structural deformations as simply another indicator of fire origin, it is believed that the distribution of structural deformations can be utilized as a benchmarking tool for validation of forensic fire models. Fire modeling is a process which utilizes a set of inputs and mathematical equations to predict the conditions (temperatures, flows, etc.) at certain points within a fire compartment. Fire modeling itself can take a number of forms from closed form hand calculations to sophisticated fluid dynamics computer programs. Forensic fire models, as with any forensic model, require field observations in order to ensure that the model is producing an accurate representation of the fire as it occurred in the field. It should be possible to integrate the temperatures developed from a forensic fire model into a structural model of the compartment to determine if the deflections observed in the field are reproduced. This comparison of deflection allows another tool for investigators to test their field hypotheses on the origin of the fire and will also provide a valid benchmark for a fire modeler to compare results from the fire model to measurable data (which is a rarity in forensic fire investigation).

1.2 Scope of Research

This dissertation addresses concepts that can be applied for any size, type, or material in a structure. While the concepts can be applied universally, the behavior of construction materials can be distinctly different. All of the equations, constants, and material properties used in this dissertation are geared toward their application to unprotected steel structures. Furthermore, the bounding of the proven concepts is limited to single story portal frame construction as used in warehouse construction or smaller commercial establishments. It is inadvisable to attempt a

structural assessment as described in this dissertation without a thorough knowledge of the mechanics of materials and the structural engineering principles that underlie the deformation characteristics of any structure involved in a fire.

The scope of the research is limited to a proof of concept accompanied by an explanation of the underlying processes. The proof of concept is explained in detail throughout the dissertation and includes literature review, research burns, field observations, and structural modeling. The underlying processes demonstrate the validity of this type of analysis when performed by a qualified individual with the requisite knowledge in both structural and fire protection engineering.

1.3 Objectives

The fundamental objective of the research reported in this dissertation is to create a "user manual" for determining the origin of a fire based on the use of structural deformations. Regardless of the extent of this research, it will be difficult to develop all of the concepts and advancements needed to answer all the questions needed for the proposed type of analysis. Nevertheless, the author presents in this dissertation a bounded solution for the use of the structural deformations as a reliable indicator of fire origin when coupled with existing indicators.

With this objective in mind, this dissertation has been structured to provide the answers to three critical questions in relation to the development of the method in discussion:

1. Can the magnitude of structural deflections be used to adequately support or discount an investigator's origin hypothesis based on visual observations?

2. Can the distribution of deformations in a post-fire building be recreated using structural modeling software and be used as a benchmark for the validation of forensic fire models?
3. If so, what are the appropriate protocols for the use of such analysis techniques?

1.4 Outline of Chapters

In order to address the questions outlined in the previous sections, the author has constructed a dissertation that begins by analyzing current knowledge then progressing through the research performed as a part of the project. The chapters of this text are laid out and briefly described below.

Chapter 2 – Literature Review

This chapter provides an in-depth literature review of topics pertinent to the development of later parts of the dissertation. This review includes a review of the fire investigation field itself including the recognition of the need for additional data in and the current methods used to conduct a post fire scene analysis. Engineering literature is reviewed to explain the properties of steel at elevated temperatures and the estimation of steel temperatures in the event of a fire.

Chapter 3 – Fire Dynamics

Chapter 3 contains an overview of the ignition, development, and decay of fires. Room fire dynamics as well as the methodologies used to model and predict fire development are discussed as pertinent to the proposed topic of the dissertation.

Chapter 4 – Tests on Scaled Buildings

Chapter 4 provides testing methodology and results for all research burns conducted as a part of this research. A total of six research burns were completed. All test design, setup, conditions, and results are presented as a part of this chapter. This chapter also contains summaries of the individual test's conclusions.

Chapter 5 – Finite Element Modeling Validation

Chapter 5 contains a narrative of the selection of the appropriate finite element modeling program. This chapter also contains a partial validation, within the boundaries of this study, of the finite element modeling program chosen for use.

Chapter 6 – Finite Element Modeling

Chapter 6 provides all relevant information regarding the modeling of the test building. This includes the material property development and the model results. This chapter also includes a comparison of modeled results versus experimental results to serve as a validation of the process used to justify the use of deflections to determine fire origin.

Chapter 7 –Methodology for Use of Structural Deformation as an Indicator of Fire Origin

Chapter 7 utilizes the information presented in the first five chapters to outline an investigation process to allow the appropriate and accurate use of structural deformations as an indicator of fire origin. Included in this chapter is not only the methodology, but also the shortcomings of the work performed in order to accurately bound the use of this process in real life investigations.

Chapter 8 – Conclusions

A summary of the work performed and outcomes of this study are presented in Chapter 8. Ideas and recommendations for future research are also recommended.

CHAPTER 2 - LITERATURE REVIEW

2.1 Goals for a Method to Determine Area of Fire Origin

The NFPA 921 Technical Committee on Fire Investigation states its goals as follows: "…to provide guidance to investigators that is based on accepted scientific principles and scientific research" (NFPA, 2011, p. 1). These methods must be underlain, not only with proven scientific principles, but also proven engineering principles.

Lentini (2008, p. 20) stated, "Other techniques for reducing bias include making strenuous efforts to disprove hypotheses, and giving full consideration to alternate hypotheses". Although the content of this address was geared toward the reduction of expectation bias, it is equally applicable to the research of new methodologies to evaluate forensic evidence. It is impossible to consider all relevant hypotheses without considering all evidence present at the scene. In fact, an investigator appropriately utilizing the scientific method is incapable of settling on a final hypothesis without considering all forensic data encountered at a scene.

Fire investigation "aims to identify where and how a given fire or group of fires started and the factors contributing to fire loss" (NFPA, 2002, p. 1). NFPA (2002, p. 5) states that, "There is a lack of scientific foundation for many methods used to identify the area of origin…" After reviewing this entire white paper, it is evident that any scientific based methodology of forensically analyzing post-fire scenes will be of benefit to the fire investigation profession.

Research performed by Tinsley and Gorbett (2013) showed that the inclusion of measurable data, as opposed to just visual data, increases both the investigator's confidence in their area of origin determination and the accuracy of their area of origin determination.

Any new method must have a significant body of scientific and engineering evidence to substantiate findings to other fire investigators, attorneys, insurance companies, and sometimes juries. The method should be able to adapt to many situations with little loss in continuity. It must also be able to be integrated and confirmed with existing methods used in the industry.

As with any existing techniques, the likelihood of a particular indicator producing a false positive has to be taken into account and should be minimized. Gorbett, Meacham, and Wood (2010) are currently pursuing a framework for quantifying the reliability of fire effects. This framework would include the consideration of a variety of factors including, but not limited to, ventilation, fuel loads and locations, ceiling heights, building size, compartment lining material, structural loads, and the initial design of the structure. The overlooking of any of these factors introduces the distinct possibility of reaching an inappropriate or incorrect conclusion. Furthermore, Gorbett has noted that with an increase in the number of fire effects and patterns noted throughout an investigation, the less likely an investigator is to reach an incorrect conclusion (Gorbett, Meacham, & Wood, 2010).

It is rare that a single dominant fire pattern will lead the investigator to the appropriate area of origin, never mind the point of origin (NFPA, 2011). Therefore, any new indicators must be able to be considered in the context of all other fire effects observed at the scene. NFPA 921 (2011) also reinforces the need for multiple methods of fire analysis prior to reaching a conclusion.

2.2 Existing Methods

Prior to the first publication of NFPA 921 in 1992, fire investigation was composed of a series of "old wives tales" which were rarely based in science (NFPA, 2002). Some of these

included large, shiny blisters or spalled concrete as an indicator of ignitable liquids, the relationship of the depth of char to the exact time of fire initiation, and the color of smoke as an indicator of the fuels. The majority of these "rules of thumb" have since been debunked through years of research and education. Although NFPA 921 has made significant leaps in the right direction, the fire investigation industry still tends to be less scientifically based in its analysis than many other forensic fields. This deficiency of scientific basis is not for lack of trying. Fire is an incredibly complex phenomena affected by countless variables within a given scenario. Research into these fire investigation topics has been performed for less than a century. Due to the lack of understanding of the root cause of the phenomena (fire) and the relative infancy of the field (fire investigation), new and improved or revised methodologies are constantly emerging.

Currently, NFPA 921 is considered the legal and ethical standard of care for fire investigators. All of the methodologies and information in the guide have been practiced and proven over years of investigation experience and is constantly revised by some of the brightest minds in the field of fire investigation. The primary investigation methodology advocated by NFPA 921, as in many other scientific fields, is the scientific method. This method of investigation involves a meticulous methodology of ensuring the inclusion of all pertinent information to the analysis at hand. As the scientific method is universally applicable to a variety of fields, NFPA 921 strives to outline the steps which are relevant to post-fire analysis.

The process of fire investigation is described in depth in a number of sources including Dehaan and Icove (2012), Icove and Dehaan (2013), Lentini (2006), and too many others to list. As such, it is not reflective of the scope of this dissertation to provide an in depth analysis of this process. However, for background purposes, a brief description of this process as it applies to the topic of this research is included below.

Within the confines of the scientific method, investigators are expected to develop and test working hypotheses to determine an appropriate area of origin. Hypotheses are developed by coordinating one or more of the following: witness information, fire patterns, arc mapping, and fire dynamics (NFPA, 2011). The proposed method in this dissertation will certainly fall under the heading of fire patterns analysis of an investigation. Fire patterns are defined as a grouping of fire effects that indicates either movement or duration/intensity. Currently, NFPA 921 (2011) lists a number of fire effects including char, calcination, melting, spalling, and thermal expansion/deformation.

Section 6.2.9 of NFPA 921 (2011) currently discusses the thermal expansion and deformation of materials. Specifically, Section 6.2.9.2 states:

> Studs, beams, and columns, and the construction components that are made of high melting point metal, such as steel, can be distorted by heating. The higher the coefficient of thermal expansion of the metal, the more prone it is to heat distortion. The amount and location of distortion in a particular metal construction can indicate which areas were heated to higher temperatures or for longer times.

While this study will ultimately seek to confirm this statement, it can be noted that there are a lot of engineering and fire behavior principles involved in such a brief notation. The oversimplification of concepts is not uncommon to this guide in its current format and really cannot be avoided due to the volume of information in the text. However, an in-depth literature review shows that there has been little research in support of the statements made. The

engineering principles behind the statement are sound, but there has been little to no research into the quantification of the effects that a dynamic fire has on the structural members of any particular building outside of the realm of structural design applications.

2.3 Properties of Steel at Elevated Temperatures

Steel is an elastoplastic material used in all types of construction. Steel can have varying properties which are dependent upon the amount of carbon and alloying agents used in the production process. Structural steel is generally produced to be ductile as opposed to having a high tensile capacity. In steel production, ductility is typically traded for strength and vice versa. Steel's behavior at room temperature as well as elevated temperatures is discussed in detail in the following sections.

2.3.1 Modulus of Elasticity and Poisson's Ratio

The elastic modulus, *E*, is the ratio of stress to the strain caused by that stress in the linear elastic range of behavior (generally thought of as the stiffness of the material). The elastic modulus of steel is typically assumed to be 210 GPa (29,000 ksi) at room temperature and is subject to variation with temperature increases (FEMA, 2002). The typical point where degradation of the strength of steel begins is approximately 100 °C (AISC, 2005).

The Ramberg-Osgood (1943) model modifies strain at a given stress by the use of three temperature dependent parameters developed through work by Kirby and Preston (1988). The governing equation and accompanying parameter calculation is outlined in Eqn. 2.1 (Ramberg & Osgood, 1943; Kirby & Preston, 1988).

$$\varepsilon_{(T)} = \frac{\sigma_{(T)}}{aA_{(T)}} + 0.01\left(\frac{\sigma_{(T)}}{bB_{(T)}}\right)^{N_{(T)}} \qquad \text{Eqn. 2.1}$$

Where:

$$a = \frac{E}{180x10^3}$$

$$b = \frac{\sigma_y}{250}$$

$$E = Modulus\ of\ Elasticity\ (MPa)$$

$$\sigma_y = yield\ stress\ (MPa)$$

And:

$$A_{(T)} = 180x10^3$$

$$B_{(T)} = .00134T^2 - .26T + 254.67$$

$$N_{(T)} = 237 - 1.58T \qquad for\ 20℃ \leq T \leq 100℃$$

$$A_{(T)} = (194 - 0.14T)x10^3$$

$$B_{(T)} = 242$$

$$N_{(T)} = 15.3x10^3(400 - T)^{3.1} + 6 \qquad for\ 100℃ < T \leq 400℃$$

$$A_{(T)} = (295.33 - 0.3933T)x10^3$$

$$B_{(T)} = 492.667 - 0.6266T$$

$$N_{(T)} = 6 \qquad for\ 400℃ < T \leq 700℃$$

$$A_{(T)} = (30.5 - 0.015T)x10^3$$

$$B_{(T)} = 306 - 0.36T$$

$$N_{(T)} = .04T - 22 \qquad for\ 700℃ < T \leq 800℃$$

Several modifications to the Ramberg-Osgood model have been proposed and included in the literature (Wong, 2001); however, the differences are too minute to warrant a detailed discussion in this dissertation. Figure 2.1 shows a sample series of stress-strain curves using the Ramberg-Osgood model with the Kirby-Preston modifications.

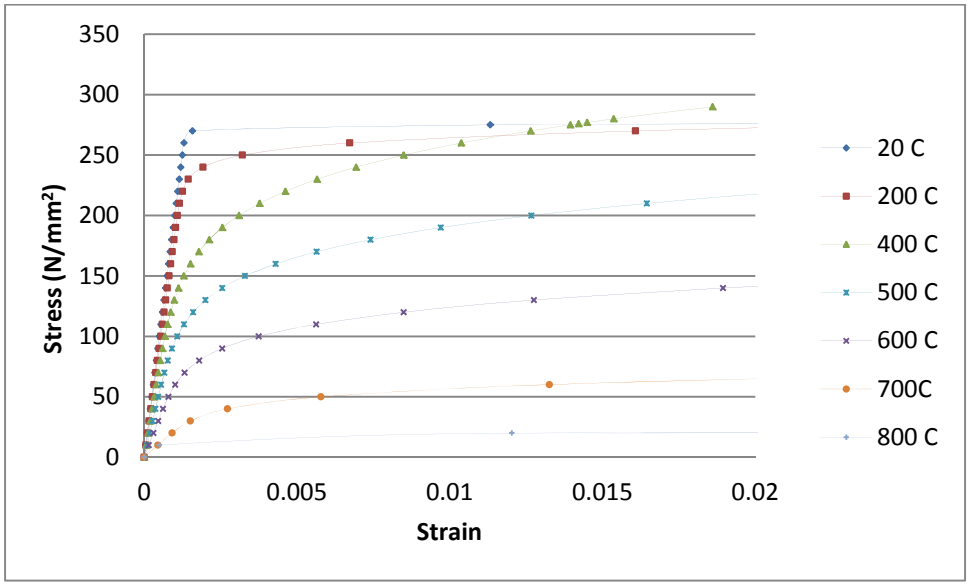

Figure 2.1: Stress-Strain characteristics for Grade 40 steel at elevated temperatures.

While the Ramberg-Osgood model is typically used for the analysis of steel at elevated temperatures, simple reduction coefficients (Table 2.1) can be computed and used for design as recommended by the American Institute of Steel Construction (2005). Design values for the variation with temperature of the modulus of elasticity (E), the yield stress (F_y), and the ultimate strength (F_u) of steel with a yield strength of less than 448 MPa (65 ksi) are shown in Figure 2.2.

Table 2.1: Properties of Steel at Elevated Temperatures (American Institute of Steel Construction, 2005)

Properties of Steel at Elevated Temperatures			
Steel Temperature (°F)[°C]	$k_e=E_m/E$	$k_y=F_{ym}/F_y$	$k_u=F_{um}/F_u$
68 [20]	*	*	*
200 [93]	1.00	*	*
400 [204]	0.90	*	*
600 [316]	0.78	*	*
750 [399]	0.70	1.00	1.00
800 [427]	0.67	0.94	0.94
1000 [538]	0.49	0.66	0.66
1200 [649]	0.22	0.35	0.35
1400 [760]	0.11	0.16	0.16
1600 [871]	0.07	0.07	0.07
1800 [982]	0.05	0.04	0.04
2000 [1093]	0.02	0.02	0.02
2200 [1204]	0.00	0.00	0.00

* Use ambient properties.

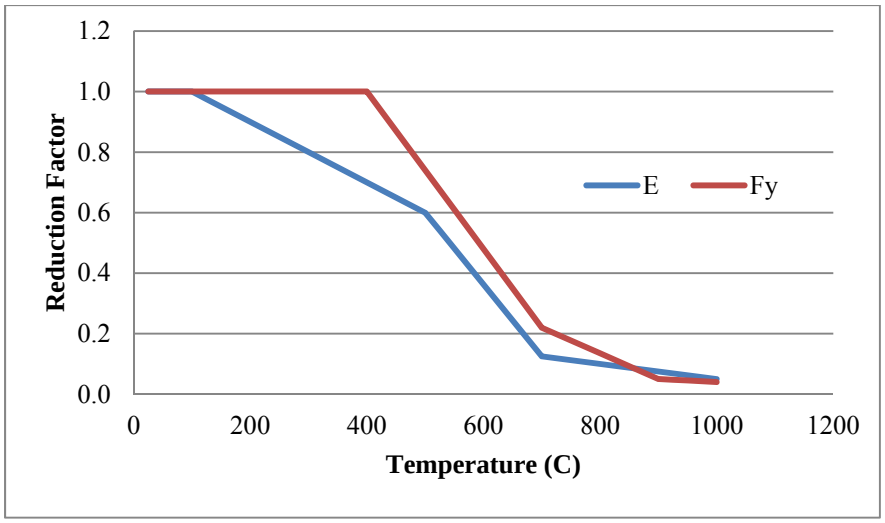

Figure 2.2: Reduction factors for Modulus of Elasticity and Yield Stress as a function of temperature.

In addition to the reduction in stiffness and effective yield strength, the well-defined yield point typically observed in steel is not nearly as well-defined (Cooke, 1988). The vanishing of this yield point dramatically affects the behavior of the steel, leading to excessive deformations at a lower stress (see Figure 2.3). Lowering the effective yield stress of the material will also increase the likelihood of the development of plastic (permanent) deformations in the steel member.

Just as important to predicting the stress-strain response of steel enduring an increase in temperature is the stress-strain response once the steel returns to ambient conditions. This topic is covered in depth in Section 2.4 of this dissertation.

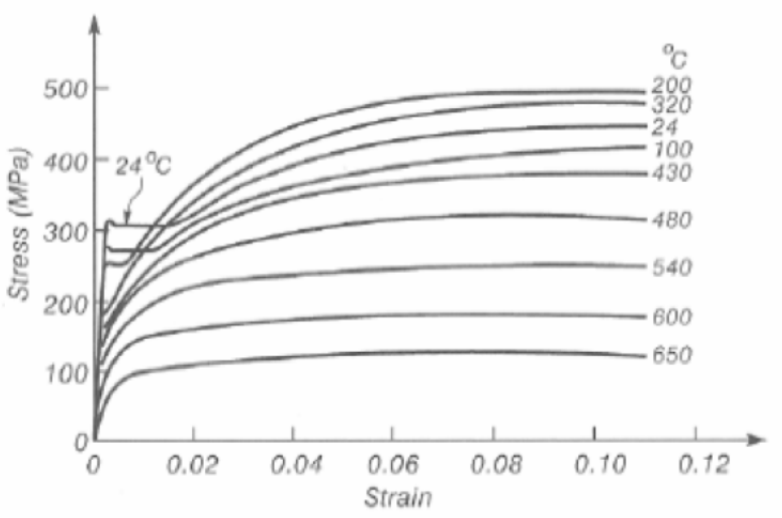

Figure 2.3: Stress Strain Curves for typical hot-rolled steel at elevated temperatures (Harmathy, 1993)

Poisson's ratio (v) is defined as the ratio of lateral strain to longitudinal strain. Poisson's ratio basically quantifies the reduction in cross sectional area as the member is placed into tension or the increase in cross sectional area when the member is placed into compression. Poisson's ratio of steel is negligibly affected by temperature (Cooke, 1988). It is recommended that Poisson's ratio for structural steel be taken as 0.3 for all calculations.

2.3.2 Strain in Steel

Deformation of steel members is a function of the strain generated by the three components of strain (Buchanan, 2002). The three components of strain that are of concern for analysis of deformations induced by fires are thermally induced strain, stress induced strain, and creep induced strain (see Equation 2.2).

$$\Delta\varepsilon = \varepsilon - \varepsilon_i = \varepsilon_{th}(T) + \varepsilon_{\sigma}(\sigma, T) + \varepsilon_{cr}(\sigma, T, t) \quad \text{Eqn. 2.2}$$

Where,

ε = total strain at time t

ε_i = initial strain at time t = 0

ε_{th} is the thermal strain

ε_{σ} is the stress-related strain

ε_{cr} is the creep strain

In a typical structural analysis of a steel member, only stress induced strain is considered since the other two are generally small enough to be neglected. Strain, regardless of type, is defined as the change in length (δ) divided by the original length of the undeformed member (L). The typical maximum strain that structural steel can endure before failure is 20-30% at room temperature (Cooke, 1988). The deformations incurred at this strain level are generally too high for this to be used as a failure criterion for steel.

Stress related strain results from the deformations caused by the loads the member in question is supporting (i.e. dead loads, live loads, wind loads, etc.). This form of strain is evident in all beams regardless of the thermal loading on the beam. It should be noted that stress related strain is a function of the modulus of elasticity of the steel which changes significantly with an increase in temperature as shown in Table 2.1.

Thermally induced strain is of primary concern during the analysis of steel members during a fire or any other scenario in which the steel is likely to be heated beyond 100 °C. Almost all materials will expand when heated. The coefficient of thermal expansion dictates

how much a certain material will expand when heated. The unrestrained length of a heated member can be found using:

$$L_t = L_0(1 + \alpha T) \qquad \text{Eqn. 2.3}$$

Where,

L_0 is the original length

α is the coefficient of thermal expansion

T is the change in temperature

The coefficient of thermal expansion is subject to minor variations at increasing temperatures. At room temperature, the thermal expansion coefficient is typically assumed to be 11.7×10^{-6}/°C (Buchanan, 2002). This value tends to increase as the temperature of the steel increases. While there are more in-depth relationships to determine the precise value of the coefficient of thermal expansion, both Eurocode 3 and the AISC Steel Construction Manual (2005) use a simple linear formula (see Equation 2.4) to represent the coefficient at a given temperature (Buchanan, 2002).

$$\alpha = \frac{\Delta L}{L} = 14x10^{-6}(T - 20) \qquad \text{Eqn. 2.4}$$

Where,

T is the temperature in degrees Celsius.

According to Franssen & Zaharia (2006), The American Society of Civil Engineers (ASCE) specifies a slightly more complicated relationship for the coefficient of thermal expansion as shown in Equation 2.5.

$$\alpha = (0.004T + 12)x10^{-6}\text{°C}^{-1} \quad for\ T < 1000\text{°C} \qquad \text{Eqn. 2.5}$$

$$\alpha = 16x10^{-6}\text{°C}^{-1} \quad for\ T \geq 1000\text{°C}$$

Where,

T is the temperature of the steel in °C

It is far more common for structural engineers to assume a constant coefficient of thermal expansion to simplify calculations. However, with the integration of computer modeling, it has become significantly easier to apply more complex relationships for values such as this.

Creep strain is a function of the mechanical loading, the temperature, and the length of time the load is in place on the member. In typical structural design of steel structures, creep is rarely a consideration for design. However, there are instances where creep becomes important such as in prestressed concrete design. Even though creep is not typically used as a design criterion, it can cause significant differences from anticipated behavior, especially at elevated temperatures. Work performed by Kirby and Preston (1988) show that creep in steel is highly dependent on temperature and stress level (See Figure 2.4). The curve of creep strain versus temperature becomes nearly vertical at higher temperatures indicating that the deflections will increase significantly without the addition of any extra load, thus demonstrating the importance of considering creep effects as members approach their collapse load.

The calculations to include this type of analysis are complicated in comparison with calculations involving the other types of strain. However, most stress-strain curves (such as Figure 2.3) used for analysis are effective curves which integrate the likely deflections from creep strain (Buchanan, 2002). It is also possible to explicitly include the effects of creep strain in computer models, but that approach is not utilized in this dissertation and, thus, is not discussed here.

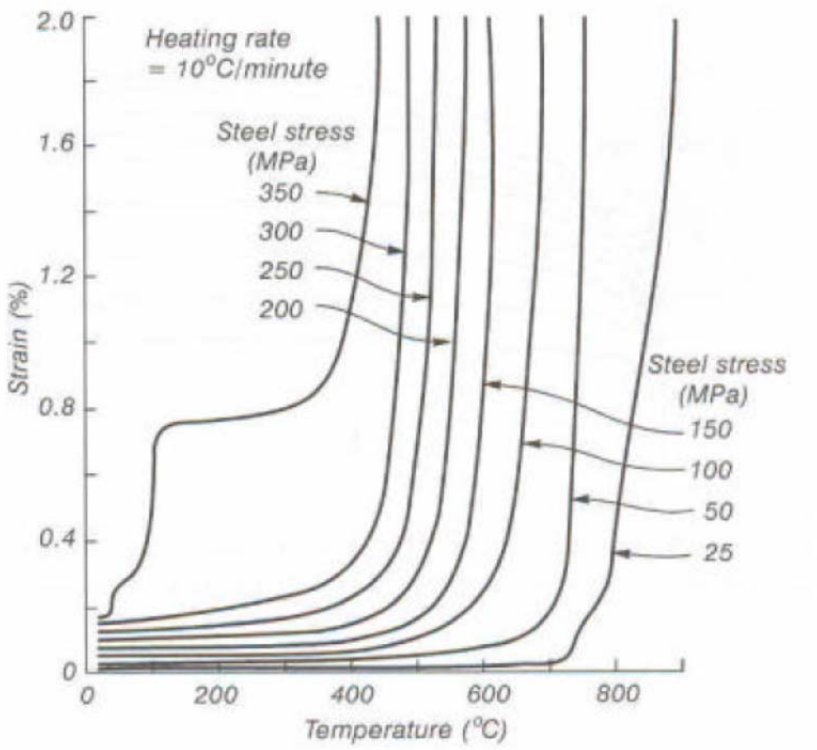

Figure 2.4: Creep of steel tested in tension (Buchanan, 2002).

2.3.3 Thermal Properties of Steel

As with the mechanical properties of steel, it is important to understand how temperature affects the thermal properties. Of most importance, and highest variance, is the specific heat and the thermal conductivity. While the specific application of these properties is discussed in the relevant sections of this dissertation, these specific properties warrant defining here. Specific heat is defined as the amount of energy necessary to raise a given mass of material one degree Celsius. This is basically a quantification of a material's ability to absorb energy without increasing in temperature. Conductors, such as steel, have a relatively low specific heat as they are easy to heat up. Thermal conductivity is a measurement of the rate at which heat transfer through conduction can occur in a given material. While there are several different thermal properties of importance to heat transfer calculations, they are minimally affected by temperature. Both ASCE and Eurocode 3 provide relationships for both thermal conductivity and specific heat (Franssen & Zaharia, 2006). The ASCE relationships are discussed below.

The thermal conductivity of carbon steel can be estimated using Equation 2.6 (Franssen & Zaharia, 2006). Buchanan (2002) recommends a constant value of 45 W/mK for simple calculations.

$$k_s = -0.022T + 48\frac{W}{mK} \qquad for\ 0 \le T \le 900℃ \qquad \text{Eqn. 2.6}$$

$$k_s = 28.2\frac{W}{mK} \qquad for\ T > 900℃$$

Where,

T is the temperature of the steel

K_s is the thermal conductivity

The specific heat of a material is dependent on the density of that material and, in most cases, the temperature. In temperatures encountered in fires, the density of steel remains fairly common at a typical value of 7850 kg/m^3 (490 pcf). For thermal conductivity, Buchanan recommends using a constant value of 600 J/kgK for simple calculations. However, ASCE gives the relationship shown in Equation 2.7 for the variation of specific heat with temperature (Franssen & Zaharia, 2006). It should also be noted that there is a large discontinuity (peak) around 735°C caused by a metallurgical change within the material.

$$\rho_s C_s = (0.004T + 3.3)x10^6 \ \frac{J}{m^3K} \qquad for\ 0 \leq T \leq 650℃ \qquad \text{Eqn. 2.7}$$

$$\rho_s C_s = (0.068T + 38.3)x10^6 \ \frac{J}{m^3K} \qquad for\ 650 \leq T \leq 725℃$$

$$\rho_s C_s = (-0.086T + 73.35)x10^6 \ \frac{J}{m^3K} \qquad for\ 725 \leq T \leq 800℃$$

$$\rho_s C_s = 4.55x10^6 \ \frac{J}{m^3K} \qquad for\ T > 800℃$$

Where,

T is the temperature of the steel

ρ_s is the density of the steel

C_s is the specific heat of the steel

2.3.4 Post Fire Behavior of Steel

As discussed in previous sections, the exposure of steel to a fire affects nearly every mechanical property based upon the temperature attained by the material. In addition to understanding the properties of steel at elevated temperatures, it is necessary to analyze the mechanical properties as the steel returns to ambient temperature. The process of steel production utilizes specific molecular formulas, but is also dependent on the heat treatment used

at the end of the process. Heat treatment produces varying molecular structures within the steel that change the mechanical properties of the steel significantly (Mamlouk & Zaniewski, 1999). This same process occurs during a fire, but under uncontrolled (and often unknown) circumstances. The heat treatment process is a function of the rate of temperature rise, ultimate temperature attained, length of stay at an elevated temperature, and the rate of cooling (Mamlouk & Zaniewski, 1999). The changes in temperature will affect the steel properties upon their cooling to ambient temperature, hence affecting the level of recovery of any elastic (or plastic) deformations which occurred during the fire event.

Research into this topic is highly complex as the properties of steel continually change given the temperature. Under normal circumstances (ambient temperatures), steel which is subject to inelastic deformations will recover any elastic deformations along a line of slope matching the modulus of elasticity. However, when the temperature has been elevated, the steel's mechanical properties change as the temperature returns to normal producing a highly complex problem. The steel does not recover deflections along a line with the slope of E; it is now following a series of different E's as the temperature decreases (see Table 2.1). This problem has been recognized and investigated by several researchers.

All reviewed methodologies of predicting the remaining plastic strain after a fire event consist of the calculation of a hysteresis curve based upon the temperatures reached by the member in a fire event (Wang, Li, & Guo, 2007; El-Rimawi, Burgess, & Plank, 1996; Franssen, 1990; Bailey, Burgess, & Plank, 1996). The methodology integrated into the modeling software Vulcan is put forward by Bailey, Burgess and Plank (1996) largely based upon the theoretical work of Franssen (1990). According to the conclusions of Franssen (1990), it is possible to find reasonable estimations of the unloading effects of members in a nonlinear stress-strain

relationship and those estimations are based on reasonable (although debatable) assumptions. Franssen (1990) also notes that this analysis will be even more complex and of more significant influence once attempted to be applied to full structures suffering from natural fires. Building on this work, Bailey, Burgess, and Plank (1996) devised a way to numerically solve the problem and integrate it into the modeling software Vulcan with relative success and analyzed its use in fire spread through multiple bays of a steel structure.

While the exact amount of plastic deformation remaining after a fire event occurs has been shown to be difficult to predict, research has been performed into the residual properties of steel after heating in a fire and then returning to ambient temperature. Tao, Wang, and Uy (2013) perform an analysis of eight other studies regarding the residual properties of steel after exposure to a fire. Of particular note are the relationships developed for residual modulus of elasticity (E_{sT}), residual yield stress (f_{yT}), and residual ultimate stress (f_{uT}) as a function of temperature attained by the steel during the fire (T). It should be noted that no changes in residual mechanical properties are observed if the steel remains under 500 °C. The residual yield stress can be calculated as (Tao, Wang, & Uy, 2013):

$$f_{yT} = f_y \qquad for\ T \leq 500℃ \qquad \text{Eqn. 2.8}$$

$$f_{yT} = [1 - 2.33x10^{-4}(T - 500) - 3.88x10^{-7}(T - 500)^2]f_y \qquad for\ T > 500℃$$

The residual ultimate stress can be calculated as (Tao, Wang, & Uy, 2013):

$$f_{uT} = f_u \qquad for\ T \leq 500℃ \qquad \text{Eqn. 2.9}$$

$$f_{uT} = [1 - 1.95x10^{-4}(T - 500)]f_u \qquad for\ T > 500℃$$

The residual modulus of elasticity can be calculated as (Tao, Wang, & Uy, 2013):

$$E_{sT} = E_s \qquad for\ T \leq 500℃ \qquad \text{Eqn. 2.10}$$

$$E_{sT} = [1 - 1.30x10^{-4}(T - 500)]E_s \qquad for\ T > 500℃$$

Figure 2.5 offers a graphical representation of Equations 2.8-2.10. Yield stress is affected the most (See Figure 2.5) demonstrating that the behavior of the recovering steel will differ significantly from its pre-yield behavior after it is heated in a fire.

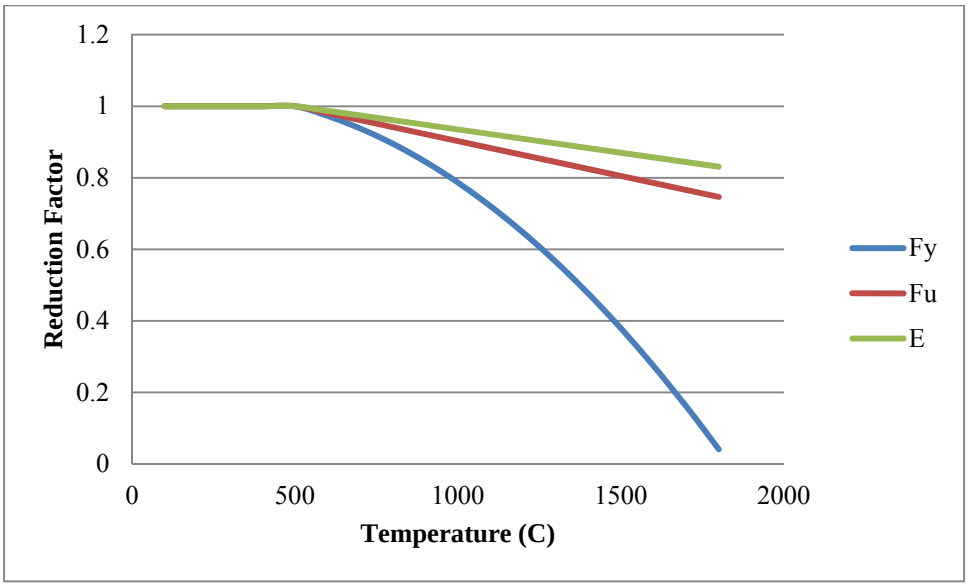

Figure 2.5: Reduction Factors for Mechanical Properties of Steel based on Temperature (Tao, Wang, & Uy, 2013).

Therefore, it is difficult to model the exact deflections present after a fire due to the difficulty of modeling the recovery of any elastic deformations. The work discussed demonstrates the difficulty in estimating the actual amount of plastic deformation that will remain after a fire has occurred.

2.4 Fire Protection for Steel Members

It is well known that exposure to excessively high temperatures can cause steel to fail in average fire conditions. There are multitudes of ways to provide protection to steel to increase its longevity under exposure to fire. Both ASCE and the International Code Council (ICC) offer guidance on the design of fireproofing for steel members. All common methods of providing extra thermal protection to steel are based on the premise of decreasing the application of energy to the surface of the steel. In most cases, this consists of placing an insulation material around the steel member to decrease the rate of temperature rise of the steel. The most common methods of providing protection to structural steel members are board protection , spray applied fire resistant material (SFRM and intumescent), and concrete or masonry encasement (Buchanan, 2002).

Board protection utilizes the insulating properties of gypsum wallboard (or another type of insulating wallboard) to encase to the steel member, thereby insulating the member from the effects of the fire. The amount of protection provided is dependent upon the composition of the wallboard (fire rated/non fire rated) and the thickness of the material applied. There are minor variations in the installation process that can result in a decrease in the afforded protection time. Common installation variations can include the spacing of connectors, the layering of joints, and the thickness of any applied joint compound.

Spray applied fire resistant material is a blend of cementitious material and another expandable material (usually vermiculite). There are also proprietary components that each manufacturer utilizes to make their product different. These materials are applied through a spray gun (similar to a paint gun) at a prescribed thickness over the entirety of the member to be protected. The amount of protection afforded is primarily dependent on the appropriate thickness of material being applied. Most manufacturers offer design guidance on the calculation of the specific thickness of their product required to provide a given amount of fire resistance.

Another type of spray applied fire resistant material is intumescent coating. Intumescent coatings are applied in a similar fashion as their cementitious counterparts, but they are much thinner when applied. Upon heating, this material will expand and create an insulating barrier around the member. Typically, this type of application would be chosen when it is visible to users of the building as it is more aesthetically pleasing than the cementitious variety of spray material.

Concrete encasement is the other method used to provide fire protection to steel. This process consists of encasing a member in concrete as concrete is minimally affected by fire. Again, both ASCE and ICC provide design guidance on calculating the required thickness of the concrete. The required thickness is mainly a function of the thermal conductivity and specific heat of the concrete itself which is heavily dependent on the type of aggregate utilized. Another closely related protection mechanism is masonry encasement. This process works similarly to concrete encasement, but the design input is obviously a little different.

2.5 Heat Transfer to Structural Elements

In order to appropriately predict the behavior of steel elements in fire, it is imperative to have an accurate depiction of the temperature of the steel members. Several methodologies exist to perform these calculations ranging from empirical formulas to advanced numerical solutions. The commonly utilized step-by-step method is a basic numerical iteration to solve for the temperature of the steel. This method works under the assumption that the heat entering is equal to the heat needed to raise the temperature. Equation 2.11 below shows the step-by-step calculation (Buchanan, 2002):

$$\dot{q}^{"} F \Delta t = \rho_s c_s V \Delta T_s \qquad \text{Eqn. 2.11}$$

Where,

ρ_s is the density of the steel

c_s is the specific heat of the steel

ΔT_s is the change in temperature at that particular time step

F is the heated surface area

V is the volume

$\dot{q}^{"}$ is the heat transfer at the surface

The heat transfer to the surface, $\dot{q}^{"}$, can be calculated as shown in Equation 2.12.

$$\dot{q}'' = h_c(T_f - T_s) + \sigma\varepsilon(T_f^4 - T_s^4) \qquad \text{Eqn. 2.12}$$

Where,

h_c is the convective heat transfer coefficient

σ is the Stefan-Boltzmann constant

ε is the emissivity

T_f is the temperature of the environment

T_s is the temperature of the steel.

These equations can be combined and rearranged to yield (Buchanan, 2002):

$$\Delta T_s = \frac{F}{V}\frac{1}{\rho_s c_s}\{h_c(T_f - T_s) + \sigma\varepsilon(T_f^4 - T_s^4)\}\Delta t \qquad \text{Eqn. 2.13}$$

As shown in the previous equations, the temperature of steel in fire is dependent upon several variables. The rate of heat transfer (and hence the rate of rise of the steel temperature) will be largely dependent upon the difference in environmental and steel temperatures. This temperature difference will also drive the radiant heat transfer. While such variables as the convective heat transfer coefficient, density, and specific heat play a large role in these calculations, they will be constant within the same material but may vary as a function of temperature.

Using the previously described methods, a series of curves can be plotted demonstrating the effects of the F/V value (commonly referred to as the section factor) on the rate of temperature rise in the steel. The fire used in this scenario was the NFPA 251 Standard Time-Temperature curve. As demonstrated in Figure 2.6, the larger the section factor, the closer the

steel temperature follows the fire temperature. This is expected as a larger section factor would be indicative of a smaller volume to heat combined with a larger heated perimeter.

The protection of steel members will also play a significant role in the magnitude of temperatures attained and the rate at which these temperatures are obtained. The entire purpose of providing protection to steel is to decrease the rate of temperature rise by shielding the steel with some sort of nonconductive material. These materials can vary widely from intumescent coatings, sprayed fire resistant materials (SFRM), fiber board, gypsum wallboard, and concrete encasement (discussed further in Section 2.5). The properties and thickness of these materials will vary widely based on the amount of fire protection required. Typically, most of these materials have been tested by independent laboratories (UL, FM Global, etc.) to validate the amount of protection provided according to the testing processes outlined in NFPA 251 (or similar standard). If more specific information regarding the protection times and steel temperature is required, this can be calculated as described below.

A best fit method can be used to calculate the time to reach a limiting temperature (T_{lim}) when exposed to the standard fire and is calculated as follows (Buchanan, 2002):

$$t = 40(T_{lim} - 140)\left[\frac{d_i k_i}{F/V}\right]^{0.77} \qquad \text{Eqn. 2.14}$$

Where,

d_i is the depth of the insulation

k_i is the thermal conductivity of the insulation

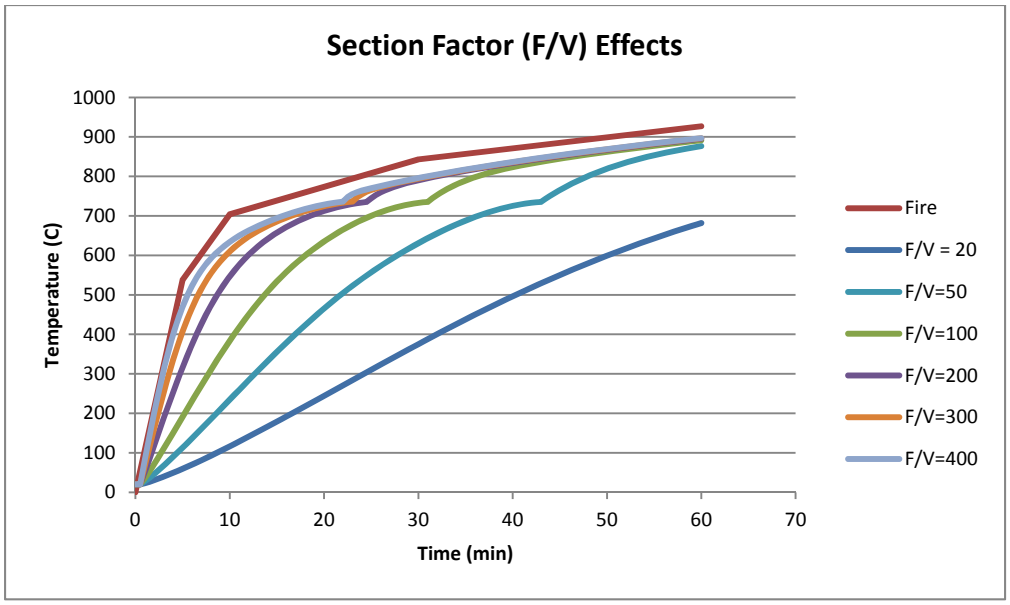

Figure 2.6: Section Factor Effects on Steel Temperature

The iterative process for calculating the temperatures of protected steelwork is similar to the method for unprotected steelwork. The primary difference is that there is no need to calculate the heat flux to the structural member due to the assumption that the outer portions of the insulating material will be the same temperature of the fire. The equation is (Buchanan, 2002):

$$\Delta T_s = \left(\frac{F}{V}\right)\left(\frac{k_i}{d_i \rho_s c_s}\right)\left\{\frac{\rho_s c_s}{\left(\rho_s c_s + \frac{\left(\frac{F}{V}\right) d_i \rho_i c_i}{2}\right)}\right\}(T_f - T_s)\Delta t \qquad \text{Eqn. 2.15}$$

Where,

c_i is the specific heat of the insulation

As can be seen, the formula is slightly more complicated than for unprotected steelwork, but the primary difference is in the inclusion of the specific properties of the insulation material.

As discussed previously, structural fire protection for steelwork requires shielding the steel from directly receiving energy from a fire. The effects of this insulating material will typically be to slow the rate of heat rise, not prevent it completely. It is still possible for structural members to exceed the temperatures set forth in the testing standards if the member is exposed to a proper duration and intensity of fire. It also warrants reiteration that testing methodologies are not typically representative of real life fire behavior, thus the rating times are merely a reference to the amount of protection provided. This also allows codes to specify protection requirements and provides the manufacturers with a relatively easy method of determining these protection requirements.

In addition to the previously shown hand/simple iterative calculations, there are multiple finite modeling programs utilized to estimate the temperature of steel in fire. Work performed at the University of Sheffield and utilizing the finite element modeling program FIRES-T3 confirmed that "steel temperatures could be predicted with acceptable accuracy by existing thermal analysis software" (Wong, 2001, p. 61).

2.6 Fire Effects on Steel Building Behavior

There have been multiple research studies focusing on the performance of steel portal frame structures under attack by fire. Research performed at the University of Canterbury investigated the full structural response of steel portal frame structures using the non-linear finite element program SAFIR (Bong, 2005). Within this project, the researcher investigated the effects of the location and severity of fires, differing support conditions at the column bases, the presence of axial restraint in the purlins, the level of out-of-plane restraint to the columns, and

the effects of concrete encasement of the columns. The conclusions of Bong's research which are relevant to this dissertation are as follows:

- For the most common case of an ISO Fire occupying the whole building, without strong axial restraint of the purlins and with common out-of-plane restraints provided by the side wall panels, the structural collapse occurs at about 15 minutes.
- External fire is less severe on the structure than an ISO fire, and the main structure may not collapse in short duration fires.
- Fire in half of the building doubles the time before collapse, and for a building with column bases pinned at the foundation, the cooler parts of the building may prevent significant sidesway from occurring.
- Fire in a smaller part of the building gives even less likelihood of collapse. (Bong, 2005, p. 257).

As demonstrated in the previous conclusions, it is possible to see isolated effects within a portal framed structure depending upon the support conditions and severity of the fire. Another finding of the study demonstrated that an appropriately designed and constructed portal frame structure provides a significant ability for load redistribution in the event of a localized fire. "If the adjacent parts of the structure remain at relatively low temperatures such that the structural stability is not significantly reduced, these cooler parts can provide adequate restraint and stiffness to the heated area and the structure may deform in a steady manner for a long period of time" (Bong, 2005, pp. 262-263). Again, this demonstrates that localized fires can cause localized deformations assuming global collapse does not occur early in the event.

Research performed at the University of Sheffield investigated the structural response of industrial portal frame structures in fire (Wong, 2001). As a part of this study, a 1:5 scale model of an industrial style steel portal framed structure was constructed and loaded to 20% of its designed failure load. A series of three tests were performed within the structure with both temperature and deflection being measured and analyzed. In order to provide adequate ventilation for the fires, the front cladding of the structure was removed possibly leading to higher temperatures on the end of the building exposed to excess ventilation. The loading was applied using water filled barrels suspended from concentrated locations on the frame supporting system, creating a concentrated load as opposed to a distributed load. Nevertheless, the study produced some interesting results regarding the distribution of deflections within the building in a post fire analysis.

The first test consisted of an equal heating of the entire roof supporting assembly by way of an elevated heptane pool fire. The results of this test showed that the building deflected in a uniform fashion as would be expected due to the consistency of the fuel load in the structure (Wong, 2001). The second test used a wood crib fire to heat one edge of the structure. The results of the second test show that the edge of the structure most intimate with the wood crib sustained higher deflections (Wong, 2001). Temperatures were highly variable within the compartment, but were more intense as proximity to the fire was increased, as expected. Of most interest was the third test in the series. In this test, the column connections were elevated by use of a metal rod with the anchor bolts loosened to allow rotation of the columns (i.e. simulated pinned connection). The building was insulated to minimize environmental heat loss and the fire was fueled by a self-replenishing heptane pool fire to allow the structural members to reach temperatures consistent with failure. As with the other tests, the front of the building was

removed to allow for adequate ventilation, in turn creating a more intense fire at that end of the structure. Deflection and, eventually, total collapse of the structure propagated from the area where the fire was the most intense (Wong, 2001). As shown in Figure 2.7, the deflection of the building occurs where the fire was most intense. While the location of highest intensity was certainly caused by the ventilation effects of the test setup, the distribution of damage certainly leads a researcher to believe that structures will deflect in direct correlation with the application of heat to the structural members.

Figure 2.7: Deflection and failure of portal frame building (Wong, 2001).

Work performed by Papadopoulos, Popadopoulou, and Papaioannou (2008) also investigated the analysis of the behavior of steel portal framed structures exposed to fires. In this study, simplifying efforts were made in order to make the analysis performable by simple, iterative methods as opposed to highly iterative finite element approaches. As a conclusion, through a series of linear simplifications of the material properties of steel, the authors were able to show that "in a simplified linear analysis of an indeterminate frame for static loading, it is observed that the stresses remain constant for any temperature T, whereas the deflections are constant up to T=300 °C and then for T>300 °C, as Young [sic] modulus decreases, they increase by the ratio of 500/(800-T)" (Papadopoulos, Papadopoulou, & Papaioannou, 2008, p. 52). While an extremely simplified relationship, this demonstrates that the deflection observed in the truss members is indeed in direct relation to the temperature of said truss member.

A study performed by Bailey, Burgess, and Plank (1996) analyzed the effects of cooling and fire spread on steel-framed buildings. A nine bay, three story steel framed structure was subjected to two scenarios. The first scenario comprised of uniform fire across three of the bays (4-6) while the second modeled fire spread across three bays (See Figure 2.8). In both scenarios, deflections were distributed evenly about the middle bay (See Figure 2.9). Bay 5 (center bay) deflected more than the neighboring bays in both scenarios. However, the second scenario in which the fire was spread produced much higher deflections within the center bay despite the fact that identical time temperature curves were used. The difference is where the energy was applied and the time at which it was applied. Since the fire originated in Bay 5 (center bay), more energy was applied at the onset of the fire. Since the center bay was heated earlier, it was heated to the point of deflection sooner than the rest of the bays.

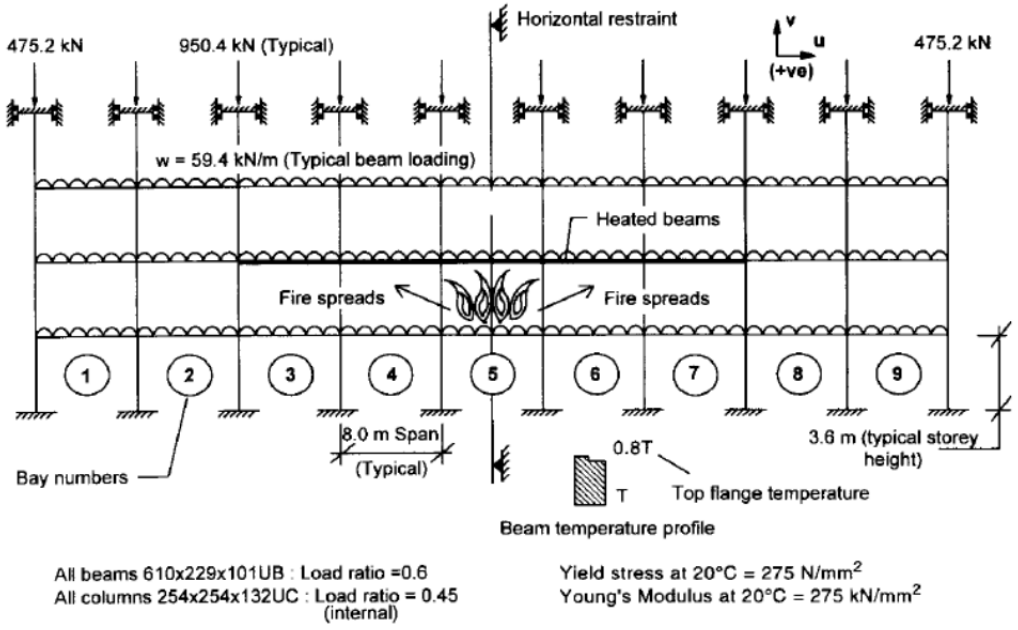

Figure 2.8: Two Dimensional Frame Subjected to fire spread (Bailey, Burgess, & Plank, 1996)

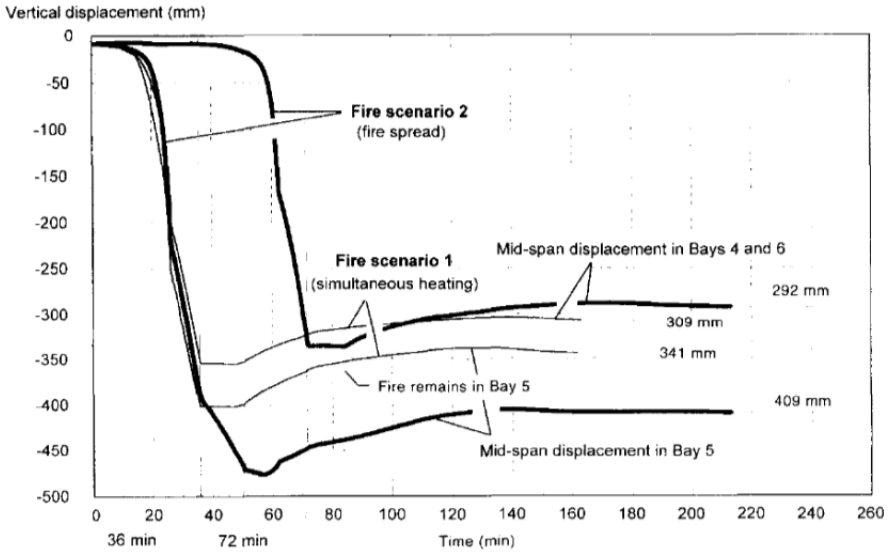

Figure 2.9: Time-displacement relationship for fire scenarios (Bailey, Burgess, & Plank, 1996)

2.7 Fire Effects on Structural Collapse

All design methods currently utilized operate using the same basic design equation which says that the nominal resistance supplied by the member (R_n) must be higher than the applied loads (M^*_{cold}) (Buchanan, 2002).

$$R_n > M^*_{cold} \qquad \text{Eqn. 2.16}$$

Current design methodologies do an excellent job in ensuring structural member's serviceability in the case for buildings constructed under normal conditions. The ratio of strength to applied load is known as the factor of safety or the load ratio. In order for a building to remain stable it is necessary that this ratio remain equal to or above 1.0.

As a steel member is exposed to fire, its nominal resistance is affected due to its decrease in both strength and stiffness. In addition, the load on these members is often seen to increase due to vibrations, pressure changes, load redistribution from other weakening members, and suppression efforts. Therefore, as the resistance provided by the member is decreased and the load applied to the member is increased, the load ratio converges on 1.0 and the eventual failure of the member.

The failure of one member in a structure does not necessarily imply that the entire structure will fail. The interaction of connections throughout a building and redistribution of loads can provide significant additional load carrying capacity. However, Buchanan discusses the concept of disproportionate collapse (progressive collapse as noted in ASCE 7) in which a small failure sets off a string of failures leading to the eventual destruction of a significant portion of the structure (Buchanan, 2002).

Applied at a more local level, this process is what will result in the increased deformations. As has been shown previously, any structural member will weaken wherever it receives the highest cumulative heat flux and the cumulative heat flux will be highest where the temperature difference is the greatest and of longest duration.

2.8 Fire Effects on Structural Deformations and Load Carrying Capacity

Deflection of any structural member in a fire scenario is a function of the modulus of elasticity (E) as well as the moment of inertia (I). The moment of inertia is a geometric property of a member and the only way it can be degraded in a fire is an actual reduction in cross section or deformation to the point of altering the shape of the member (i.e. buckling). These geometric deformations are the general method of failure of wood structures since the modulus of elasticity of wood remains fairly constant throughout the temperature range at which it will not combust. Steel, however, has a melting temperature well over 1100 °C in most cases and will suffer little, if any reduction in cross sectional area. Steel will begin to experience a decrease in modulus of elasticity at temperatures as low as 100 °C as demonstrated in Figure 2.1. This ability to retain its geometric integrity while losing much of its structural integrity is one of the reasons steel structures fail in such a dramatic (and often unexpected) fashion under temperature loadings. This same ability to retain its geometric integrity is one of the advantages of steel structures in fire as well.

The primary forces of concern in building design are bending (moment), shear, and axial loads. All of these individual design parameters are controlled at their fundamental levels by the yield strength and modulus of elasticity. Bending and axial capacities are also subject to bracing requirements and connection types. Fire's effects on yield strength and modulus of elasticity

have already been discussed at length and their effects should be obvious at this point. Provided bracing greatly effects both the moment and axial capacities of the member and can provide significant increases in durability to temperature changes when utilized appropriately. It is also worth noting that the bracing is typically exposed to the same or similar conditions as the main structural members and they will decrease in effectiveness as energy is applied.

Bending over long, unbraced spans can often lead to lateral torsional buckling being the primary mode of failure. The AISC Steel Construction Manual contains detailed processes for calculating the capacities of these members based on a number of geometrical and strength properties of the member in question. AISC also allows the design equations in the specification to be used for elevated temperature design assuming that strength modifiers are appropriately applied as described in Appendix 4 of the Specification.

Axial capacity is a function of the unbraced length of both the strong and weak axes. While the degradation of strength and elasticity does not affect the unbraced lengths, it changes the calculation of the critical buckling stress, F_{cr}, which is a critical component when determining the axial strength based on flexural buckling (American Institute of Steel Construction, 2005). In addition, decreases in strength can change the compactness classification of the member in question leading to the use of differing limiting equations.

2.9 Structural Design in Fire Conditions

Conceptually, there are few differences in the design processes utilized to design structures under fire conditions and structures under normal conditions. With regard to the differences, there are a few items which must be considered when performing this type of analysis. According to Buchanan (2002) these are:

- Lower applied loads
- Induction of internal forces by thermal expansion
- Reduction of the strengths of materials
- Reduction of cross sectional areas (by charring or spalling – not applicable to steel)
- Decrease in size of needed safety factors (due to unlikelihood of occurrence)
- Decreased importance of deflections
- Consideration of different failure mechanisms

While the method of analysis may be similar in fire and non-fire affected structures, the path to failure will surely vary. For failures in buildings not subjected to fire, members are typically stressed by the addition of loads to the point of failure. In a fire affected building, however, the member can fail with no addition of, or even a reduction in, applied load due to the decreasing material properties.

CHAPTER 3 - FIRE DYNAMICS

Fire is defined as an oxidation reaction resulting in the emission of varying degrees of light and heat of varying intensities (NFPA, 2011). Fire behavior is covered in a wide array of textbooks, codes, manuals, white papers, and technical reports. This section outlines the pertinent facts about fire behavior as they relate to the specific purpose of this dissertation. It is not intended to be an all-inclusive overview of fire behavior.

3.1 Compartment Fires

In order for a fire to occur, there are four essential components which must be united within a particular set of conditions. The most common way of demonstrating the components of a sustained fire is referred to as the fire tetrahedron. The four components are a reducing agent (fuel), an oxidizing agent (typically oxygen), a heat source, and a self-sustained chemical reaction to link them all together.

The combustion process itself consists of a highly complicated chain of chemical reactions. The intricacies of this process are not relevant to this dissertation and are discussed very briefly. Combustion actually occurs only in a gaseous form. In other words, solids themselves do not burn; the gases generated by the heating of the product will burn. Gases will burn in their natural state, liquids will burn after they are heated past their flash point, and solids are turned into a combustible gaseous form through the process of pyrolysis (or thermal decomposition) (Drysdale, 1998).

A compartment fire's development can be broken down into three separate stages:

1. Growth or pre-flashover in which the average temperature in the compartment is relatively low and the fire's effects on the compartment are relatively minor and localized to the area of origin.
2. Fully developed or post flashover in which the majority of the combustibles in the compartment are involved and the flames appear to fill the room.
3. The decay period which consists of the fire reducing in intensity from its peak value ending at the point of extinguishment.

Figure 3.1 is a graphical representation of the development of a compartment fire in the context of the heat release rate within the compartment. The transition between stage 1 (growth) and stage 2 (fully developed) typically occurs through a process known as flashover which involves the rapid spread of fire throughout the compartment and the majority of the combustibles within it. This progression is possible without the occurrence of flashover as the circumstances necessary to produce flashover are fairly complex. As noted by kirbey (2006), the effects of a fire on a structural member are primarily dependent on the intensity of the fire and the duration of exposure to higher temperatures. Therefore, the fully developed stage of a fire is of most danger to the structural members, as this period is not only long lasting, but the point at which the fire is at its peak heat release rate and producing the highest temperatures within the compartment.

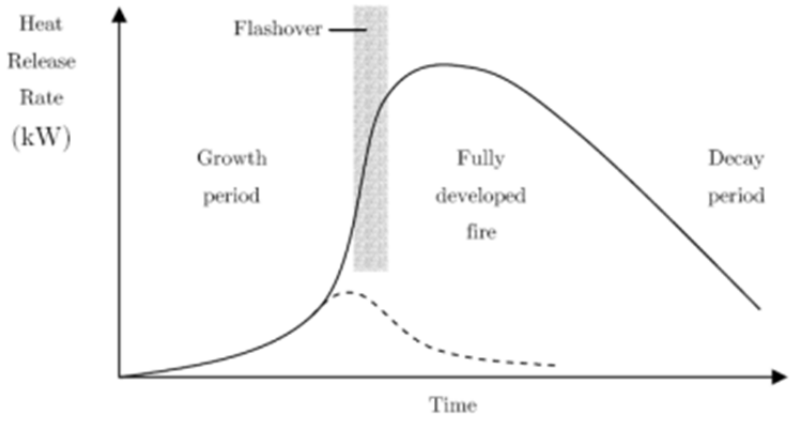

Figure 3.1: Development of a well-ventilated compartment fire as the rate of heat release as a function of time. The broken line represents depletion of fuel/ventilation prior to progression to fully developed (Drysdale, 1998).

3.2 Growth

Following the ignition of a fire in a compartment, several events can take place depending on the specific properties of the geometry of the compartment, availability of oxygen, and the presence/orientation/composition of fuel within the compartment.

1. The fire may self-extinguish due to inadequate fuel. This inadequacy can be caused by lack of fuel, the orientation of the fuel with relation to the origin of the fire, or the composition of the fuel.
2. The fire may self-extinguish due to a lack of ventilation caused by an insufficient supply of oxygen within the room. Poor ventilation can cause the fire to begin to die out prior to exiting the growth phase or can result in a long, smoldering fire (which will eventually burn out as well).

3. Given sufficient fuel and ventilation, a fire may progress to fully developed.

If the compartment's ventilation and fuel characteristics are suitable, a fire can progress beyond the growth phase, typically through a phenomenon known as flashover. The precise definition of flashover has been a much debated topic between fire protection engineers. For purposes of this dissertation, the review performed by Gorbett, Hopkins, and Kennedy (2008) will be utilized. Flashover is defined as "A transitional phase in the development of a compartment fire in which surfaces exposed to thermal radiation reach ignition temperature more or less simultaneously and fire spreads rapidly throughout the space resulting in full room involvement or total involvement of the compartment or enclosed area" (NFPA, 2011). The technical indicators demonstrating that flashover have occurred are an average upper layer temperature of ~600 °C or radiant flux at floor level of approximately 20 kW/m^2. Flashover does not occur in all fires as the circumstances necessary to produce this phenomenon are fairly complex. According to Gorbett, Hopkins, and Kennedy (2008) many factors affect the likelihood of the occurrence of flashover including:

- Ambient temperature at the beginning of the fire
- Size, shape, area, and volume of the compartment
- Area, height, width, and soffit (header) height of open doors and windows, or other vents
- Surface areas, materials, thickness, thermal inertia, and thus the conductance of the surface lining materials
- Heat loss fraction

- Heat release rate (kW)
- Fire growth rate (kW/s)
- Location of the fire within the compartment
- Active HVAC

As previously stated, it is possible for fires to progress to full room involvement without flashover occurring. The transition from the growth phase through the fully developed phase will still occur, but the transition will take longer. This phenomenon is common in large compartments (especially ones with high ceiling heights) or compartments with high rates of ventilation.

The modeling of the growth rate of a pre flashover fire is characterized by a parabolic curve known as a t-squared fire where the heat release rate of the fire is proportional to the time squared (Buchanan, 2002). The equation governing the growth rate is:

$$Q = \left(\frac{t}{k}\right)^2 \qquad \text{Eqn. 3.1}$$

Where,

Q is the heat release rate (MW)

t is the time (s)

k is the growth constant ($s/\sqrt{MW}$).

Typical fire growth rates depending on the material ignited are shown in Table 3.1 (Buchanan, 2002). A graphical representation of the different growth rates are shown in Figure 3.2. Based on this method, a representative heat release rate curve can be formulated for a variety of materials with relatively little experimental testing. In addition, multiple fuel packages

inside the room can be modeled to produce a composite heat release rate for the room. This process involves a lot of assumptions as far as ventilation and fire spread are concerned, but has been shown to produce results which closely match observations of actual fires.

Table 3.1: Fire Growth Rates for t^2 Fires (Buchanan, 2002)

Fire Growth Rate	Value of k	Typical Real Fire
Slow	600	Densely packed wood products
Medium	300	Solid wood furniture such as desks
Fast	150	Some Upholstered Furniture
		High stacked wood pallets
		Cartons on pallets
Ultrafast	75	Most upholstered furniture
		High stacked plastic materials
		Thin wood furniture such as wardrobes

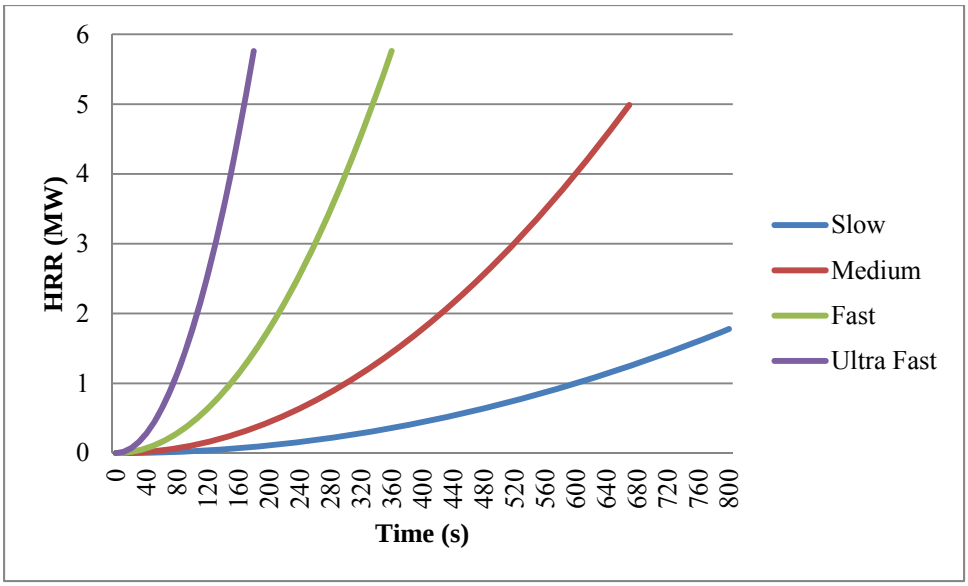

Figure 3.2: Heat Release Rate for t^2 fires (Buchanan, 2002)

3.3 Fully Developed

As previously mentioned, the fully developed fire is the most dangerous type of fire when considering effects on structural members. After progressing through the growth phase into the fully developed phase, the conditions within the compartment have changed drastically. Depending upon ventilation, fire will appear to consume the entire compartment, and the majority of the combustibles will be actively producing pyrolyzates and contributing to the intensity of the fire.

In most fully developed fires, the fire is ventilation controlled in that the size of the fire is limited by the amount of oxygen the fire is able to entrain into the compartment. If there is adequate ventilation, it is possible to see a fire remaining in the fuel controlled state where the size of the fire is limited by the rate at which fuel can be pyrolysized. This is common in very large compartments and compartments with large amounts of ventilation.

The longevity of a fire in its fully developed phase is primarily a function of the amount of fuel in the compartment along with the rate at which that fuel is consumed. Therefore, the more important aspect to look at when comparing compartments with similar fuel loads is the peak temperature. There have been a number of studies measuring the peak temperatures reached in compartment fires which have resulted in a considerable amount of spread in results. This spread illustrates that the estimation of temperatures within a compartment fire is not only highly variable, but highly complex. An in depth analysis of these studies can be found in Section 3, Chapter 6 of SFPE's Handbook of Fire Protection Engineering (2008). Most of these methods rely on some form of empirical correlation that is related to a conservation of energy equation with regards to energy output into and out of the compartment in question. But, in the final analysis the general principles of each of the methods are similar. With this similarity in mind, Law's Method is chosen for discussion here. Law's method is one of the simpler processes for approximate temperature prediction, but it provides a look at how the variables within a compartment will affect the ultimate peak temperature. According to Law's Method, the maximum temperature in a fire is defined as (Society of Fire Protection Engineers, 2008):

$$T_{max} = 6000(1 - e^{-0.1\Omega})/\sqrt{\Omega} \qquad \text{Eqn. 3.2}$$

$$\Omega = \frac{A_t - A_v}{A_v\sqrt{H_v}}$$

Where,

A_t is the total surface area of the compartment

A_v is the total ventilation area of the compartment

H_v is the height of the ventilation in the compartment

As observed in Equation 3.2, the maximum temperature in a compartment fire is largely a function of the room size and the size of the ventilation openings. This is to be expected as the primary driver of a post flashover fire is adequacy of ventilation and radiant heat transfer from the upper layer.

As stated previously, the above analysis is based on the heat balance which is the conservation of energy applied to the compartment in question. The variables demonstrated in Figure 3.3 allow the following heat balance equation to be written:

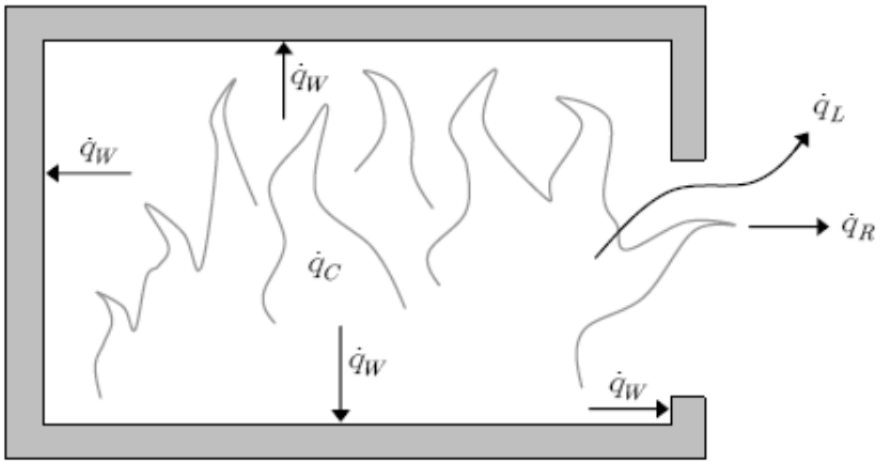

Figure 3.3: Heat losses during a fully developed fire (Buchanan, 2002)

$$\dot{q}_c = \dot{q}_L + \dot{q}_W + \dot{q}_R \quad \text{Eqn. 3.3}$$

Where,

$\dot{q}_C$ is the rate of heat release due to combustion

$\dot{q}_L$ is the rate of heat loss from replacement of hot gases by cold gases

$\dot{q}_W$ is the rate of heat loss through the boundaries

$\dot{q}_R$ is the rate of heat loss by radiation through the openings

All values in Equation 3.3 can be estimated through a variety of methods with varying accuracies. The large number of variables that play a role in this relatively simple looking equation should be noted. These can include, at a minimum, the compartment geometry, the type and configuration of the fuel, compartment lining thermal properties, and the flow characteristics of the ventilation opening(s).

3.4 Decay

The decay period of a fire is marked by the point at which the fuel and/or oxygen has been depleted, thus causing the fire to self-extinguish. The decay phase of the fire is of little to no concern to the analysis of structural members due to the rapid decrease in the temperatures present in the compartment. Residual heat will remain in the compartment, but it will dissipate rapidly.

The length and intensity of the decay period of the fire can vary based on ventilation characteristics and compartment lining material. Simple assumptions of this phase can be made for modeling purposes. The Eurocode, for instance, estimates that the length of the decay period will be approximately the same as the full burning duration and marked by a linear decrease in

released energy (Buchanan, 2002). The total energy released during this phase is estimated to be 1/3 of the total potential energy in the compartment, demonstrating that the fire is still actively burning. However, the slower rate of energy release results in temperatures low enough to be of no concern to structural members within the compartment.

CHAPTER 4 - FIRE TESTS ON SCALE BUILDING

In order to validate the effectiveness of the use of structural deformations, it was necessary to devise a scenario where deflections can be measured while other variables are as controlled as possible. This scenario was set up by using a scale model structure. The relative distribution of heat flux and the reactions from the steel supporting structure are expected to be representative of a much larger burn scenario. The test building was assembled outdoors and was, therefore, subject to wind, rain, etc. on the days of the burns. All efforts were made to ensure that the burns did not occur on days with abnormal weather (very cold, windy days, or rainy days, etc.). Environmental factors, such as ventilation, were controlled as much as possible.

A total of three test buildings were assembled and utilized. The first building was used to validate the fuel loading, ventilation conditions, and structural loading to be used in the later tests. The last two buildings were used to provide two test scenarios on which the conclusions can be based. The specific test set up and findings of each burn are discussed at length later in this dissertation.

4.1 Building Construction and Materials

The structure used for this series of tests is an Arrow GA1017 steel shed. The company refused to disclose details about the design and manufacturing process of the structure, but they claim when appropriately assembled and anchored it should meet the codes of the majority of states. It is modularly constructed with steel trusses. The trusses themselves are very similar in configuration to portal frame connections in that the hip connections are moment bearing. All structural members were composed of galvanized steel with the truss members having a thickness of 0.84 mm (0.033 in.) and all other members having a thickness of 0.53 mm

(0.021in.). The front and back walls are not load bearing though they are incorporated in a way that will allow them to act as shear walls. The exterior of the structure is covered in 26 gauge, vinyl covered standing seam metal sheeting. The building was anchored on 0.6 meter (2 foot) centers using 13 mm (½ inch) Tapcon masonry screws. Figure 4.1 shows a cutaway of the structural system of the test building and Figure 4.2 is a picture of the building as assembled.

The structure's nominal exterior dimensions are 3.05 m wide by 5.18 m deep (10 ft x 17 ft). The peak of the roof sits 2.4 m (7.88 ft) off the concrete slab. The hips of the trusses are 1.93 m (6.33 ft) off the slab. The doorway is approximately 2.29 m (7.5 ft) wide composed of two hinged doors attached with simple hinges.

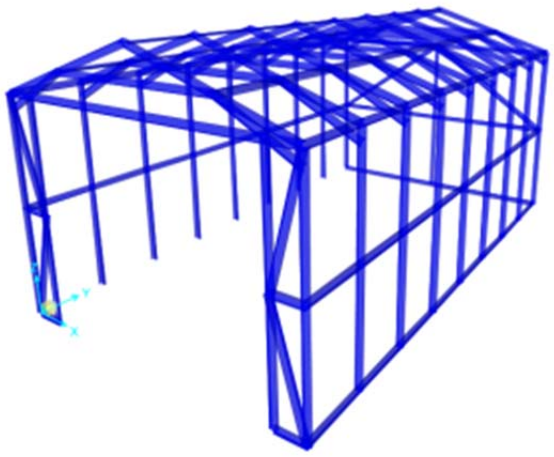

Figure 4.1: Cutaway showing structural members of test building.

Figure 4.2: Overview of test building as constructed.

4.2 Experimental Design

A total of 5 burns were conducted as part of this experimental series. Three preliminary burns, noted as PB-_, were conducted to evaluate experimental parameters in the original test building. Two test burns, noted as TB-_, were also conducted, each in a new building. The experimental set up is discussed later in the dissertation. A summary of the primary variables which were changed in each test is given in Table 4.1.

Table 4.1: Test parameters.

Test ID	Date	Ignition (Origin)	Fuel Load	Roof Load kN/m^2
PB-1	5/10/11	Pan Fire (SE Corner)	Symmetric, 6 stacks, 2 pallets each	None
PB-2	5/25/11	Pan Fire (SE Corner)	Non-Symmetric, 3 stacks, 2-3 pallet stacks, 1 6 pallet stack	None
PB-3	7/6/11	Pan Fire (SE Corner)	Symmetric, 6 stacks, 6 pallets each	0.359
TB-1	9/30/11	Pan Fire (SE Corner)	Symmetric, 6 stacks, 5 pallets each	0.091
TB-2	11/11/11	Pan Fire (SE Corner)	Symmetric, 6 stacks, 5 pallets each	0.182

4.2.1 Ventilation Conditions

Ventilation conditions were held constant throughout all test burns. The main source of ventilation for the fire was a 50 mm gap running the length of the peak of the roof and 25 mm gaps around all sides of the front door. In addition, each eve had two ventilation holes measuring approximately 50 mm by 100 mm. Observation of the building showed smoke exiting the structure through the joints in the corrugated metal sheathing of the structure;

however, there is no way to quantify the area of ventilation from this source, only to note that it should have remained fairly consistent from test to test. The gap in the peak of the roof can be seen in Figure 4.2. The ventilation in the front and rear of the structure is shown in Figure 4.3*(a)* and 4.3*(b)*.

(a) *(b)*

Figure 4.3: Test Building. *(a)* front. *(b)* rear

4.2.2 Instrumentation

The main purpose of these burns was to measure the deflections caused by the fire and to relate these deflections to measured temperatures. Typically, high temperature strain gages are used to monitor deflections in this type of research. Due to the high cost and lack of data acquisition equipment, a Nikon total station with prism was used to measure the deflections both before and after the burns took place. The accuracy of this instrument is better than 0.25 mm at

the distance it was utilized and the deflections anticipated were two orders of magnitude larger. Any measurement error should be negligible in the end analysis of the deflections.

A series of 20 gauge, Type K thermocouples (TC) with twisted ends were used to monitor temperatures in the structure at the ceiling level. In addition, a thermocouple tree of the same composition was placed in the middle of the structure with the leads placed one foot apart. All thermocouple data were logged and stored at a regular interval of three seconds. Figure 4.4 shows the location of the thermocouples and their associated labels in a plan view and Figure 4.5*(a)* demonstrates the method of routing the thermocouple wiring in order to avoid any interference from contact with the structure. All figures in this dissertation are oriented to reflect the layout of Figure 4.4.

Additionally, each test had a series of heat flux transducers (radiometers) placed at the ceiling level. The total heat flux at the ceiling level was measured with a water cooled, Schmidt-Boelter type heat flux transducer with a viewing window of approximately 180^{o} (Medtherm model 64-15SB-4-10MgO-20665A with no window, Range of 0-150 kW/m^2). The transducers were installed through holes drilled in the roof of the building looking downward. Figure 4.4 shows the locations of the heat flux sensors on the structure and Figure 4.5*(b)* demonstrates the radiometer's installation with respect to the building.

A Bullard T-4 Max thermal imaging camera was utilized to record each experiment. This thermal imaging camera is primarily designed for firefighting applications, but was equipped with digital video recording capabilities. It utilizes an uncooled microbolometer with digital processing as its detector type and has a temperature sensitivity of 0.5 °C. In addition, this model is equipped with Bullard's Thermal Throttle function allowing for distinct differences in temperature to be easily recognizable through the use of a color display.

In addition to the above instrumentation, digital still and video photography were used during each test to document the growth and progression of the fire. Photographic records of the compartment fire were supplemented by direct observations and written notes.

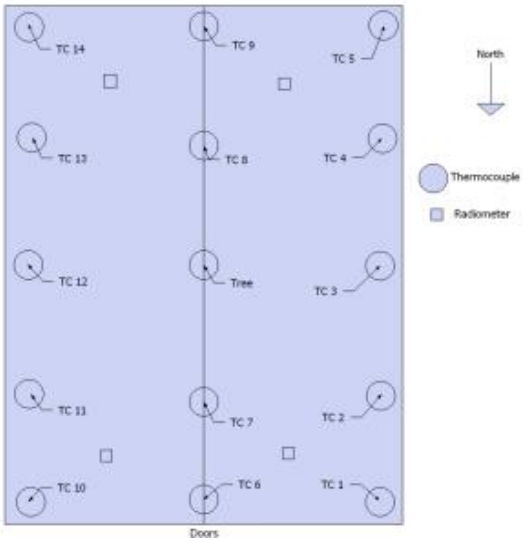

Figure 4.4: Location of thermocouples and radiometers.

(a) *(b)*

Figure 4.5: Instrumentation. *(a)* thermocouple routing. *(b)* radiometer placement through roofing material.

4.2.3 Fuels

All fires were fueled using wooden pallets. It has been demonstrated that an accurate peak heat release rate of a stack of pallets can be determined from (Zalosh, 2003):

$$Q_{max} = 1450(1 + 2.14h_s)(1 - 0.027M_w) \quad \text{Eqn. 4.1}$$

Where

Q_{max} is the heat release rate (kW) of the pallet stack

h_s is the height of the pallet stack (m)

M_w is the moisture content of the pallets (weight %).

The number and orientation of the pallets varied based on the test, and all variations are outlined in Table 4.1. The majority of the tests were performed using a symmetrical fuel load with 6 stacks of pallets, varying from 2-6 pallets per stack. Figure 4.6 demonstrates a symmetrical fuel load with two pallets per stack. All symmetrically loaded tests appeared similar, with only the height of the pallet stack being varied.

Figure 4.6: Symmetric fuel configuration (PB-1).

A 9-inch diameter heptane pool fire was chosen to ignite the fires because of its consistency of energy production. A small pool fire was selected for this experimental series due to their extensive use in fire research and the data provided by these studies that enable the heat release rate and duration of burning to be calculated by Equation 4.2 (Society of Fire Protection Engineers, 2008).

$$\dot{Q} = \dot{m}''\Delta H_{c,eff} A_f \left(1 - e^{-k\beta D}\right) \quad \text{Eqn. 4.2}$$

Where,

$\dot{Q}$ is the heat release rate (kW).

$\dot{m}''$ is the mass loss rate

$\Delta H_{c,eff}$ is the heat of combustion

A_f is the area of the fire

$k\beta$ is an empirical constant

The mass loss rate for heptane was estimated to be (C_7H_{16}) $\dot{m}'' = 0.101 \frac{kg}{m^2 - sec}$; the heat of combustion as $\Delta H_{c,eff} = 44{,}600 \frac{kJ}{kg}$; the area, A_f=0.04 m^2; and the empirical constant as $k\beta = 1.1\ m^{-1}$. This ignition scenario resulted in a calculated 48 kW peak heat release rate fire with an approximate burning duration of 4 minutes.

4.2.4 Roof Loads

After several of the preliminary burns were completed and the behavior of the buildings observed, it became clear that the building was unlikely to deflect under its own weight as the structural members were lightweight in nature. In order to simulate an evenly distributed load, concrete masonry units (CMUs) were placed in an evenly distributed manner on the roof over

each of the trusses. While the selection of these loads appears a bit arbitrary, they are not outside of the realm of expected dead loads on structures such as this building. In the instance of the research building, the entire building weighed less than 340 kg (750 lbs). As such, it is unlikely that the structure would deflect under its self-weight to a point that was measurable with a total station. The loading was varied from test to test to produce the magnitude of deflections required to be measurable and meaningful (see Table 4.1). In all variations, the loads were kept equally distributed and evenly placed; only the magnitude of the load was changed in an attempt to realistically simulate a roof load.

4.3 Preliminary Burns

A series of preliminary burns were conducted in the first test building. As in any case of fire testing there are a number of variables that must be evaluated and held constant to ensure that accurate results can be obtained. As such, these preliminary burns were aimed at the evaluation of several test parameters including fuel load, ventilation conditions, roof loading, and instrumentation placement and operation. Three burns were conducted with varying degrees of success as part of this phase of the study.

4.3.1 Preliminary Burn 1 (PB-1)

The test parameters for PB-1 were a "best guess" at the conditions required to produce a fire of high enough intensity to produce deflection in the test building. At this point in the research, there were a number of unknowns including the adequacy of the ventilation, appropriate fuel loads, effects of heat loss through the thin metal skin, and the actual behavior of the structure once affected by elevated temperatures. As initial conditions, PB-1 consisted of a fuel load of 6 stacks of 2 pallets each. There was no external roof load applied to the structure.

Upon analyzing the results of PB-1, the fuel configuration proved to be too small to produce adequate intensity or duration of temperatures to cause deflection of the steel support system. The fire experienced difficulty spreading from the initial pallet stack to the surrounding stacks due to the relatively small heat release rate of the pallets. Ventilation throughout the test appeared to be adequate for fuel consumption, but the heat release rate of such a small stack of pallets was unable to produce sustained temperatures over 500 °C for any sustained period of time. In addition, the high thermal conductivity of the walls caused excessive amounts of heat loss to the environment. While there was no way to completely stop this heat loss, the overall effects could be minimized by increasing the heat release rate of the fire. Both the thermocouple and radiometer data provided little to no insight into the fire as much of the data was lost due to an acquisition problem outside of the researcher's control. One unique aspect of this burn was the use of a thermal imaging camera (TIC) elevated above the building. Figures 4.7*(a)* – 4.7*(f)* show still photographs from directly over the building at varying times using a digital video recording Bullard TIC.

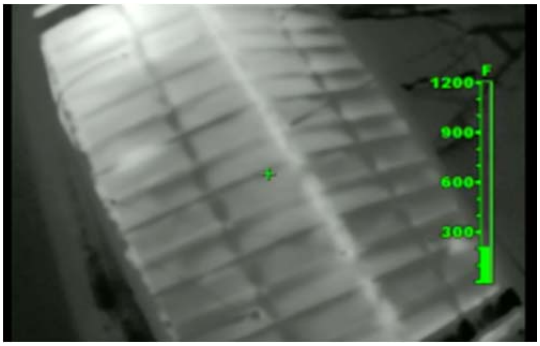

(a) t=18 minutes.

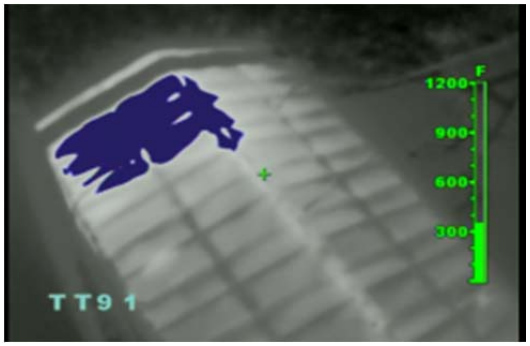

(b) t=21 minutes.

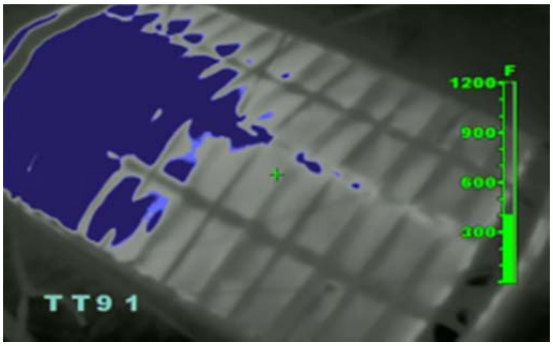

(c*)* t=24 minutes.

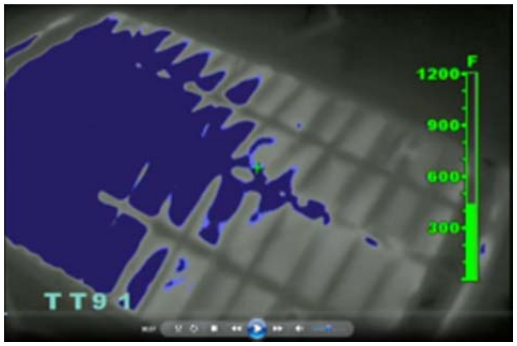

(d) t=27 minutes.

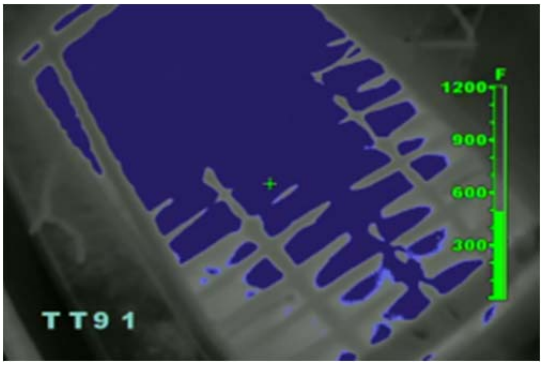

(e) t=30 minutes.

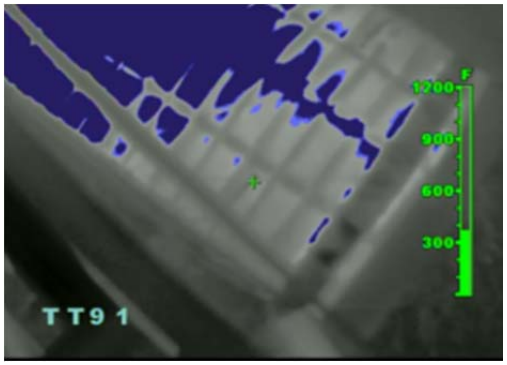

(f) t=33 minutes.

Figure 4.7: TIC images of PB-1 at given times.

4.3.2 Preliminary Burn 2 (PB-2)

Similar to PB-1, PB-2 was used to investigate several parameters with regard to the optimum test setup. The biggest change made to the test procedure before this burn was the fuel loading and distribution. Since PB-1 demonstrated the reluctance for the fire to spread to additional pallet stacks, a non-symmetric fuel load with one stack of six pallets and 2 stacks of 3 pallets each were utilized. The fire was initiated using a pan fire in the larger stack of pallets.

As seen in PB-1, the fire did not produce temperatures of high enough intensity or long enough duration to produce any sustained deflections. However, this burn demonstrated that the fire would spread from the initial pallet stack and that the ventilation within the structure was adequate for a higher heat release rate fire. A plot of the temperature data from the thermocouple tree can be found in Figure 4.8.

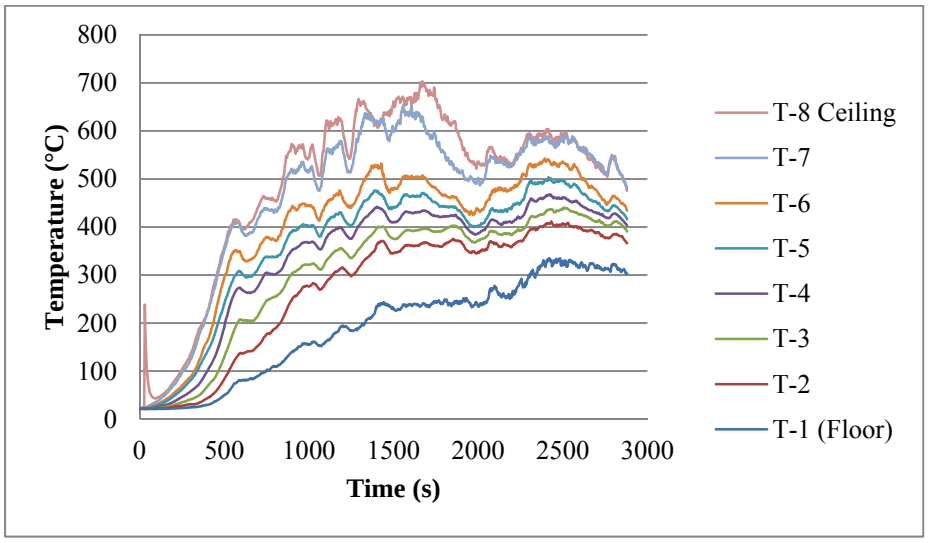

Figure 4.8: PB-1 Thermocouple Tree Data

As shown in Figure 4.8, the temperatures at the ceiling level reached 500 °C and stayed at this temperature for well over 30 minutes. It should be noted that these were the temperatures recorded in the center of the structure and temperatures were relatively higher over the fire origin within the building. PB-2 still produced no measurable deflections, most likely due to the nonexistence of any real load on the roof.

4.3.3 Preliminary Burn 3 (PB-3)

The results of the first two preliminary burns were integrated into the third test scenario. Thus far, the researcher had been unable to produce temperatures of high enough intensity and duration to produce meaningful deflections. As a result, the fuel load was increased to six stacks of six pallets. In addition, an evenly distributed roof load was added to the building in order to obtain higher magnitude deflections. Roof loads and the methodology for their development and use have been discussed previously in this dissertation.

The combination of increased fuel load and the addition of a roof load proved to be too much for the building to handle, causing the building to totally collapse. This made the obtaining of deflection measurements impossible. However, the movement in the building was of sufficient magnitude to be observed in pictures. The collapse began at the end of the building where the fire originated as was expected. Figures 4.9*(a)* – 4.9 *(f)* shows the collapse progression of the building. Thermocouple data is not available for this burn due to equipment malfunction outside of the researcher's control.

(a)T~35 mins

(b)T~37 mins

(c)T~41 mins

(d)T~43 mins

(e)T~45 mins

(f)T~50 mins

Figure 4.9: PB-3 Progression of Collapse. In time sequential order from a-f. Approximate times given from ignition of first fuel package.

4.4 Test Burn 1 (TB-1)

Test burn 1 (TB-1) was conducted in an entirely new building as the previous one had collapsed. The fuel load was reduced to six stacks of five pallets each. The roof load was also reduced to one CMU per truss simulating a roof load of 0.091 kN/m^2 (1.9 psf). This test was instrumented as discussed in the methodology section of this dissertation. However, due to errors in the data collection, much of the temperature data were lost. The temperatures from the thermocouple tree were retained and are shown in Figure 4.10. In addition, the total heat flux in each quadrant of the structure can be seen in Figure 4.11. Figure 4.12 contains a contour plot of the deflections.

The thermocouple data provide insight into the conditions within the structure from a temperature standpoint. The temperatures largely reached a relative plateau, despite several localized peaks. This plateauing of the temperatures indicated a ventilation controlled fire, which was expected with such a small compartment volume and large fuel load. Temperatures consistently averaged over 500 °C at the ceiling level which is clearly high enough to produce deflections in the structural members.

More interesting than the thermocouple data is the heat flux data. The reader can recall from information presented earlier that the ultimate temperatures obtained by the steel members are dependent on this cumulative (over time) heat flux. The fire originated in the southeast quadrant of the building. Both the SE and SW quadrants appeared to receive comparable heat flux to the ceiling. It is not until a time of nearly 80 minutes when the north end of the structure begins to see more heat flux than the south end of the structure. By this time, the majority of the fuel has been consumed. Additionally, it can be noted that the duration of exposure to the higher heat flux is much more severe in the southern half of the structure. The average heat flux

exposure (in kW/m^2) per quadrant is 32.86 in the SW quadrant, 28.2 in the NW quadrant, 30.81 in the SE quadrant, and 22.9 in the NE quadrant, again demonstrating that the southern end of the building received significantly more energy from the fire than the northern end. Specifically, the SW quadrant received the highest average heat flux, which is somewhat of an anomaly as the fire originated in the SE corner, a phenomena that will be discussed later in this dissertation.

The deflection data reflect the findings of the heat flux data. The largest deflections appear to occur in the SW quadrant of the building. This relationship shows that the amount of deformation is in fact dependent upon the amount of cumulative heat flux received by a specific structural member (or area of a building in this case).

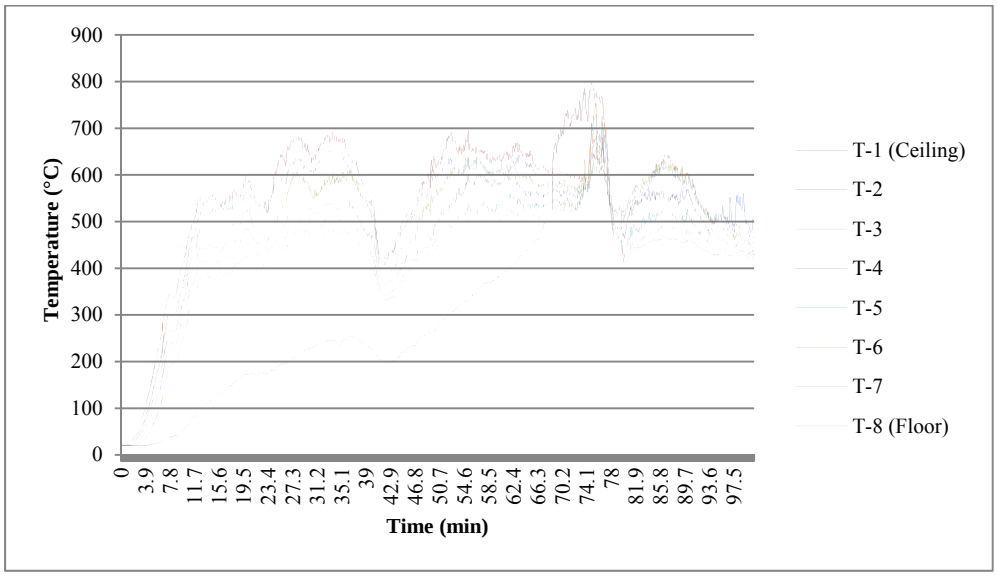

Figure 4.10: TB-1 thermocouple tree temperatures.

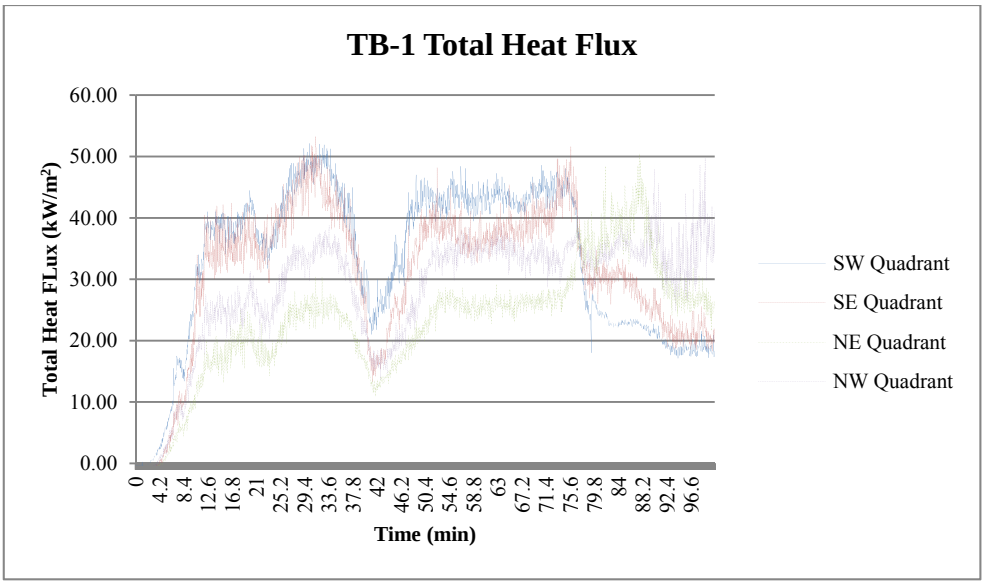

Figure 4.11: TB-1 total heat flux by quadrant. SE quadrant was area of origin.

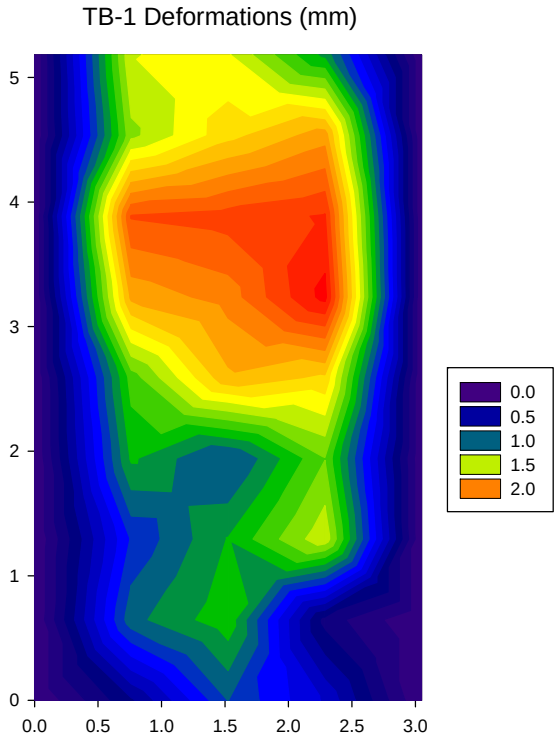

Figure 4.12: TB-1 deformations (mm)

4.5 Test Burn 2 (TB-2)

Test burn 2 (TB-2) was conducted in an entirely new building to ensure that no residual effects from the previous tests would affect the outcomes of this burn. The fuel load remained the same at six stacks of five pallets each. The roof load was increased to two CMUs per truss simulating a roof load of 0.182 kN/m^2 (3.8 psf). This test was instrumented as discussed in the methodology section of this dissertation. The temperatures from the thermocouple tree are shown in Figure 4.13 below. In addition, the total heat flux in each quadrant of the structure can be seen in Figure 4.15. Figure 4.16 shows a contour plot of the cumulative relative heat flux. Figure 4.17 contains a contour plot of the deflections.

In regard to the thermocouple data, there were several peaks in the temperatures indicating the fire to be ventilation controlled, which was expected with such a small compartment volume and large fuel load (See Figure 4.13). The peaks are not as prevalent as noted in TB-1. The ventilation was consistent between the two tests, so a reason for these variations is not readily apparent. Temperatures consistently averaged well over 500 °C at the ceiling level which was certainly high enough to produce deflections in the structural members. The distribution of temperature within the building as a function of time can be seen in Figure 4.14*(a)* - 4.14*(l)*.

The heat flux data (see Figure 4.15) in this case show the SW quadrant receiving significantly more heat flux than the SE quadrant (which is where the fire started). It is not until a time of nearly 110 minutes when the north end of the structure begins to see more heat flux than the south end of the structure. By this time, the majority of the fuel had been consumed. As in TB-1, it can be noted that the duration of exposure to the higher heat fluxes is much more severe in the southern half of the structure. The average heat flux exposure (in kW/m^2) per

quadrant is 29.6 in the SW quadrant, 24.3 in the NW quadrant, 18.4 in the SE quadrant, and 24.4 in the NE quadrant, again demonstrating that the southern end of the building received significantly more energy from the fire than the northern end. Again, as in TB-1, the SW quadrant received the highest average heat flux, which is somewhat of an anomaly as the fire originated in the SE corner. Again, this anomaly is discussed further later in the dissertation.

Since there were only four radiometers present, a better picture of the cumulative heat flux distribution can be developed by integrating the area under the time-temperature curves for each of the thermocouples mounted at ceiling level. The units of Figure 4.16 are rather meaningless; it is presented merely as a comparative tool, but it can be equated to heat flux units. In this case, the concentration of the heat flux is definitely in the southern end of the structure with a slight skew toward the eastern side (toward the quadrant of fire origin).

The deflection data reflect the findings of the heat flux data (see Figure 4.17). The largest deflections appear to occur in the SW quadrant of the building.

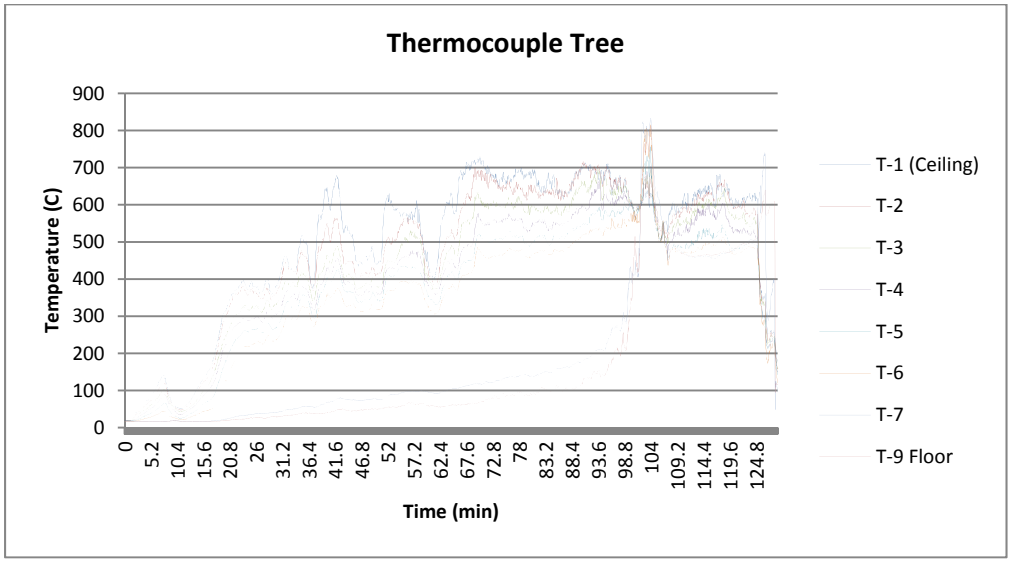

Figure 4.13: TB-2 thermocouple tree temperatures.

Figure 4.14: TB-2 Temperature Contour Plots

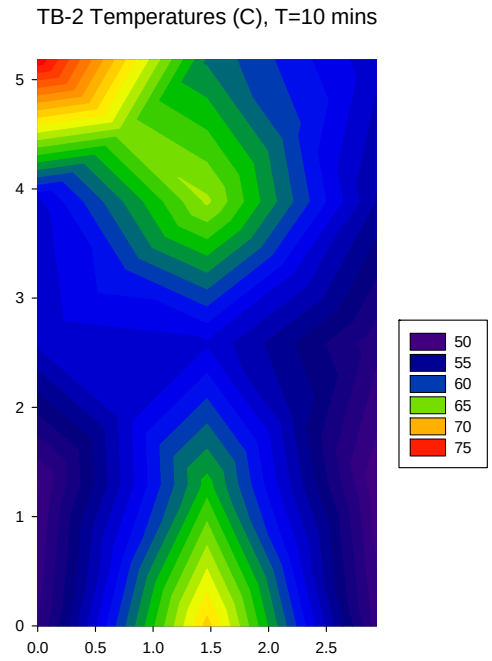

(a) t=10 mins

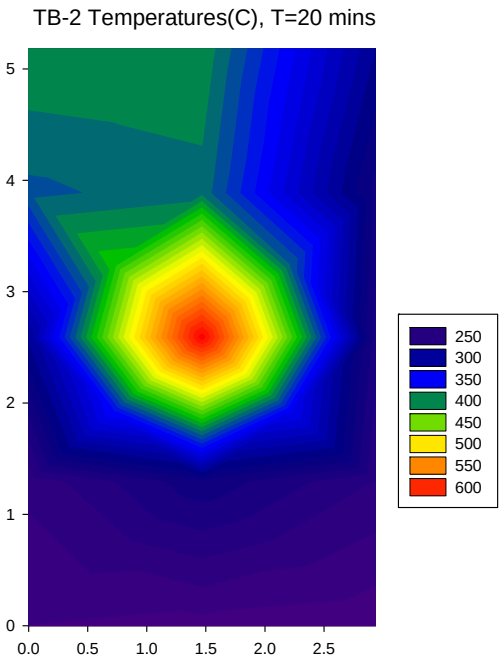

(b) t=20 mins

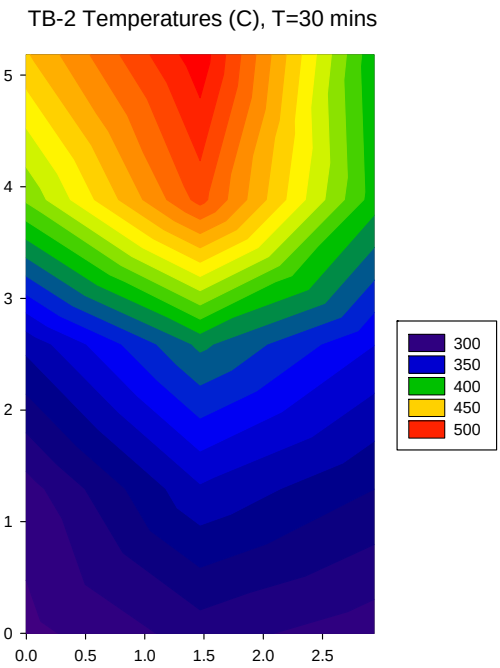

(c) t=30 mins

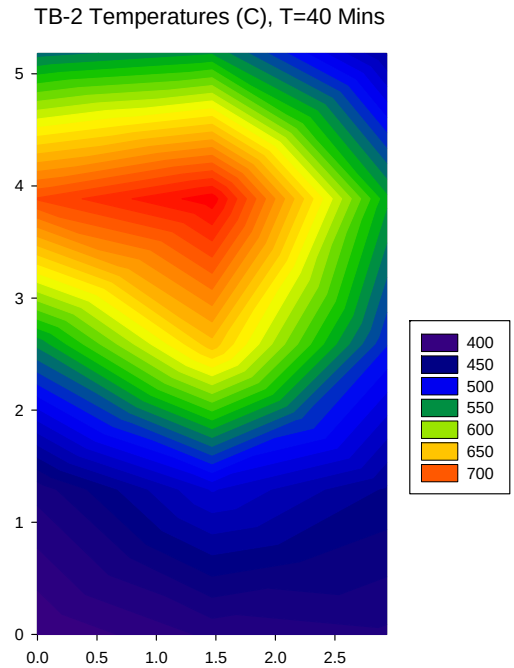

(d) t=40 mins

Figure 4.14. Continued

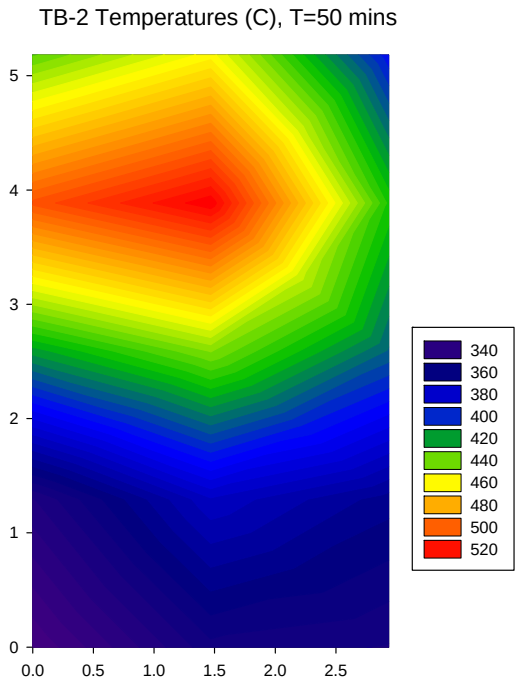

(e) t=50 mins

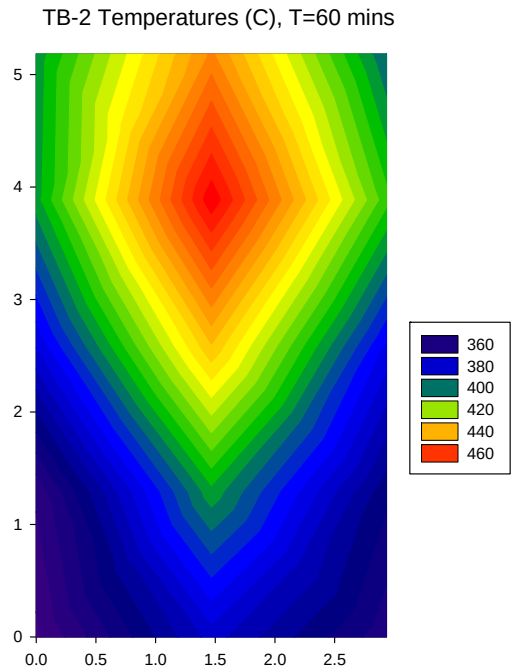

(f) t=60 mins

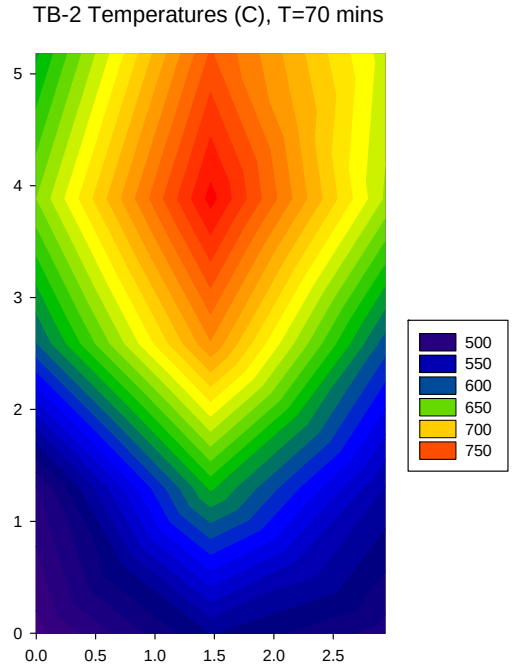

(g) t=70 mins

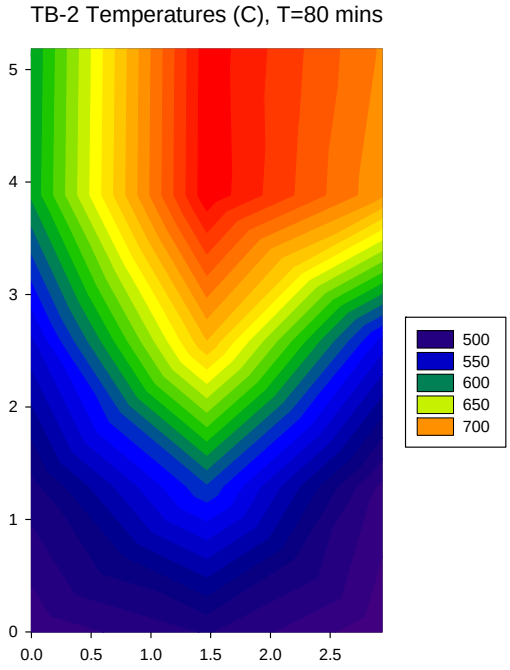

(h) t=80 mins

Figure 4.14. Continued

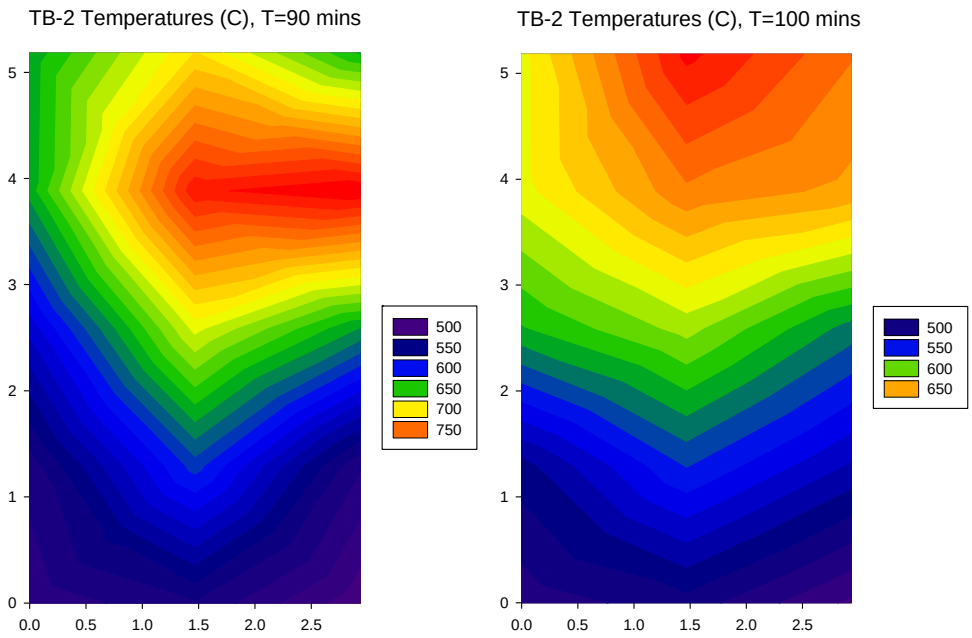

(i) t=90 mins *(j) t=100 mins*

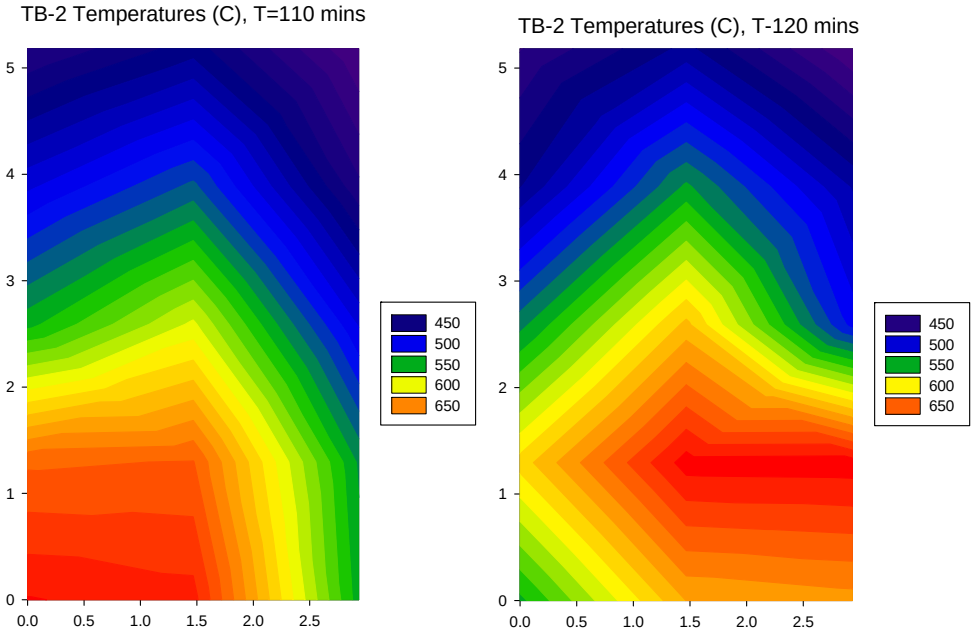

(k) t=110 mins *(l) t=120 mins*

Figure 4.14. Continued

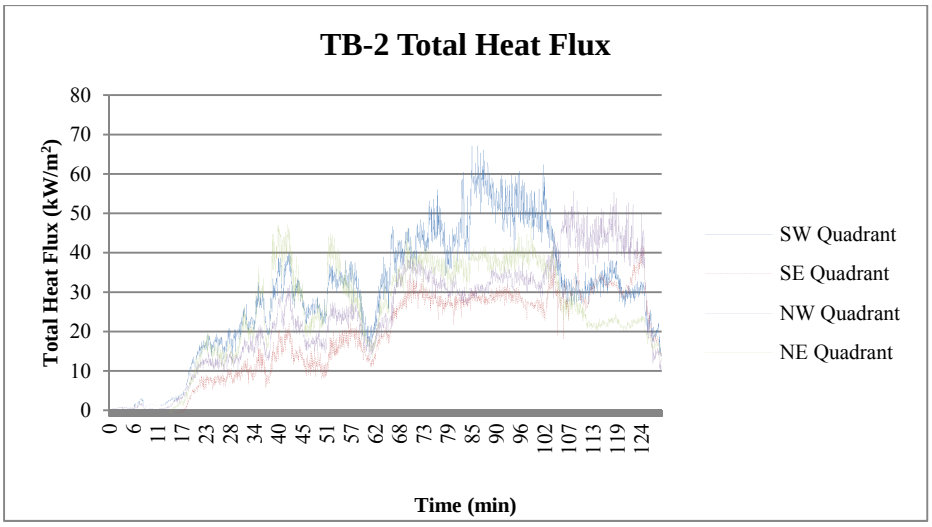

Figure 4.15: TB-2 total heat flux. SE corner was area of origin.

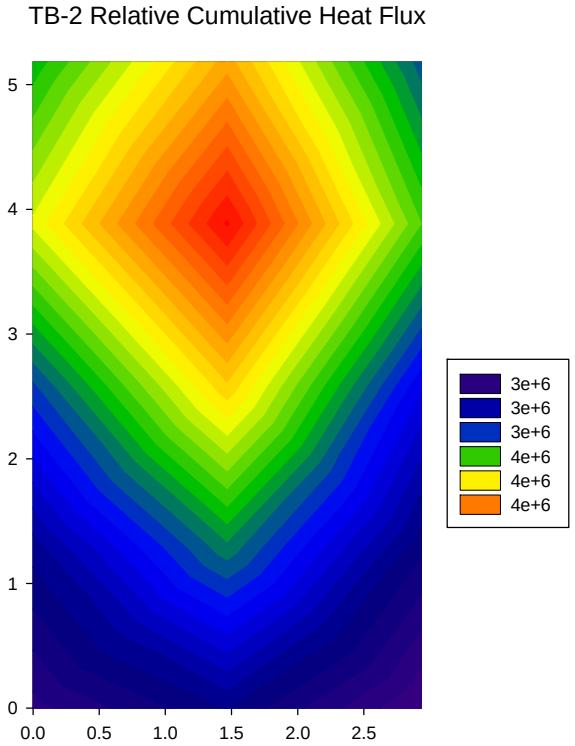

Figure 4.16: TB-2 relative heat flux

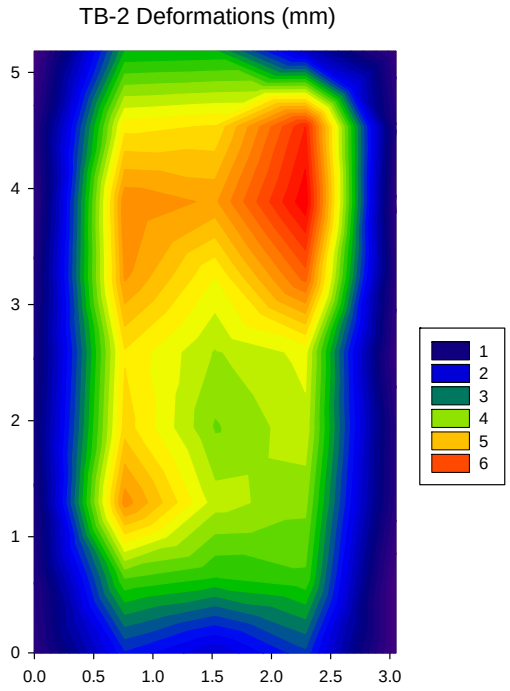

Figure 4.17: TB-2 deformations (mm)

4.6 Discussion

The main anomaly noted was the tendency of the highest magnitude deflections and the highest average heat flux accumulation to be in the southwest quadrant of the structure despite the origin being in the southeast corner. The researcher believes that this apparent anomaly is due to a variety of reasons. First of all, the high conductivity and low amount of thermal insulation provided in the building allowed a significant amount of energy to escape the structure. This energy loss could be somewhat negated by an increase in the heat release rate. Therefore, as the fire developed and moved beyond the initial pallet stack, there was more fuel involved creating a more intense fire. By that time, the majority of the fuel in the original pallet

stack was consumed. In addition, much of the energy from the first pallet stack was used in preheating the structure itself.

Another observation was the location of flaming combustion within the structure. As the fire progressed beyond the initial stack of pallets, the fire had a tendency to burn in the southwest corner of the structure. Fire dynamics will dictate that flaming combustion will occur where the ratio of fuel to air is in a specific range, not necessarily in relation to the fuel packages itself. In this building's case, pyrolysized fuel from other pallets was actually burning significantly in the southwest quadrant for the majority of the burning duration. This can be confirmed by looking at the temperature distributions on the ceiling and the heat flux data.

The buildings tested were, in comparison to "typical" buildings in which determining the point of origin of a fire is important, relatively small. Thus, the SE quadrant (fire origin) and SW quadrant (highest temperature) of the test buildings were in close proximity to each other. Even with the relatively small size of the building, the researcher recorded significant variances in both temperature and heat flux based on the time during the fire and location.

While these phenomena do not specifically support the anticipated findings of this study, neither do they negate them. While the largest magnitude of deflection was not directly over the area of origin, the deflection data can still be used to locate the quadrant of origin. An area weighted average of the deflections actually places the area of origin in the southeast quadrant (the actual area of origin). The area weighted average is calculated by multiplying the deflection measured times an attributed area similar to the weighting of load distributions from a slab to a selected beam. In both TB-1 and TB-2, this method accurately arrived at the correct area of origin (See Table 4.2 for results). The units in Table 4.2 are actually $mm*m^2$, but this is rather

meaningless. The important observation is that the area of highest area weighted average deformations occurs in the quadrant of origin.

This method of weighting attributed areas with their deflection shows that even though the most severe single measurement of deflection was in the SW quadrant of the structure, the largest deflection when weighted by area will lead the investigator to the SE quadrant. In addition, the differences noted between the north and south end of the structure are also important. In large loss investigations, the possible elimination of half of the structure can certainly be useful to any investigator.

Table 4.2: Area Weighted Average for TB-1 and TB-2 by Quadrant

	Area Weighted Average	
Location	TB-1	TB-2
SE Quadrant*	5.5	15.0
SW Quadrant	5.1	14.6
NE Quadrant	3.8	13.2
NW Quadrant	3.6	12.0

* Quadrant of Origin

CHAPTER 5 FINITE ELEMENT MODELING VALIDATION

5.1 Modeling Software

In order to accomplish the objectives stated in Chapter 1, it is necessary to provide a readily utilizable methodology for analyzing structural deformations in the context of an origin investigation. In the selection of a finite element modeling program, several characteristics were considered, all of which took into consideration the complexity and cost of the use of the particular analysis tool. These considerations included the following:

- Cost of Program – Most finite element software is relatively expensive to purchase and maintain. Also, the more complex a package is, the more it typically costs. Therefore, choosing a package designed specifically for structural analysis will help to keep overhead costs to a minimum.
- Availability – The availability of specific software packages at local or regional offices of engineering firms was important as the ability to work with local engineering firms is often more cost effective than working with national firms that have the expertise to run full service FEM packages.
- Ease of Use – While no FEM program is particularly easy to use, structural analysis packages contain a wide array of pre-built sections, connections, and other commonly encountered structural implements making the construction of models simpler than with full service FEM packages like Abaqus or Adina. Again, this approach will help to lower costs and increase the number of engineering firms with the requisite skills necessary to develop and analyze a model of a particular structure.

- Applicability – The program chosen must be capable of performing the specified analysis including accounting for inelastic behavior of materials past yield, consideration of fire effects on the material, and the ability to model the material as it returns to ambient temperature from its elevated temperature.

With these considerations in mind, Vulcan was the chosen software package for this analysis. Vulcan is a proprietary modeling software designed at the University of Sheffield based on several previous analysis tools and marketed through Vulcan Solutions Limited. "Vulcan is a finite element analysis program, which is capable of modelling the global 3 dimensional behavior of composite steel-framed buildings under fire conditions" (Vulcan Solutions Limited, 2014). Vulcan is a program designed specifically for the analysis of the behavior of steel structures exposed to fire conditions. Although Vulcan is a specialized program, the cost is relatively inexpensive at around $1500 per year for a commercial license. Because it is specialized, the developers have only included input and output options as are relevant to the intended analysis.

While a true finite element program (such as Abaqus or Adina) could be deemed appropriate for this kind of analysis, the costs and expertise associated with analysis using these programs would be prohibitive to all but the highest tier of forensic analysis. As discussed previously, utilizing a more limited but specialized program (such as Vulcan) for the analysis keeps cost under control and increases the likelihood that this kind of an analysis of deformations will be available for use in forensic settings.

Vulcan Solutions, Ltd. has also performed verification work which is listed on its website (Vulcan Solutions Limited, 2014). The Vulcan program has also been used successfully in

several dissertations and peer-reviewed articles including: Bailey, Burgess, & Plank (1996), Bong (2005), El-Rimawi, Burgess, & Plank (1996), Franssen (1990), and Wong (2001).

5.2 Ambient Temperature Validation

As with any finite element analysis, it is necessary to evaluate the capabilities of the chosen program with the proposed analysis in mind. In order to partially validate Vulcan for use in this study, it is necessary to ensure that the program produces reliable results when handling both temperature loading and unloading and can properly account for the yielding of steel as the yield stress is surpassed.

In order to assure that Vulcan is capable of producing accurate deflections at normal temperatures within the elastic range of loading, a series of beams with varying end configurations were analyzed within the program and compared to hand calculations. To perform the analysis, a 6 m long UB 203x102x23 was used with differing end configurations. A modulus of elasticity of 210,000 MPa (30,500 ksi) was used in both the calculations and the model. A concentrated load of 1000 N (lower than the load to cause yield) was applied to each configuration at the center of the beam. To reinforce the match, the process was repeated with a load of 10,000 N (also lower than yield load). Calculated hand deflections are for the center of the beam and are performed using Equation 5.1 for the simple beam, 5.2 for the propped cantilever, and 5.3 for the fixed end beam (American Institute of Steel Construction, 2005).

The modeled and calculated deflections for the center of the beam are contained in Table 5.1. The match between Vulcan and hand calculations is considered acceptable although there is a small unexplained difference between Vulcan and hand calculations associated with each of the calculations.

$$\Delta = \frac{Pl^3}{48EI}$$ Eqn. 5.1

Where,

P = Magnitude of Concentrated Load (N)

l = Length between supports (mm)

E = Modulus of Elasticity (N/mm^2)

I = Moment of Inertia (mm^4)

$$\Delta = \frac{7Pl^3}{768EI}$$ Eqn. 5.2

$$\Delta = \frac{Pl^3}{192EI}$$ Eqn. 5.3

Table 5.1: Deflection Results

	P=1,000 N		P=10,000 N	
Beam Configuration	Hand (mm)	Vulcan (mm)	Hand (mm)	Vulcan (mm)
Simple	1.02	1.04	10.18	10.49
Propped Cantilever	0.45	0.46	4.45	4.64
Fixed End	0.25	0.26	2.54	2.87

The simple beam validation is not capable of demonstrating Vulcan's ability to model inelastic behavior when a structure is loaded to stresses beyond the yield of the material. When a simple beam is stressed to the point of yield, it becomes an unstable member and produces non-convergence within Vulcan. Thus, a second model beam was analyzed by hand and by Vulcan. A W18x71 with a length of 6.1 meters (20 ft) was used for this example. The beam was simply supported at one end and fixed at the other (i.e. propped cantilever) and had a concentrated load placed in the center. The steel was assumed to have a yield stress of 344.7 N/mm^2 (50 ksi) and a modulus of elasticity of 199,950 N/mm^2 (29,000 ksi). For purposes of the hand calculations, the steel was assumed to be elastic-perfectly plastic; that is, the stress in the beam remained constant after it reached its yield stress. Vulcan, on the other hand, models the behavior of steel a bit differently as it used the Ramberg-Osgood model for inelastic behavior of steel (Refer to Section 2.3.1).

The propped-cantilever beam modeled is indeterminate to the first degree; therefore, when a plastic hinge forms at the point of highest bending moment (fixed end), the structure becomes inelastic, behaving under further loading like a simple beam. Upon formation of a second plastic hinge at mid-span, the beam becomes a mechanism and fails.

Elastic deformation of a propped cantilever at its midpoint was calculated using Equation 5.3. The self-weight of the member was also factored in as a distributed load. For a W18x71, the self-weight is 1.04 N/mm (71 lb/ft). The elastic deflection caused by this load can be calculated using Equation 5.4 (American Institute of Steel Construction, 2005).

$$\Delta = \frac{wx}{48EI}(l^3 - 3lx^2 + 2x^3) \qquad \text{Eqn. 5.4}$$

Where:

x = Distance from Support to Calculate Deflection (mm)

After yield, additional deflection was calculated using Equation 5.1 since the beam behaves similar to a simple beam once the hinge is formed at the fixed end.

To do an analysis using Vulcan, the user typically inputs a load which remains constant and then inputs a fire loading which varies with increasing temperature. In this example several analyses were done to partially validate the ability of Vulcan to handle inelastic behavior, without consideration of fire loading. A series of model iterations were run at varying concentrated loads below, at, and above the calculated yield stress of the beam. Deflections greater than that at the yield stress would not be expected to match the hand calculated values perfectly because of the way the steel stress-strain behavior was modeled after yield.

Figure 5.1 shows an idealized load-deflection curve calculated by hand. The Figure also contains four separate deflections calculated at varying loads (both above and below yield) utilizing Vulcan. Vulcan consistently predicted lower deflections when compared to hand calculations. However, Vulcan did not yield at the same point as predicted using the elastic behavior of the beam. Hand calculations produce a yield load of approximately 625 kN while Vulcan begins to yield around 800 kN. The change in slope of the P-Delta curve after yield is also significantly different than predicted by hand calculations.

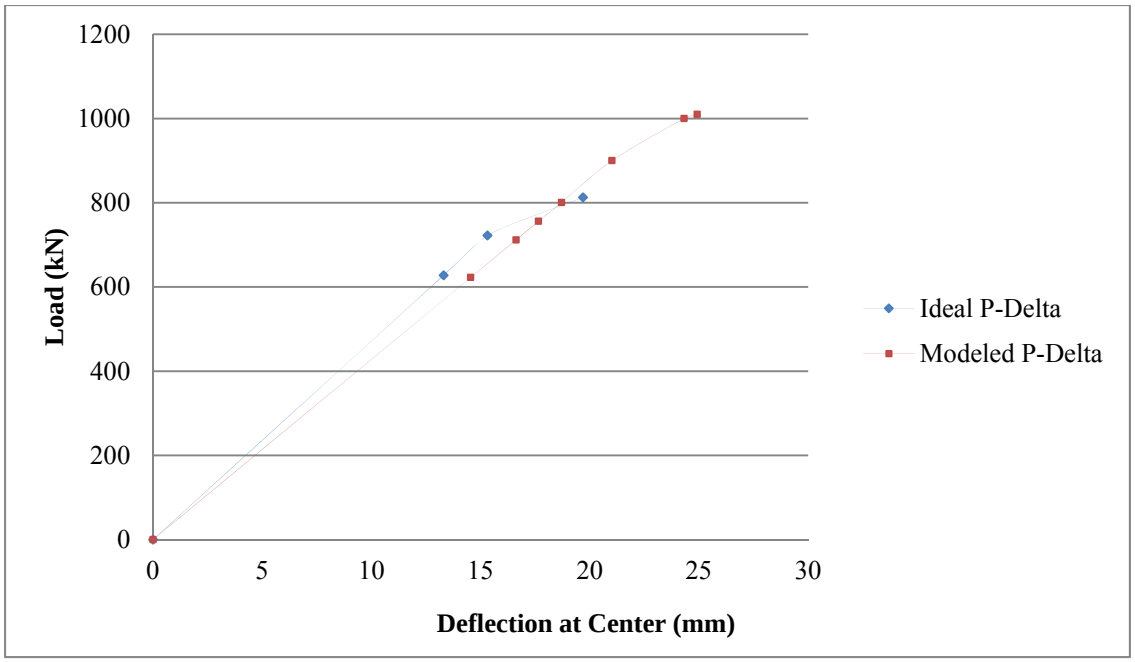

Figure 5.1: Load Deflection Curve Comparison

In order to determine whether Vulcan is capable of accurately accounting for differing yield strengths, several scenarios were considered. The scenarios are based on a 6 m long UB 203x102x23 beam with varying support conditions. Yield strength was varied between 330.9 MPa and 344.7 MPa (48 and 50 ksi).

Figures 5.2 and 5.3 show the load deflection curves for the described scenarios in a propped cantilever and fixed end beam configuration, respectively. Behavior is as expected when varying yield strength in that a higher yield strength material takes longer to yield.

Table 5.2 shows the only discrepancy noted in this analysis. Specifically, Vulcan does not seem to yield at the same loads which should produce yield according to basic hand calculations as shown in the previous example. While a slight variation is expected between

hand calculations and finite element modeling, the discrepancy is well over expected limits without any ability to explain the error.

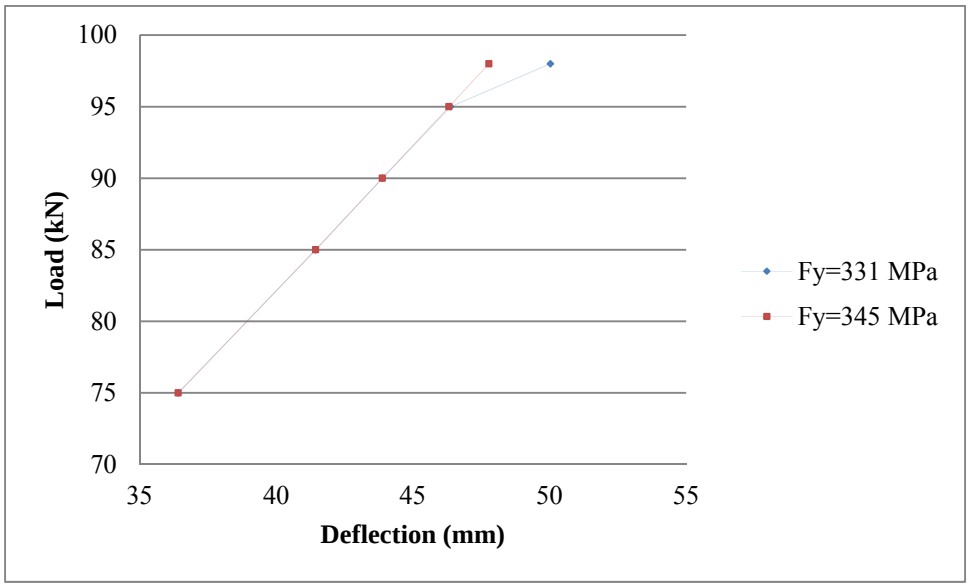

Figure 5.2: Propped Cantilever Load Deflection Curve

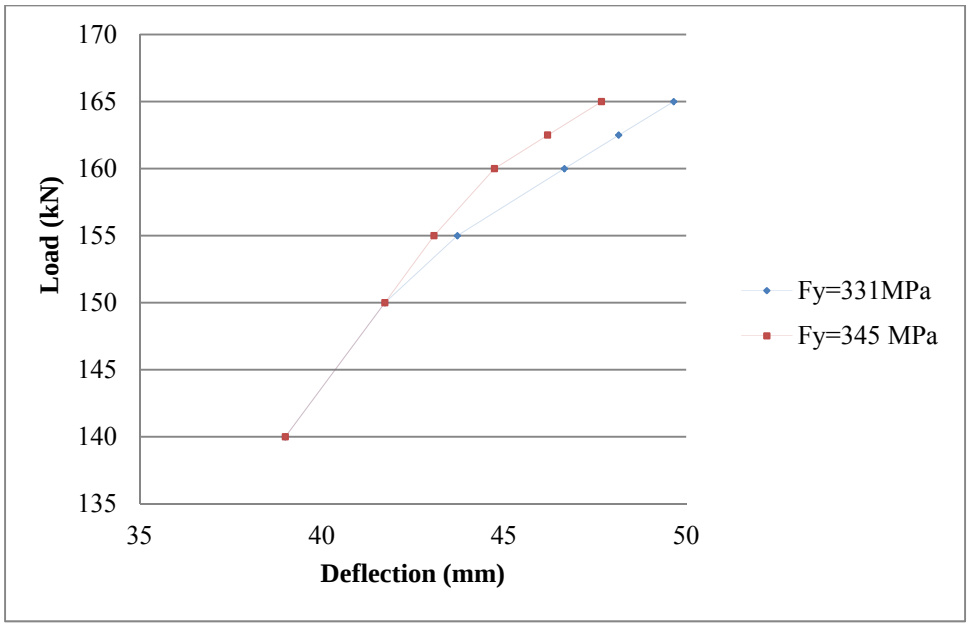

Figure 5.3: Fixed End Load Deflection Curve

Table 5.2: Yield Load Calculations

	Yield Load (N) for Yield Strength of 330.9 MPa (48 ksi)	
Beam Configuration	Hand Calculations	Vulcan (appx)
Simple Beam	45,750	49,000
Propped Cantilever	73,200	95,000
Fixed End	91,500	152,000

Next, a simple frame was analyzed in Vulcan. Two columns with pinned bases and a height of 3 m were connected by a horizontal member of 3 m in length. All columns and beams were composed of UB 203x102x23. A horizontal load was applied to the frame with the intention of performing a push over analysis. Hand calculations indicate a yield load of approximately 46 kN. The same frame in Vulcan yielded at approximately 56 kN. Again, Vulcan shows a significant disparity from hand calculations.

Overall, Vulcan appears to have some difficulty in modeling fixed ends and predicting yield at ambient temperatures. The amount of information regarding the development and background equations of Vulcan is not readily available to investigate. However, Vulcan was not designed as a program for use in the ambient temperature range, but for analysis at elevated temperatures. Section 5.3 describes an investigation of the ability of Vulcan to calculate behavior under elevated temperatures.

5.3 Elevated Temperature Validation

As previously stated, Vulcan was developed as a tool for structural analysis at elevated temperatures. To validate Vulcan's performance at elevated temperatures, a series of analyses have been performed.

The first analysis consisted of a simply supported UB 203x102x23. The length of the beam was set at 6 m (19.7 ft) and the steel was assumed to have a modulus of elasticity of

210,000 N/mm^2 (30,500 ksi) and a yield strength of 275 N/mm^2 (39.9 ksi). Two iterations were run including a concentrated load of 1000 N (228.4 lb) and a line load of 0.2 N/mm (13.7 lb/ft). The temperature was varied between 20 °C and 900 °C as shown in Figure 5.4. Hand calculations were performed using Equation 5.1 for the concentrated load and Equation 5.2 for the distributed load. The modulus of elasticity was reduced with an increase in temperature as outlined in Table 2.1. Results are shown in Figures 5.5 and 5.6.

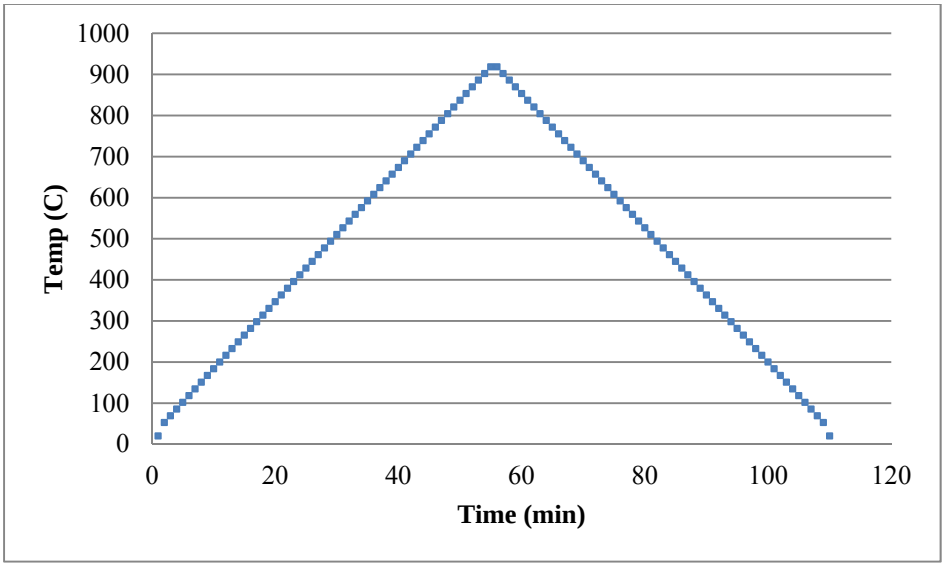

Figure 5.4: Temperature Curve used for Simple Beam Validation

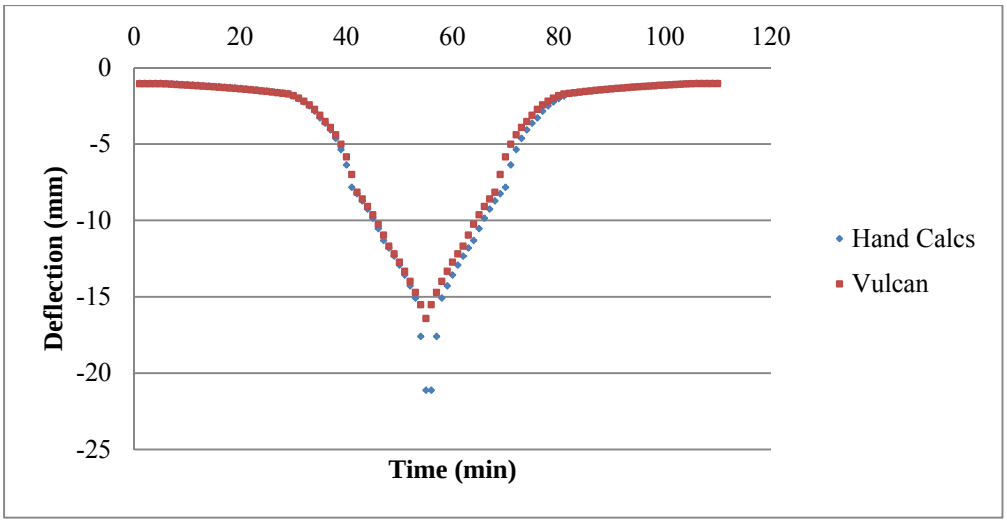

Figure 5.5: Simple Beam, Point Load Validation

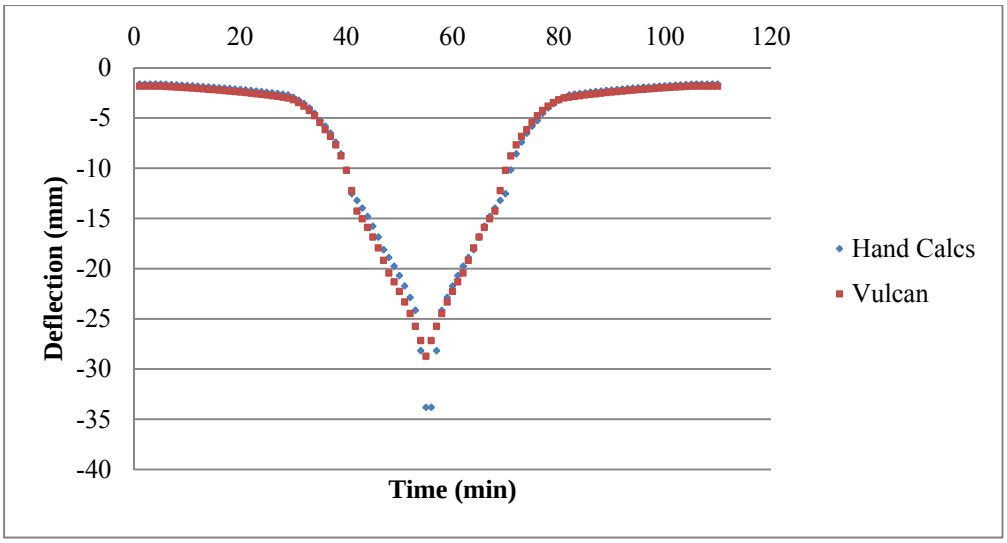

Figure 5.6: Simple Beam, Line Load Validation

As shown in the figures, the agreement between Vulcan and the hand calculations can be considered satisfactory. The only area where the two diverge in any relevant amount is where the temperature is very high (over 850 °C). This difference can be explained through the

difference in the model used to reduce the modulus of elasticity. The hand calculations utilize the design values given by AISC and outlined in Table 2.1 (American Institute of Steel Construction, 2005). Since these are design values, they are very conservative at higher temperatures basically making the modulus of elasticity nonexistent at these temperatures. The Ramberg-Osgood model (discussed in Section 2.3.1) utilized by Vulcan is less conservative at these higher temperatures. Hence, the hand calculations generate higher deflections at these extremely high temperatures.

It is also worthy to note the lack of yielding by these examples even though they reach fairly high levels of deflection. As the temperature is increased and modulus of elasticity decreases, the yield point occurs at higher strain levels. In relatively lightly loaded members (like these) it is difficult to reach yield until the yield strength has become almost completely degraded.

Next, an attempt was made to demonstrate Vulcan's ability to predict the behavior of an indeterminate beam that is capable of yielding without failing. To model this, a 6 m long UB 203x102x23 configured as a propped cantilever was utilized. A yield strength of 344.7 MPa (50 ksi) was used for the steel. Two iterations of this analysis were performed. The first analysis used a relatively light load coupled with an extreme temperature increase. The indeterminate beam was loaded with a concentrated load of 47 kN (10.6 kips). The temperature was then increased as shown in Figure 5.7. The deflection vs. time curve can be seen in Figure 5.8.

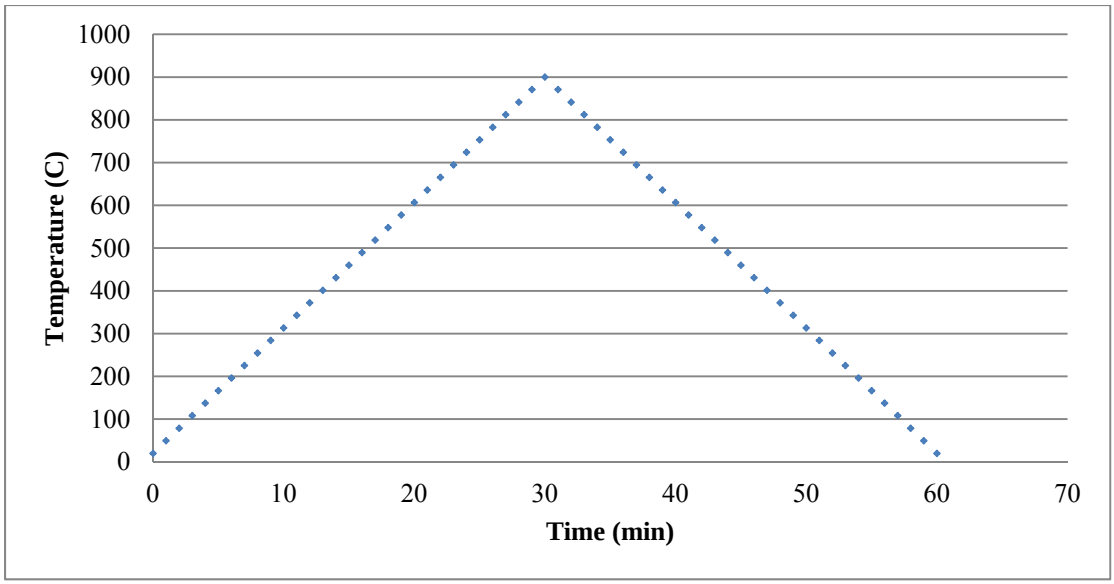

Figure 5.7: Time Temperature Curve

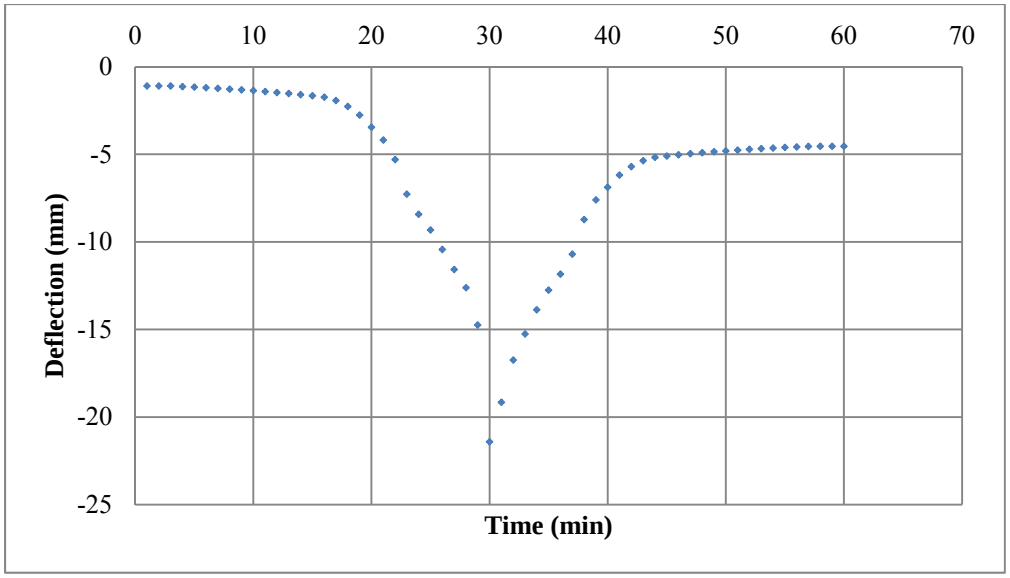

Figure 5.8: Deflection vs. Time

The next iteration used a relatively large concentrated load of 550 kN (123.6 kips) and a less extreme temperature increase (See Figure 5.9). The deflection vs. time results are shown in Figure 5.10.

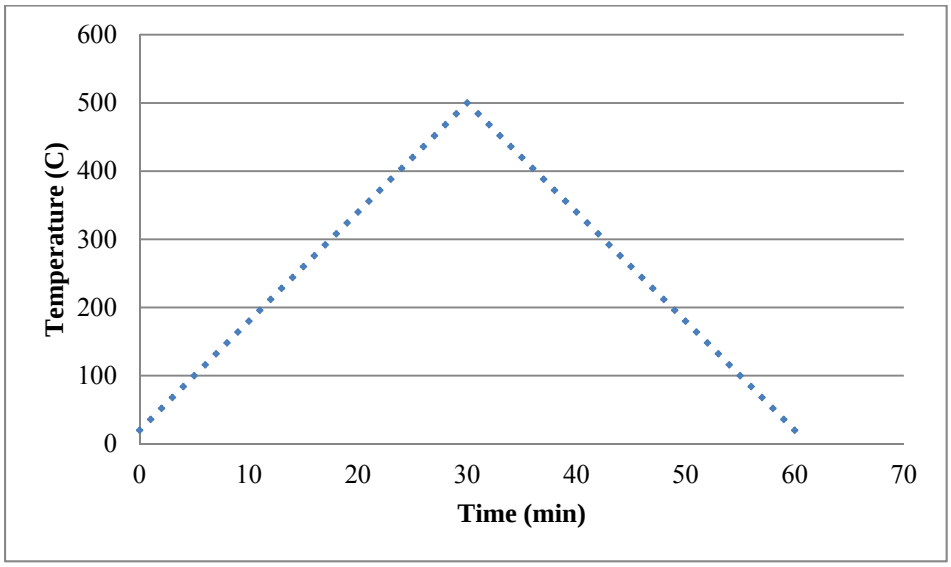

Figure 5.9: Time vs. Temperature Curve

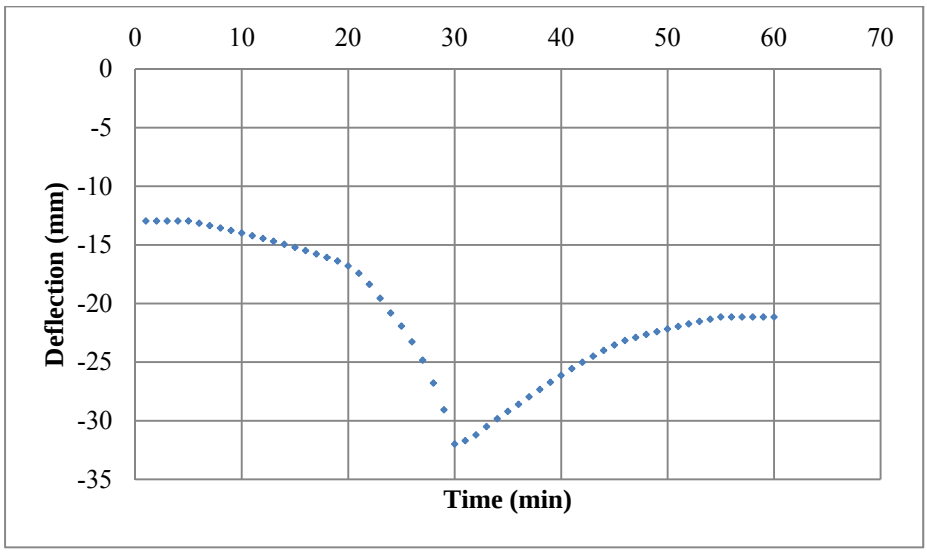

Figure 5.10: Deflection vs. Time

In both iterations, the beam was loaded to less than that which would produce yield under normal temperature conditions. However, the structure did in fact yield due to the lowered yield stress due to high temperatures, as demonstrated by the non-linear load vs. temperature plots showing that Vulcan will correctly produce yield due to high loads or high temperatures. As the temperature returned to ambient, the structural deflection decreased, recovering some of the deflection caused by high temperature. However, not all of the added deflection was recovered, indicating that plastic deformation did occur in the analysis.

In the previous section, problems were noted with Vulcan's ability to recognize yield at ambient temperatures. In order to analyze the effects of yield strength on a member under non constant temperature loading, a 6 m long W18x71 configured as a propped cantilever was analyzed. A constant load of 40 kN was applied in the center of the beam and the temperature was applied as shown in Figure 5.11. Under identical loading and support conditions, the yield strength was adjusted from 275.8 -244.7 MPa (40-50 ksi). The results of this analysis are contained in Figure 5.12.

At a yield stress of 275.8 MPa (40 ksi) the beam yields as the temperature increases. There is residual deflection as the member is returned to ambient temperature as shown in Figure 5.12. At yield stresses of 310.3 and 344.7 MPa (45 and 50 ksi), the beam does not yield and regains all of the deflection. As expected, higher yield stresses produce a smaller deflection as the temperature increases.

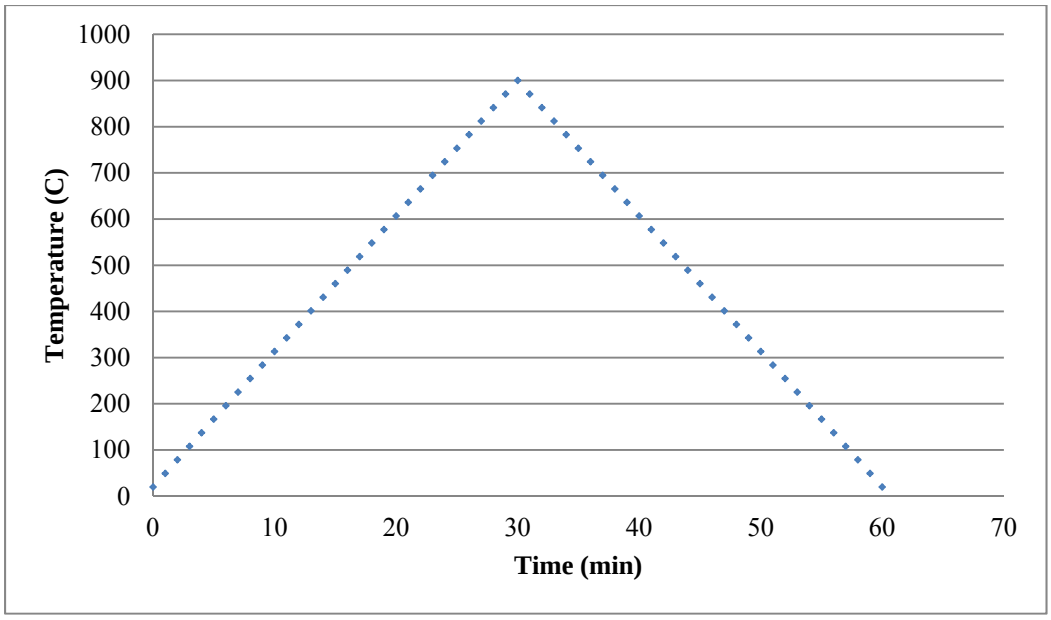

Figure 5.10: Time Temperature Curve

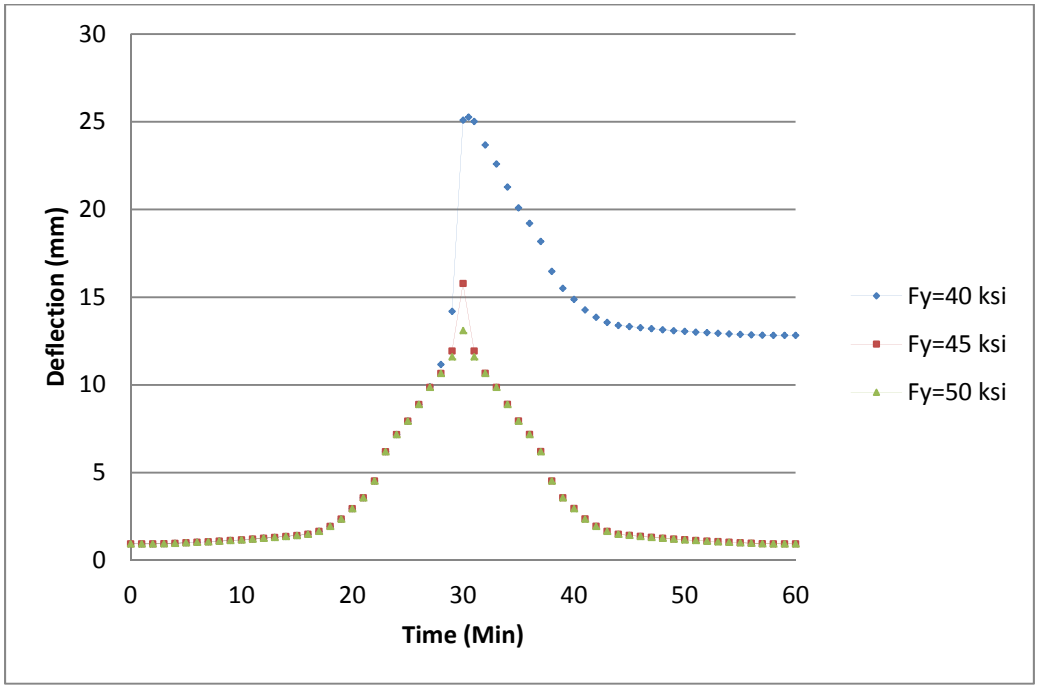

Figure 5.11: Time vs. Deflection

5.4 Conclusion

Vulcan has shown weaknesses in correctly predicting yield deflections at ambient temperatures as well as unexplained inaccuracies handling fixed end beams. However, these weaknesses, while troubling, are not considered sufficient to invalidate the usefulness in the comparisons made in this dissertation.

Vulcan has shown the capability of predicting the behavior and deflection of members under elevated temperatures to a reasonable degree of accuracy. It is important to note that the primary focus of this dissertation is the reproduction of patterns within the structure, not necessarily the exact replica of the deflections obtained in the field tests. Thus, Vulcan was deemed capable of performing the analysis required in this dissertation.

CHAPTER 6 - FINITE ELEMENT MODELING

Once the scale tests discussed in Chapter 4 were completed, a series of finite element model (FEM) runs were made to show that a relatively simple FEM program was able to reproduce deflection patterns reasonably close to those observed in the field. The ability to reproduce these patterns in a model was pivotal to the validation of the use of structural deformations as an indicator of fire origin. Test results from TB-2 were utilized for this analysis as it was the only test burn in which all temperature and deformation data were retained.

6.1 Input Properties

6.1.1 Steel Properties

The structural members of the test building were constructed of ASTM A563 hot dipped galvanized steel. All steel was purchased as sheets and broken into a series of non-standard channel sections. The truss members had a thickness of 0.84 mm (0.033") and all bracing and other support members had a thickness of 0.53 mm (0.021"). According to the company that manufactures the buildings, the steel was purchased from US Steel and was specified as CS Type B, non-chemical treated, minimum spangle (Coated Sheet, 2012).

The properties of the steel were varied as a function of temperature using the Ramberg-Osgood methodology (discussed in Chapter 2) which is programmed into Vulcan as part of the software package. A starting F_y of 331 MPa (48 ksi) was utilized as input for the model. Ultimate strength was not required as input into the model.

Certain values were kept constant throughout the temperature range. While the density of steel does vary slightly with temperature, the change is, for the most part, negligible and was

assumed to remain constant at 7850 kg/m^3 (490 lb/ft^3). Poisson's ratio was also shown to remain essentially constant with temperature and was taken as 0.3.

6.1.2 Frame Properties and Connections

The building itself was composed of three frame elements incorporated into multiple places in the structure; hence, three separate frame sections were utilized for the analysis. Measurements for these members were taken from the actual constructed building and constructed as a general cross section within Vulcan. The locations of the members within the model can be seen in Figure 6.1. Truss members are displayed as green, upper support members are shown in yellow, and other support members are shown in blue. As discussed in previous sections, the building is composed of a number of repeating truss shapes that are tied together using various supports, similar to full size portal frame structures.

Connections proved more difficult to model. The bases on the columns were treated as pins. While there is some fixity associated with this type of connection, it is not designed to be a moment connection and was treated as a pin. The truss connections (See Figure 6.2), specifically the mid-truss connections, were designed to be moment bearing connections. At room temperature, they would function and be modeled as such. However, when modeled at an elevated temperature, these connections are expected to behave much more like pins as opposed to fixed connections. This behavior is due to the fact that the gusset plates are merely flat sheet metal connected to the trusses with 6 mm (¼ inch) sheet metal screws through pre-drilled, oversized holes in the truss members. When heated, it would be expected that this connection would lose a large amount of its rigidity. The front and back walls were integrated as shear

walls, even though this is likely an overestimate of their actual structural integrity, even under normal temperatures.

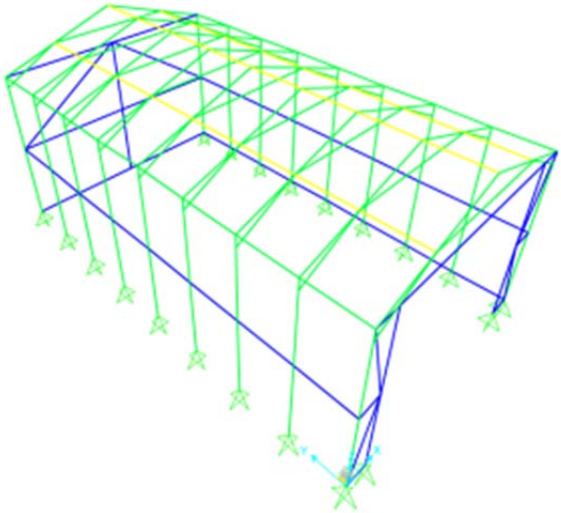

Figure 6.1: Locations of specific frame elements

Figure 6.2: Truss Connections

The skin of the building was not included in the model. This decision was made for a couple of reasons. The building was completely constructed, squared, and anchored to the concrete pad prior to installing the skin. There seemed to be little additional strength or rigidity added when the skin of the building was installed. This decision was reinforced by the connection method of the skin to the building's frame. Sheet metal screws (appx. 0.6 mm long) were placed through holes in the skin that were nearly the size of the head of the screw attaching to predrilled holes in the building's frame. The holes were oversized to make installation by novice assemblers easier, but this installation would allow a significant amount of movement in the structure prior to the skin offering any additional rigidity to the structure.

6.1.3 Loads

Loads placed on the building consisted of self-weight and loads from the concrete masonry units (CMU) placed on the roof. Wind conditions did not warrant the inclusion of any loads reflecting ambient conditions. Self-weight proved fairly inconsequential to the structure as the entire building (including the skin) weighed approximately 350 kg (772 lbs). Loads from the added roof weight (CMU's) were input into the model as point loads on the trusses in the same positions as in the actual building (see Figure 6.3). Point loads placed on the trusses constituted a realistic model as the CMU's were placed directly on the trusses in the research burns.

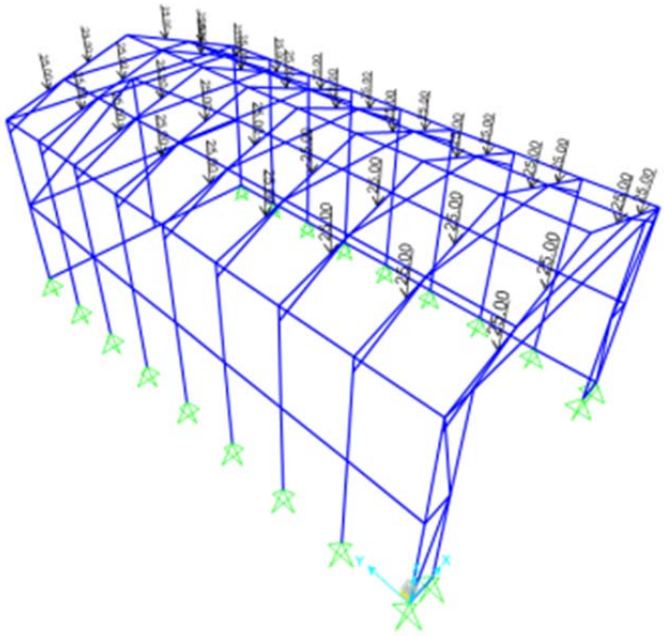

Figure 6.3: Modeled loads

6.1.4 Temperatures

Temperature input was obtained from field measurements via Type K thermocouples as discussed in Section 4.2.2 of this dissertation. The actual time temperature curves recorded in the fire were used as input into Vulcan. The only concern regarding accuracy of input is the distribution of temperatures in the vertical direction as temperature data were only collected at roof level. In order to account for this concern regarding temperature distribution, several different approximations were attempted based upon the readings of the thermocouple tree in the center of the structure. It turned out that the exact percentage of the weightings did not appear to affect the end result as the loads on the columns were relatively small. Nevertheless, the time temperature curves were scaled using the following criteria:

- Floor level to 0.3 m = 40% measured temperature
- 0.3 m to 0.6 m = 60% measured temperature
- 0.9 m to 1.2 m = 80% measured temperature
- 1.5 m to 1.8 m = 90% measured temperature
- Above 1.8 m = 100% measured temperature

A sample time temperature curve along with its scaling is shown in Figure 6.4.

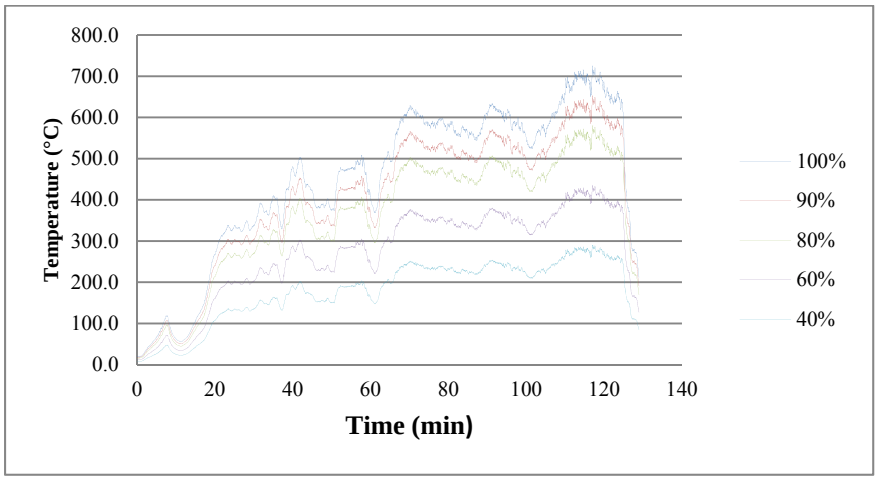

Figure 6.4: Sample Time Temperature Curve with Scaling

6.2 Model Output

The result of primary interest in the analysis of this model was the pattern of structural deformations and their relationship to the observed deformations. Figure 6.5 shows the deflected shape of the model. Model outputs were obtained for each truss at the hip, peak, and in the middle of the truss (the same locations measurements were taken in the field).

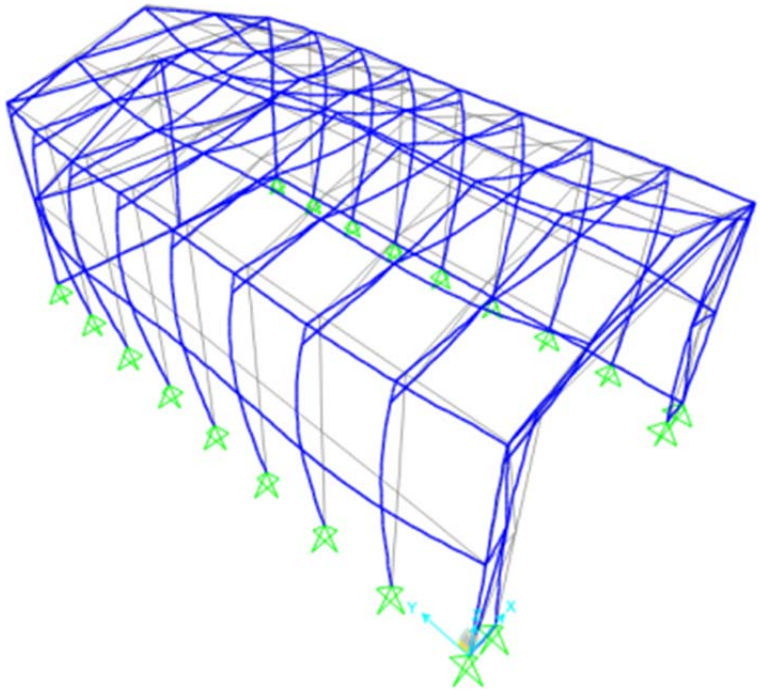

Figure 6.5: Deformed Shape

To show the behavior of the structure throughout the fire, Figures 6.6 through 6.9 provide plots of the time vs. deflection curves at the center of each of the quadrants. To aid in interpretation, the time-temperature curves have also been imposed on the plots. There is no comparison to these plots as measurements were only taken at the beginning and end of the experimental burns.

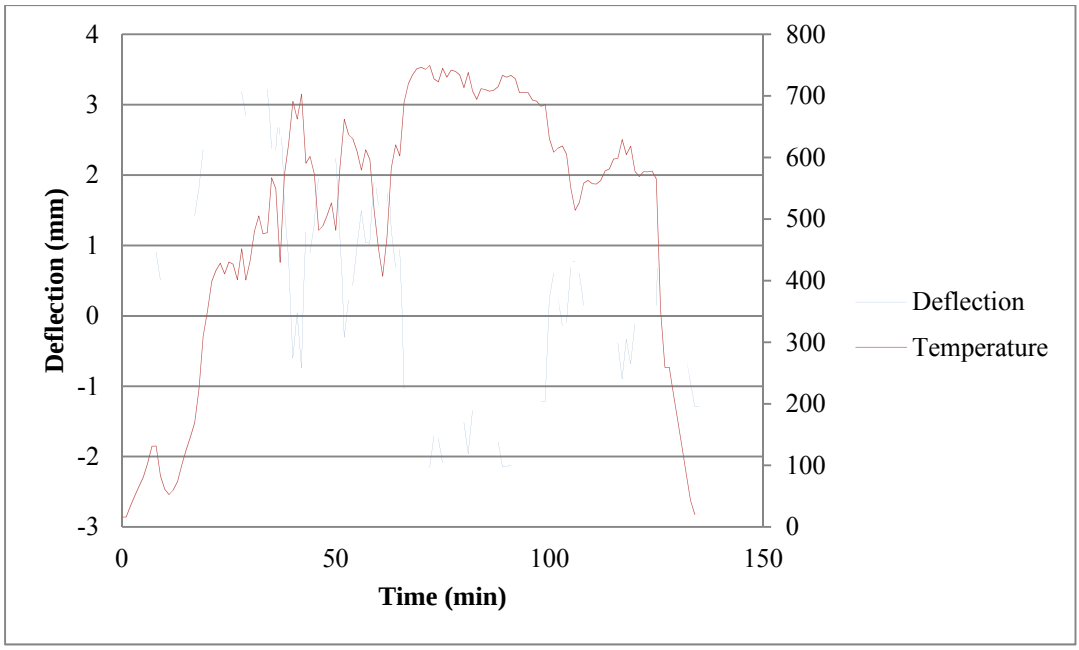

Figure 6.6: Southeast Quadrant Time vs. Deflection

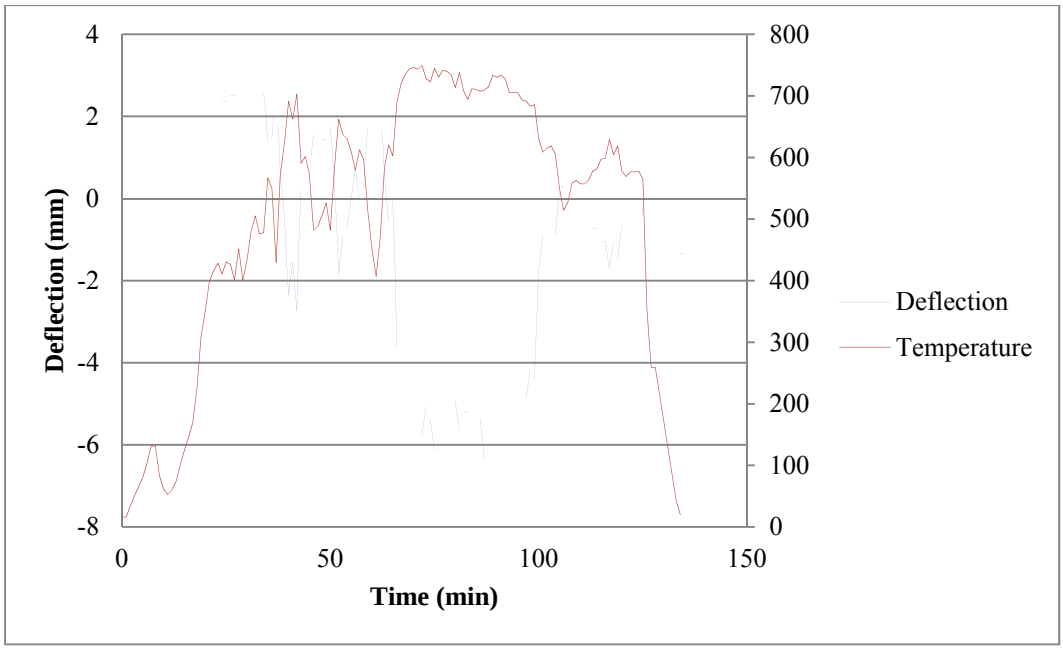

Figure 6.7: Southwest Quadrant Time vs. Deflection

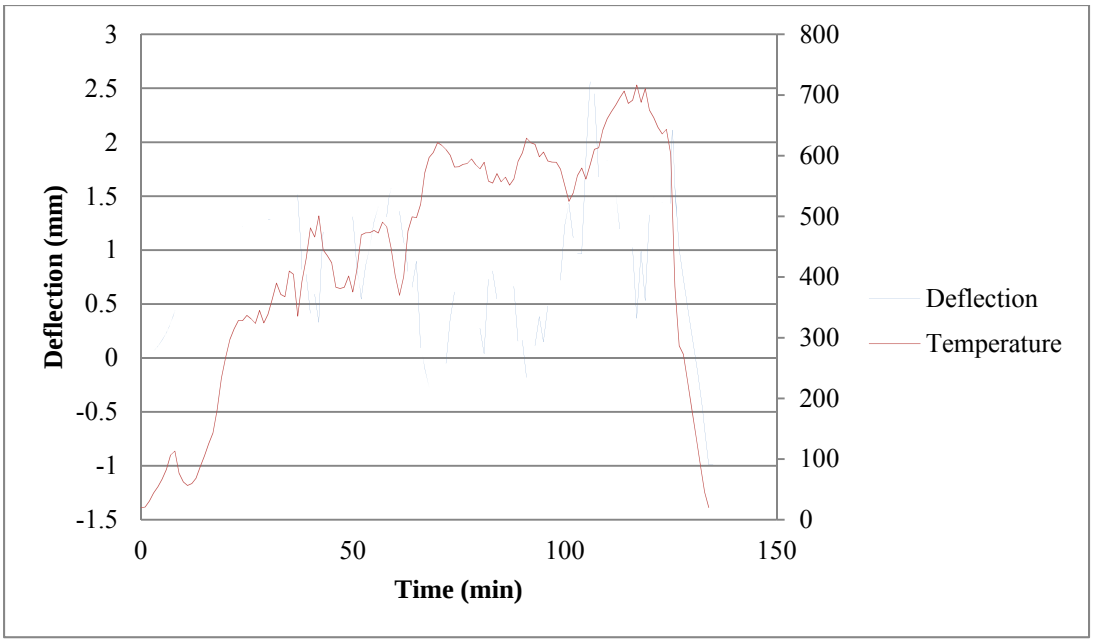

Figure 6.8: Northeast Quadrant Time vs. Deflection

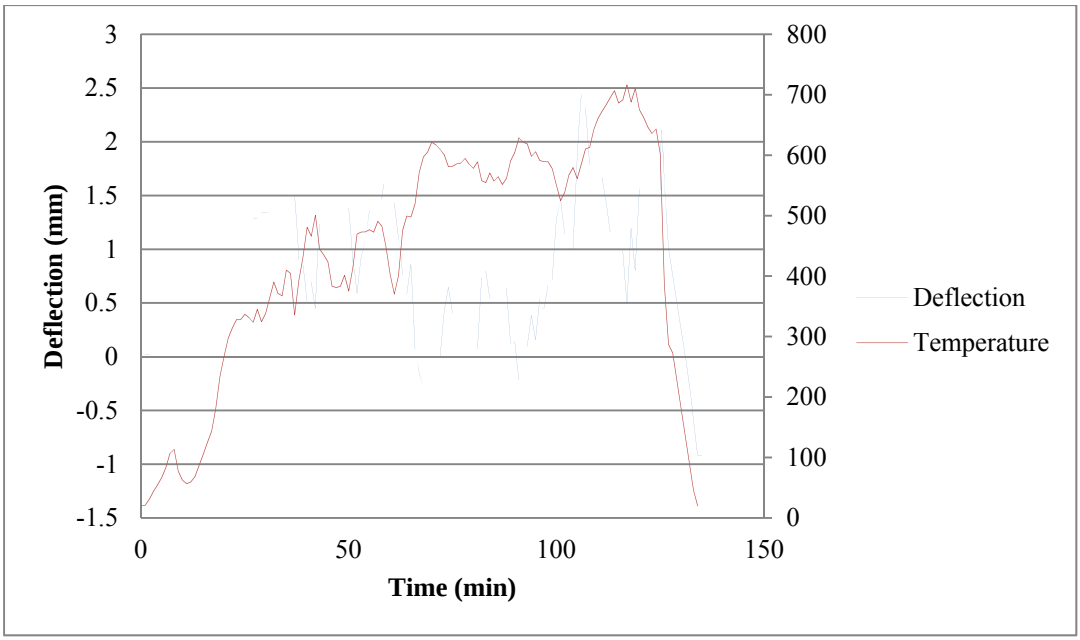

Figure 6.9: Northwest Quadrant Time vs. Deflection

6.3 Comparison of Model Output to Field Observations

Table 6.1 contains a comparison of the actual deflections at various locations (note that all values are after the building has returned to ambient temperatures). In Tables 6.1-6.3, the x and y coordinates are based on the same x-y coordinate system as Figures 6.10-6.12. Coordinate (0, 0) represents the northeast corner of the building.

Table 6.2 is a reproduction of Table 6.1 eliminating all measured deflections less than 1 mm to aid the reader in their comparison. Overall, the deflections over 1 mm tended to be much more accurate with most points having a percent error of plus or minus 40%.

For comparison purposes, Table 6.3 includes raw data without the normalization process applied (described later). Vulcan showed a tendency to under predict the observed deflections away from the edges of the building. The source of this error is discussed further in Section 6.4.

Table 6.1: Measured vs. modeled deformations[#]

X (m)	Y (m)	Measured (mm)	Normalized Measured	Modeled (mm)	Normalized Modeled	Normalized Percent Error	Corrected Percent Error
0	5.1816	0.051	0.008	0.062	0.038	-396%*	0%
0	4.5339	0.533	0.081	0.243	0.151	-85%*	0%
0	3.8862	0.406	0.062	0.516	0.320	-416%*	0%
0	3.2385	0.660	0.101	0.597	0.371	-268%*	0%
0	2.5908	0.787	0.120	0.486	0.302	-151%*	0%
0	1.9431	0.914	0.140	0.328	0.204	-46%*	0%
0	1.2954	0.762	0.116	0.202	0.125	-8%*	0%
0	0.6477	0.610	0.093	0.131	0.081	13%*	0%
0	0	0.457	0.070	0.022	0.014	80%*	0%
0.762	5.1816	3.200	0.488	0.249	0.155	68%*	0%
0.762	4.5339	4.521	0.690	1.025	0.636	8%	8%
0.762	3.8862	5.359	0.818	0.838	0.520	36%	36%
0.762	3.2385	5.232	0.798	0.332	0.206	74%	74%
0.762	2.5908	4.572	0.698	-0.157	-0.097	114%	114%
0.762	1.9431	4.699	0.717	0.084	0.052	93%	93%
0.762	1.2954	5.309	0.810	1.004	0.623	23%	23%
0.762	0.6477	3.607	0.550	0.483	0.300	46%	46%
0.762	0	2.362	0.360	0.304	0.189	48%*	0%
1.524	5.1816	3.238	0.494	1.407	0.873	-77%*	0%
1.524	4.5339	4.623	0.705	1.611	1.000	-42%	-42%
1.524	3.8862	5.156	0.787	1.107	0.687	13%	13%
1.524	3.2385	4.394	0.671	0.489	0.304	55%	55%
1.524	2.5908	3.975	0.607	0.409	0.254	58%	58%
1.524	1.9431	3.772	0.576	0.478	0.297	48%	48%

Table 6.1 (Con't): Measured vs. modeled deformations[#]

X (m)	Y (m)	Measured (mm)	Normalized Measured	Modeled (mm)	Normalized Modeled	Normalized Percent Error	Corrected Percent Error
1.524	1.2954	4.089	0.624	1.489	0.924	-48%	-48%
1.524	0.6477	3.391	0.517	0.997	0.619	-20%	-20%
1.524	0	1.803	0.275	0.101	0.063	77%*	0%
2.286	5.1816	1.727	0.264	0.678	0.421	-60%*	0%
2.286	4.5339	6.198	0.946	1.092	0.678	28%	28%
2.286	3.8862	6.553	1.000	1.345	0.835	17%	17%
2.286	3.2385	5.690	0.868	1.409	0.875	-1%	-1%
2.286	2.5908	4.267	0.651	1.298	0.806	-24%	-24%
2.286	1.9431	4.140	0.632	1.170	0.726	-15%	-15%
2.286	1.2954	3.861	0.589	0.934	0.580	2%	2%
2.286	0.6477	3.556	0.543	0.451	0.280	48%	48%
2.286	0	2.540	0.388	0.301	0.187	52%*	0%
3.048	5.1816	0.279	0.043	0.154	0.096	-124%*	0%
3.048	4.5339	0.610	0.093	0.256	0.159	-71%*	0%
3.048	3.8862	0.381	0.058	0.423	0.263	-352%*	0%
3.048	3.2385	0.508	0.078	0.463	0.287	-271%*	0%
3.048	2.5908	0.254	0.039	0.406	0.252	-550%*	0%
3.048	1.9431	0.559	0.085	0.334	0.207	-143%*	0%
3.048	1.2954	0.508	0.078	0.232	0.144	-86%*	0%
3.048	0.6477	0.051	0.008	0.074	0.046	-493%*	0%
3.048	0	0.051	0.008	0.035	0.022	-180%*	0%

*indicates measurement is on edge of structure.

[#] Measurements are reported to three decimal places. This should not be taken as an indication of accuracy. Measurements were taken at the levels indicated in Chapter 4.

Table 6.2: Measured vs. Modeled Deformations (Measurements less than 1 mm removed)[#]

X (m)	Y (m)	Measured (mm)	Normalized Measured	Modeled (mm)	Normalized Modeled	Normalized Percent Error
0.762	5.1816	3.200	0.488	0.249	0.155	68%*
0.762	4.5339	4.521	0.690	1.025	0.636	8%
0.762	3.8862	5.359	0.818	0.838	0.520	36%
0.762	3.2385	5.232	0.798	0.332	0.206	74%
0.762	2.5908	4.572	0.698	-0.157	-0.097	114%
0.762	1.9431	4.699	0.717	0.084	0.052	93%
0.762	1.2954	5.309	0.810	1.004	0.623	23%
0.762	0.6477	3.607	0.550	0.483	0.300	46%
0.762	0	2.362	0.360	0.304	0.189	48%*
1.524	5.1816	3.238	0.494	1.407	0.873	-77%*
1.524	4.5339	4.623	0.705	1.611	1.000	-42%
1.524	3.8862	5.156	0.787	1.107	0.687	13%
1.524	3.2385	4.394	0.671	0.489	0.304	55%
1.524	2.5908	3.975	0.607	0.409	0.254	58%
1.524	1.9431	3.772	0.576	0.478	0.297	48%
1.524	1.2954	4.089	0.624	1.489	0.924	-48%
1.524	0.6477	3.391	0.517	0.997	0.619	-20%
1.524	0	1.803	0.275	0.101	0.063	77%*
2.286	5.1816	1.727	0.264	0.678	0.421	-60%*
2.286	4.5339	6.198	0.946	1.092	0.678	28%
2.286	3.8862	6.553	1.000	1.345	0.835	17%
2.286	3.2385	5.690	0.868	1.409	0.875	-1%

Table 6.2 (Con't): Measured vs. Modeled Deformations (Measurements less than 1 mm removed)[#]

X (m)	Y (m)	Measured (mm)	Normalized Measured	Modeled (mm)	Normalized Modeled	Normalized Percent Error
2.286	2.5908	4.267	0.651	1.298	0.806	-24%
2.286	1.9431	4.140	0.632	1.170	0.726	-15%
2.286	1.2954	3.861	0.589	0.934	0.580	2%
2.286	0.6477	3.556	0.543	0.451	0.280	48%
2.286	0	2.540	0.388	0.301	0.187	52%*

*Indicates measurement on edge of structure.

[#] Measurements are reported to three decimal places. This should not be taken as an indication of accuracy. Measurements were taken at the levels indicated in Chapter 4.

Table 6.3: Raw Data Comparisons[#]

X (m)	Y (m)	Measured (mm)	Modeled (mm)	Percent Error
0	5.1816	0.0508	0.062	-22%*
0	4.5339	0.5334	0.243	54%*
0	3.8862	0.4064	0.516	-27%*
0	3.2385	0.6604	0.597	10%*
0	2.5908	0.7874	0.486	38%*
0	1.9431	0.9144	0.328	64%*
0	1.2954	0.762	0.202	73%*
0	0.6477	0.6096	0.131	79%*
0	0	0.4572	0.022	95%*
0.762	5.1816	3.2004	0.249	92%*
0.762	4.5339	4.5212	1.025	77%
0.762	3.8862	5.3594	0.838	84%
0.762	3.2385	5.2324	0.332	94%
0.762	2.5908	4.572	-0.157	103%
0.762	1.9431	4.699	0.084	98%
0.762	1.2954	5.3086	1.004	81%
0.762	0.6477	3.6068	0.483	87%
0.762	0	2.3622	0.304	87%*
1.524	5.1816	3.2385	1.407	57%*
1.524	4.5339	4.6228	1.611	65%
1.524	3.8862	5.1562	1.107	79%
1.524	3.2385	4.3942	0.489	89%
1.524	2.5908	3.9751	0.409	90%
1.524	1.9431	3.7719	0.478	87%

Table 6.3 (Con't): Raw Data Comparisons[#]

X (m)	Y (m)	Measured (mm)	Modeled (mm)	Percent Error
1.524	1.2954	4.0894	1.489	64%
1.524	0.6477	3.3909	0.997	71%
1.524	0	1.8034	0.101	94%*
2.286	5.1816	1.7272	0.678	61%*
2.286	4.5339	6.1976	1.092	82%
2.286	3.8862	6.5532	1.345	79%
2.286	3.2385	5.6896	1.409	75%
2.286	2.5908	4.2672	1.298	70%
2.286	1.9431	4.1402	1.17	72%
2.286	1.2954	3.8608	0.934	76%
2.286	0.6477	3.556	0.451	87%
2.286	0	2.54	0.301	88%*
3.048	5.1816	0.2794	0.154	45%*
3.048	4.5339	0.6096	0.256	58%*
3.048	3.8862	0.381	0.423	-11%*
3.048	3.2385	0.508	0.463	9%*
3.048	2.5908	0.254	0.406	-60%*
3.048	1.9431	0.5588	0.334	40%*
3.048	1.2954	0.508	0.232	54%*
3.048	0.6477	0.0508	0.074	-46%*
3.048	0	0.0508	0.035	31%*

*Indicates measurement on edge of structure.

[#] Measurements are reported to three decimal places. This should not be taken as an indication of accuracy. Measurements were taken at the levels indicated in Chapter 4.

Figure 6.10 shows a contour plot of the measured deformations after the building returned to ambient temperature. Figure 6.11 contains contour plots of the same description but utilizes the modeled deflections, again, after the building returned to ambient temperature. The pattern of deflections is generally similar through visual comparison. The deformations appear to be of greatest magnitude in the SE corner of the structure in the model just as they were in the research burn. The actual location of the fire and the location of the greatest deflections are discussed at length in Chapter 4, and the same reasoning is still relevant (See Section 4.6).

As can be seen from Table 6.1, the edges contain much more error than the rest of the building. Note that an edge measurement is considered any measurement taken directly on the edge of the building. This error around the edges is due to the relatively small amount of deflection measured on the edges of the experimental building. The maximum deflection measured along the edge of the building was typically less than 1 mm, so a small difference in the modeled and measured values produces a large percent error value.

Figure 6.12 is a contour plot of the percent difference between the normalized measured vs. normalized modeled deflections (with corrections as discussed in the next paragraph). The rest of the model shows acceptable agreement with the measured values. Normalization is the statistical process of adjusting values to a common scale to allow better comparison. To normalize the deflection values, the largest deflection in the model is found. All deflections are divided by the largest deflection in order to obtain a valid comparison of where the large/small deflections fall in relation to each other. Normalized values are used for the comparison as the desired accuracy is largely focused on the pattern of deflection as opposed to the actual values.

As previously discussed, the percent error near the edges is abnormally large. For purposes of Figure 6.12, the edges have been treated as outliers and the percent difference was

set to 0 for any edge measurement. Eliminating these large percent error values allows the relative accuracy of the rest of the model to be shown. For the areas of the building where "significant" deflections occurred during the experiment, the percent error is generally within plus or minus 20%. The areas where the model seems to have difficulty predicting the deflections are in areas where the measured deflections were relatively small.

Also of interesting note is the general variability of the analysis. While an analysis of the variance of the measured and modeled deflections is not a comparison of the differences in specific points, it does offer a view into the disparity of measurements as a whole. The experimental data has a variance of 0.098 and the modeled data has a variance of 0.085. The relatively similar variances show that the spread within the data is similar in nature.

The distribution of deflections leads to a conclusion that an analysis based on the model results can be taken as a reasonably accurate representation of the field observations of the distribution of the deflections. Final conclusions are outlined further in Chapter 8.

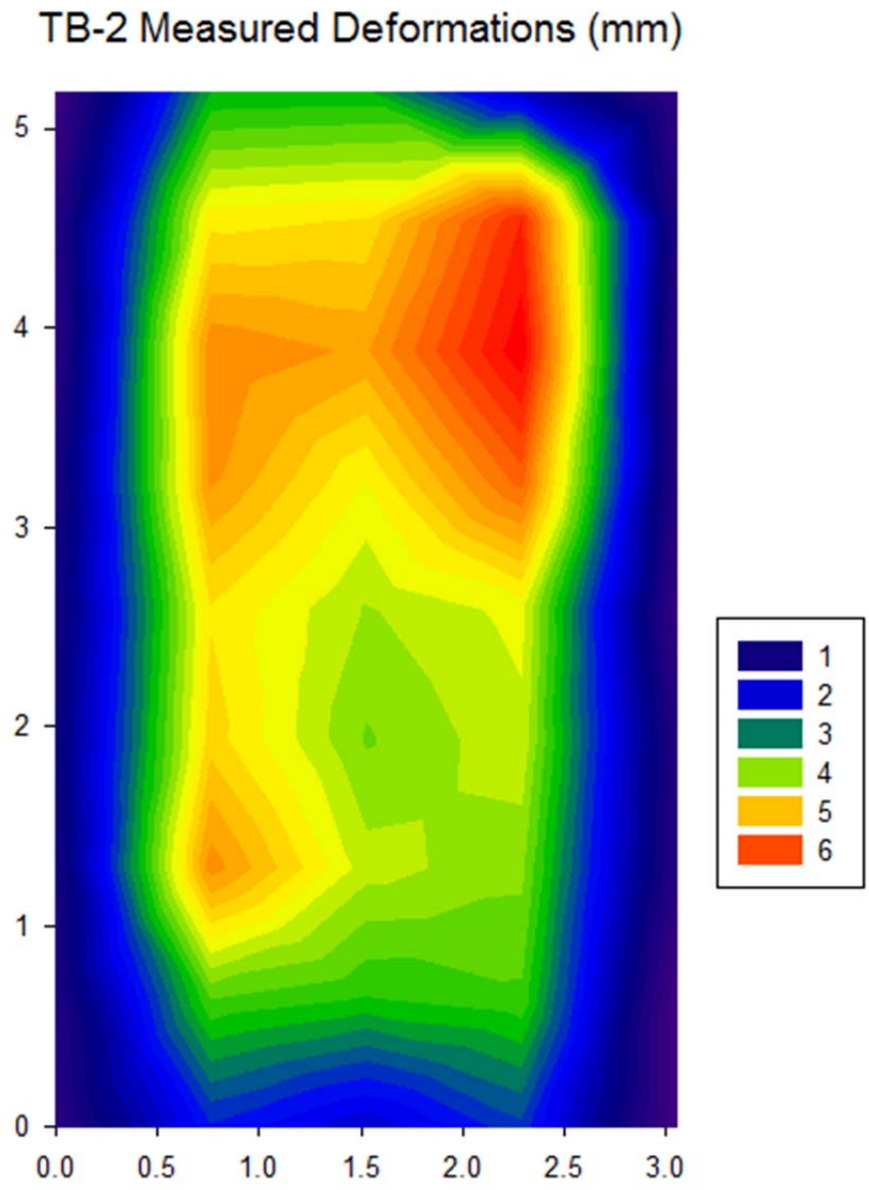

Figure 6.10: Measured Deformations

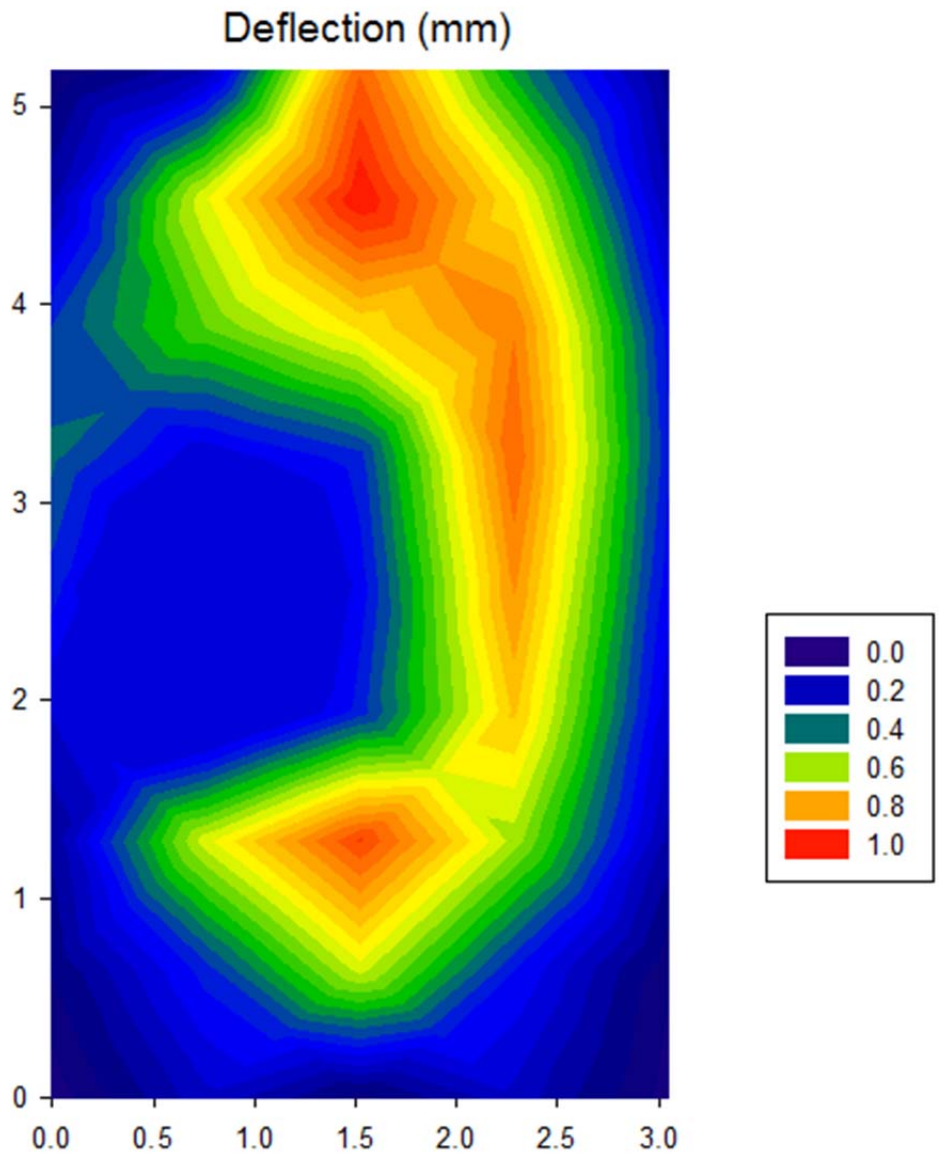

Figure 6.11: Modeled Deflections

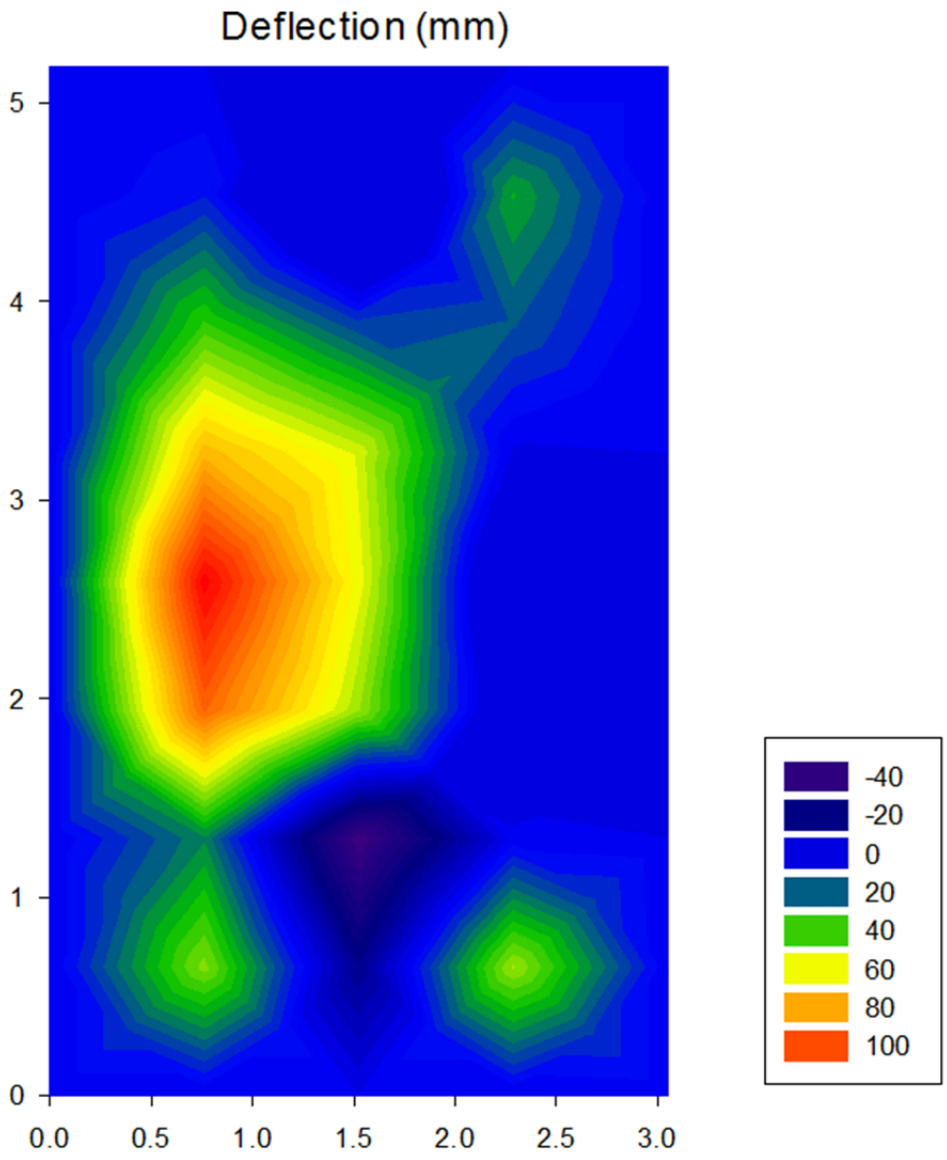

Figure 6.12: TB-2 Corrected Percent Difference (Measured vs. Modeled)

6.4 Sensitivity Analysis

As shown in the previous sections, there is noticeable error present within the predicted (modeled) structural deformations. This introduces somewhat of a limitation to the analysis since modeling efforts were unable to reproduce structural deformations to a confident level. Again, as previously discussed, the analysis will focus on the pattern of deformations present.

To ensure that a reasonable replication of the model is given, it is necessary to perform a limited sensitivity analysis. The truss system of the structure in question is close to being statically determinate. Upon yielding, a statically determinate structure will become a mechanism and fail. A number of variables can affect a structure's possibility and magnitude of yielding including applied load, yield stress, and temperature effects. Temperature effects are known on this structure as they were measured as part of the experimental process. Applied load and yield stress, while affecting different parts of the yielding criteria, essentially have the same effect. Unfortunately, no coupon testing was performed on the material used to construct the structure, so these properties are unknown. However, to analyze these effects and to show that the predicted deformations are within the realm of possibility, the loads can be adjusted on the building. A decreased load can reflect the possibility that the yield stress was underestimated while an increased load will reflect the possibility that the yield stress was overestimated.

The purpose of this analysis is to investigate whether or not Vulcan can predict behavior that appears to reflect behavior consistent with the various introduced changes.

Figure 6.13 shows a contour plot of the model with no applied load beyond the self-weight of the structure. Temperature loading is consistent with the actual model discussed in Section 6.4. As seen in the figure, the deflections are minimal with the maximum being around

0.4 mm at the end of the fire. As expected, these deflections are significantly smaller than those reported in the model loaded to reflect experimental conditions. The deflections are also relatively evenly spread throughout the structure as opposed to concentrated in certain areas. This lack of concentration can be attributed to the overall lack of yielding in the building. While yielding did occur as there are residual deflections, overall, the amount of yielding was so small as to be virtually immeasurable. The "higher" deflections tend to be skewed toward the rear of the building, as expected due to the point of origin of the fire. It is almost symmetrical about the vertical axis. This symmetry occurs because the loads applied were virtually nothing (only self weight) and that there were not any substantial forces to increase the yieilding. The same lack of measurable deflection was observed in the PB-1 and PB-2 tests discussed in Chapter 4. Since this pattern matches the general observations in the field, it is considered an accurate representation of the structural behavior.

Figure 6.14 is a contour plot of the applied load doubled with any dead load deflections removed. The maximum deflections are approximately four times the maximum deflection in the actual model, indicating non-linearity. While a purely linear relationship was not expected, these results indicate that Vulcan is taking into account the additional loads as well as accounting for additional yielding. Doubling the load does not result in the localized deflections seen in Figure 6.11. This changed pattern is reasonable as much more of the building would be loaded to the point of yielding when doubled load is applied, and the building is subjected to the same temperature increase.

Overall, this analysis indicates that the presented results are at least calculated within reasonable bounds of certainty. The pattern of computed and modeled deflections is consistent with visual observations during the testing process. While there continues to be a number of

unknowns associated with the analysis, this sensitivity testing has shown that Vulcan is able to account for additional loading to the structure and to produce reasonable results within the model as reported in Section 6.2.

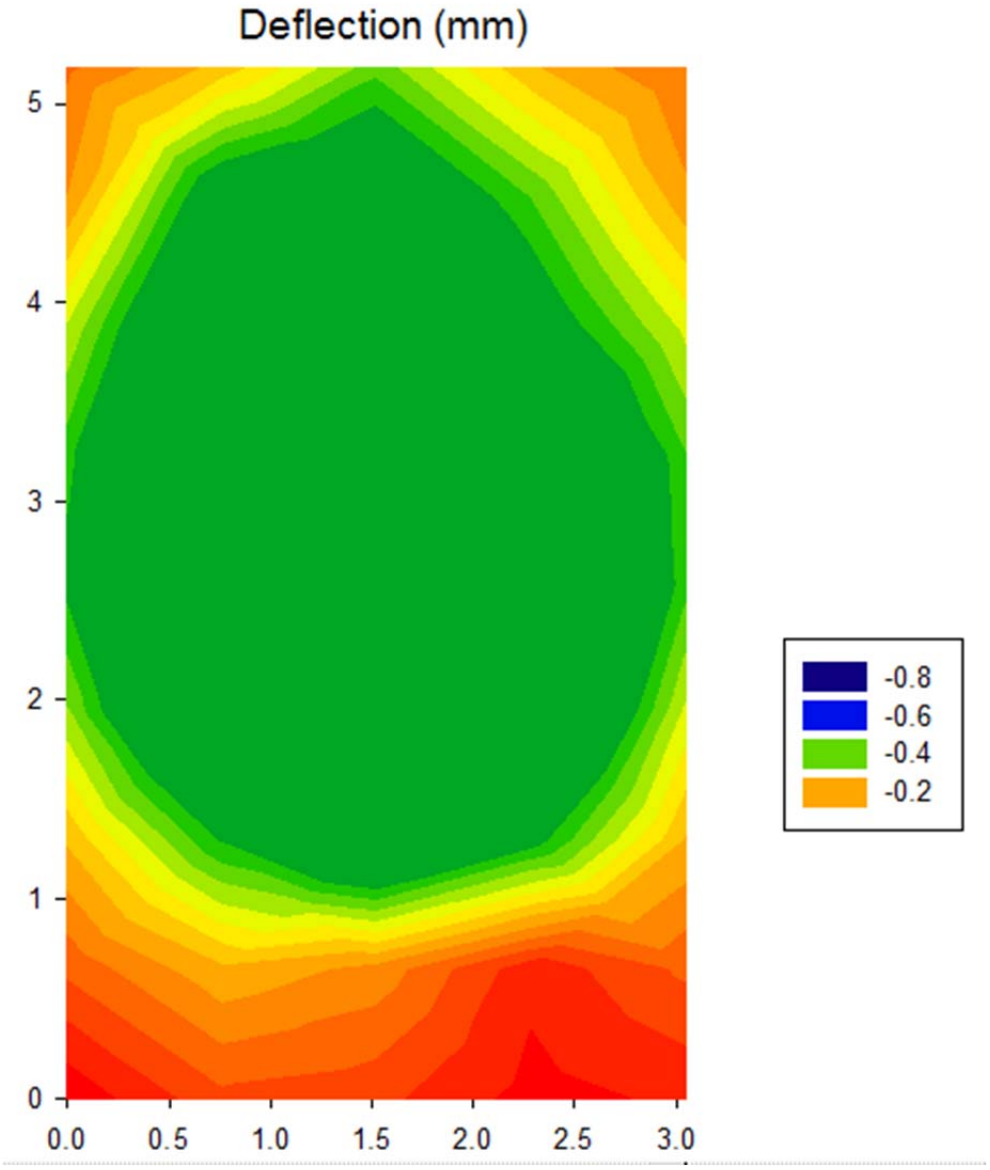

Figure 6.13: Deflections. No Applied Load.

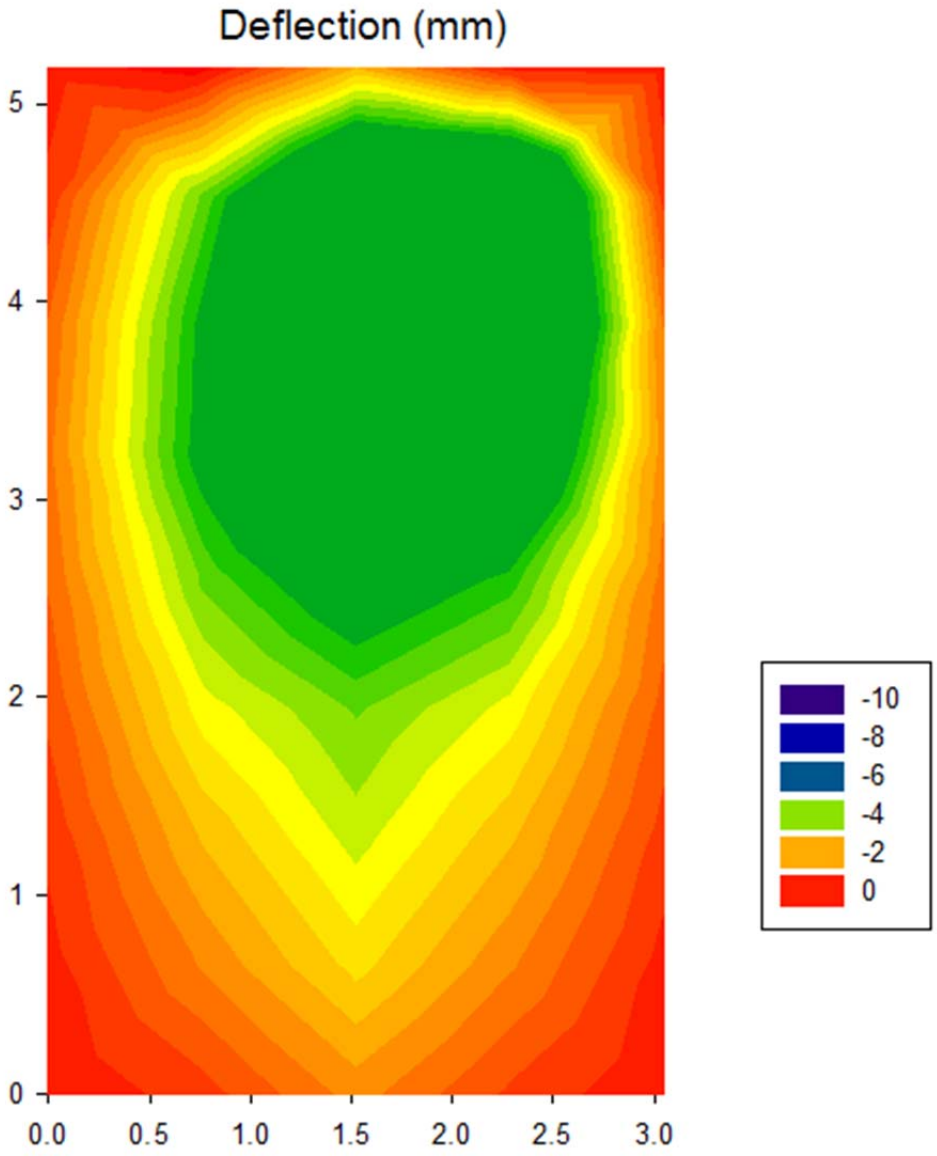

Figure 6.14: Deflections. Double applied load.

CHAPTER 7 – METHODOLOGY FOR USE OF STRUCTURAL DEFORMATIONS AS AN INDICATOR OF FIRE ORIGIN

As with any investigative methodology, for it to be useful an in-depth guide to its particular use and its limitations is necessary. This chapter of the dissertation is meant to serve as a guide to the forensic investigator in the use of structural deformations as an indicator of fire origin. This author views two distinct methods of using structural deformation data in regard to origin determination in a post fire setting.

7.1 Visual Observations

The first, and simplest, use of structural deformations is by observation. As discussed in Chapter 2 of this dissertation, many of the current fire effects noted by fire investigators consist of visual data and the recognition of contrasts in their intensity as a primary tool in investigation. This same methodology can be applied while incorporating structural deformations. It is widely recognized, and already noted in NFPA 921, that structural deformations will have a tendency to be of the greatest magnitude where the fire was the most intense. The fact that most current writing has failed to point out is the complexity of most structural systems and the inter-connection between several members (load redistribution). As noted several times previously, it is entirely possible (due to ventilation and room geometry) that the fire is not the most intense at the area of origin. Trained investigators are taught to recognize these effects with their observations of other patterns, and this training can certainly be applied to the use of structural deformations.

That being said, the complexities of structural behavior require personnel who are knowledgeable in structural design and mechanics as well as the fire behavior. The behavior of

the fire and the behavior of the structure are so intermingled in a post-scene analysis, that anyone performing this sort of analysis "on the fly" should be able to demonstrate his/her competence in both areas of the investigation.

As with any other investigative methodology, these data should not be relied upon as the sole source of information. Fire leaves a multitude of distinctive indicators that can lead an investigator to the area of origin. NFPA 921 and the scientific method dictate that all sources of information must be utilized and integrated for a valid hypothesis to be determined. Nothing in this dissertation is advocating the separation of data sources or the non-inclusion of multiple data sources.

7.2 Use of Structural Deformations as a Benchmark for Validation of Forensic Fire Models

One of the main purposes in performing the research for this dissertation was to utilize measured structural deformations from a post-fire analysis to act as a validation tool for computer fire models. Fire modeling encompasses a wide range of mathematical modeling techniques, typically grouped by their level of precision, used to predict the conditions at certain areas or points within a fire compartment. Fire models can take forms ranging from closed form hand calculations to sophisticated, computer-based fluid dynamics simulators. Depending on the type of computer fire model, outputs can include the temperatures, gas concentrations, and flow velocities throughout the compartment. The validity of computer fire modeling has been extensively researched and reported in a variety of publications (NIST, 2010; Rein, Empis, & Carvel, 2007) and is not discussed at length in this dissertation. It has been noted that the validated methodology currently used in computer fire modeling provides a range of outputs

based on a range of reasonable inputs, especially for the variables that are not specifically known (Society of Fire Protection Engineers, 2008).

Computer fire models, as discussed in this dissertation, are fluid dynamics simulators utilized to solve hundreds of simultaneous equations mainly focused on the energy balance within a cell (see Figure 3.3). The most commonly utilized fire modeling code was developed by the National Institute of Standards and Technology (NIST) and is referred to as FDS (Fluid Dynamics Simulator). Extensive detail on this computer fire modeling code can be found in the technical reference manual published by NIST (2010). For the purposes of this discussion, FDS behaves similarly to a finite element program in that a fire compartment is meshed into cells for which a number of energy balancing equations are solved at specified time steps. The output from FDS can vary based on the way the model is set up, but most fundamental to this research is its ability to predict temperatures at specific points within the fire compartment.

As with any simulation model, there must be some true benchmarks in order to ensure the model's validity. In most cases, fire models are designed to match internal damage to the structure, timelines constructed through witness statements, and the expected behavior of the fire using more rudimentary calculations. Given the appropriate data, it will be possible to utilize structural deformations of the building's load bearing system as another indicator. This ability to analyze deformations becomes significant as it is certainly within the realm of possibility that a fire progresses to the point of not leaving distinguishable fire patterns (significant post-flashover burning) and few witness statements are available to corroborate a model. Even with the availability of witness statements, they have been noted as estimates at best (NFPA, 2011). In these cases, a modeling endeavor becomes a battle of the expert witnesses with little to no ability to determine who is correct.

The best aspect of using structural modeling to validate a fire model is that the structural deformations will typically remain (to a large extent) after the fire has been extinguished (unless the building has been entirely demolished by the fire and extinguishing efforts). Given the previous comments, it should be apparent that that the use of another tool to validate a forensic fire model will be a welcome addition to the fire investigation process.

In order to utilize structural deformations to assist in the validation of a fire model, certain data must be collected at the time of the scene investigation. This data collection has to be comprehensive, as all information to create both a fire model and a structural model must be collected. Much of these data are not typically included as part of a fire investigator's post-scene analysis, so the decision to use this method must be made early on in the investigation process. The following data will be required to complete the fire model and structural analysis.

- All typical data relevant to fire modeling performance (See NFPA 921 for further discussion of the requirements). The required data will include, at a minimum, building geometry, ventilation openings (both geometric size and location), fuel load, and ambient temperature conditions.
- An elevation survey of (at a minimum) the roof of the structure. The survey should be performed in such a way that an adequate representation of the contour of the roof can be produced. Depending on the size of the building in question, 2 m (6.6 ft) intervals should suffice.
- As-built construction documents for the building in question. Construction documents are a necessity for an accurate portrayal in the structural modeling process. If these documents are not available, in-depth documentation of the

structure must be performed. This documentation must include all member sizes, connection types, and existing loads at the time of the fire.

- Ambient weather conditions. Snow, wind, and rain loads must play a part in any successful forensic structural analysis. These conditions are typically easily found through a number of weather history sites such as weatherunderground.com. More detailed information can be obtained from organizations like the National Oceanic Atmospheric Administration and the National Weather Service, but these sources typically have a cost associated with them. Ambient temperature can have an effect on the behavior and growth of a fire. Required ambient conditions must include ambient temperatures for both the inside of the structure and the outdoor conditions.
- Extinguishment efforts. While extinguishment is nearly impossible to model, the location and extent of extinguishment efforts will assist in the explanation of any discrepancies between the structural model and the measured field observations. Extinguishment efforts are also a necessity in refining the input to the fire model.

Once all appropriate data are collected, a fire model can then be run to determine the temperatures for input into the structural model. It is worth noting that it is possible to do a "coupled" analysis using FEM programs like SAFIR, but as noted earlier, the expertise necessary to run these types of models will often make them cost prohibitive. In addition, structural fire programs are designed to analyze the integrity of a building during fire attack as opposed to producing post fire deflections. Based on the temperatures obtained from the computer fire model, the structural model, using Vulcan or other suitable structural modeling program, can be

constructed and run. Deformation patterns over the roof of the structure can be compared in a way similar to the methods that other fire patterns are matched with the output of a fire model. If the pattern of modeled deformations shows reasonable agreement, it can be said that the fire model produced representative fire conditions within the compartment. This agreement will lend credence to the investigator's fire origin hypothesis. If the results are deemed not to match within reasonable bounds, a new look at and a possible revision to the fire model are called for.

In this dissertation, a number of simplifying assumptions were made in order to ensure that the analysis was as practical as possible. "Agreement" between measured and modeled data must be carefully considered prior to a determination of an acceptable level of accuracy. The nature of the problem makes the probability of precise comparison between measured data and calculated values low. However, even with the simplifying assumptions made in this dissertation, the analysis produced percent errors which were generally within 40% in areas away from the edge of the structure. When applied in the field with a fire model, there is an extra level of uncertainty, so higher percent errors in those conditions could be justified, but should be done so judiciously.

It should also be noted that this dissertation focuses on the pattern of deflections as opposed to the exact matching of observations in the field. For reasons discussed throughout the dissertation, the exact recreation of the conditions of the fire and structural system is unlikely. Comparison of patterns allows for certain deviations in the produced deflections while still analyzing the general fire pattern. This approach is consistent with methodologies generally used for fire investigation as discussed in Chapter 2.

If the modeled deformations do not follow a pattern reasonably similar to the observed (measured) deformations, then the computer fire model can be deemed not to have produced an

adequate representation of the fire – assuming no errors are present in the structural model. In the case where reasonable agreement between the fire model and structural model is judged not to have occurred, an iterative process of analyzing inputs would then be necessary to discover the reason for the disagreement. Inputs should be adjusted within boundaries based on reasonable assumptions of their values as they relate to the fire scenario being analyzed. While a number of variables can cause disagreement between the models, it is anticipated that the inputs for the fire model will be subject to the most error. As already noted, there are a number of variables that go into providing an adequate representation of a fire. While the initial model may have postulated the correct area of origin, there are certainly a plethora of other variables that can affect the end product. From the fire model side, the sequence of ignition, rate of growth, and the heat release rate of individual fuel packages are all common sources of error. From the structural model side, estimates of the material properties, distribution of temperature within the structural member, and poor estimation of the degrees of joint fixities within the structure can result in inaccurate modeling results.

Once an investigator is able to produce adequate agreement between the structural and fire models, it is reasonable to assume that the postulated ignition scenario and fire origin are correct within acceptable limits. Of course, the modeling results should be corroborated with existing fire patterns, witness statements, and other forensic evidence prior to being deemed entirely accurate.

All of the variables listed in the previous paragraphs (which do not constitute a comprehensive list of all the possibilities) can have an effect on the outcome of the mathematical models. A sensitivity analysis, whereby the variables identified above are varied within

reasonable limits, can prove useful in comparing the computed pattern of deflection to the actual pattern.

Based on the limitations just noted, it becomes obvious that the use of observed deformations is not, nor was it intended to be, a stand-alone method for post-fire analysis. However, with appropriate input data and modeling expertise, it can be expected that the process of evaluating and enhancing the traditional fire model through the use of structural modeling will lead to reasonably accurate and useful results, thus enhancing the ability of a fire investigator to identify the location of origin of a fire.

CHAPTER 8 - Conclusions

8.1 Summary of Findings

The research described in this dissertation was conducted in order to explore the potential use of structural deformations as an indicator of fire origin. With regard to the use of this methodology, the following conclusions may be drawn:

- Very little literature exists to explicitly warrant the use of structural deformations as an investigative tool for fire origin analysis.
- Even though little literature exists explicitly outlining the use of structural deformations as a post-fire scene analysis tool, most of the needed background research has been completed and is generally well accepted in both the fire protection and structural engineering fields.
- The pattern of residual deflections that will be present after a fire has been extinguished and the structure has returned to ambient temperature can be modeled to a reasonable extent using appropriate finite element modeling programs.
- The methodology of using structural deformations as an indicator of fire origin fits within the requirements of investigative methodologies within NFPA 921.
- A large number of variables (both from the fire and structural standpoint) must play a role in any analysis that uses the deformation of a structure as a post-fire analysis tool. These variables are discussed at length in Chapter 2 and reviewed in Chapter 7.

- The highest magnitude deformation does not necessarily indicate the origin of the fire. While it is certainly possible that the highest magnitude does reflect the fire's origin, the location of maximum deformation must be considered with regard to the fire's growth and behavior as well as the structural support system and existing loading of the structure.
- Tests performed as a part of this dissertation have shown that the parts of the structure intimate with the area of origin are likely to sustain higher cumulative heat fluxes over the entire duration of the fire. While exposure to the most cumulative heat flux may not lead to the highest magnitude of deformation (as it is also affected by the rate of heat flux receipt), the quadrant of origin within the test building showed the most deformation when taking into account the area weighted average deflection across a given area as discussed in Section 4.6.
- If ventilation and fuel loading conditions are taken into consideration, the structural deformations can potentially be used to narrow the origin of a fire to specific areas of the buildings (i.e. a certain half of the building).
- It is possible to recreate, within reasonable limits, the conditions experienced by the structural system of a building and the resulting deformations that occur during a fire by using a structural finite element modeling program and appropriate input from field measurements and fire modeling.
- Based on the tests performed in this dissertation, the pattern of structural deformations obtained from Vulcan can serve as a valid benchmark for comparison with fire modeling results.

8.2 Proposed Future Research

There are several topics of future research that would potentially aid in the full development of the topic of this dissertation.

The tests performed in this dissertation were primarily on smaller scale structures. The lack of full scale testing leads to issues with the ability (or inability) to scale certain aspects of both the structural systems and the fire's output/behavior. Tests on a complete, large scale structure (obviously difficult and expensive) would be necessary to completely validate this methodology as a valid and useful technique.

Full scale research could feasibly be conducted at actual fires occurring in the field, assuming there was a reasonable level of certainty where the origin of the fire was (i.e. witnesses to fire's ignition, etc.). However, buildings of the nature conducive to the use of structural deformation analysis are typically commercial or industrial in nature. Whenever these sorts of buildings catch fire, there are often years of litigation and subrogation following the claims. This legal activity effectively makes the investigation and publishing of results out of the realm of practicality.

Because of questions raised in this dissertation regarding the technical validity of the Vulcan model in structural analysis, further work needs to be done which is directed either toward a refinement of Vulcan or toward developing another modeling program altogether. Ideally, a "one-step" process whereby a fire model and a structural model such as Vulcan are combined to evaluate fire origin.

The other option for full scale research would involve the construction of a structure specific to this research topic. While plans are underway to pursue this topic in the future, a project of this magnitude, as just noted, will be very expensive in nature.

This dissertation has primarily focused its literature review and research on the use of structural deformation analysis of post-fire scenes with regard to steel as the construction material. Multiple other structural materials are in common use for building construction, including wood, masonry, and concrete. The principles outlined in this dissertation are expected to apply similarly to any construction material. Of course, different materials will behave drastically different when exposed to fire. While most of these materials have been analyzed in-depth with regard to their behavior under fire attack, studies such as the one performed in this dissertation should, if feasible, be performed prior to the use of this methodology in the field.

LIST OF REFERENCES

Coated Sheet. (2012, July 11). Retrieved from U.S.Steel: www.ussteel.com/corp/sheet/coated/hot-dip-application.asp

(2014, May 27). Retrieved from Vulcan Solutions Limited: www.vulcan-solutions.com

American Institute of Steel Construction. (2005). *Steel Construction Manual* (13th Edition ed.). AISC.

Bailey, C. G., Burgess, I. W., & Plank, R. J. (1996). Analyses of the effects of cooling and fire spread on steel-framed buildings. *Fire Safety Journal*(26), 273-293.

Bong, M. (2005). *Structural Fire Protection of Steel Portal Frame Buildings.* (Master's thesis). Univeristy of Canterbury: Christchurch, New Zealand.

Buchanan, A. H. (2002). *Structural Design for Fire Safety.* Chichester: John Wiley and Sons.

Cardin, L. P., & Itani, A. M. (2007). Performance of an unprotected steel structure subjected to repeated fire at a firefighter training facility. *Fire Safety Journal 42*, pp. 81-90.

Computers and Structures, Inc. (2011). *CSI Analysis Reference Manual.* Berkley, CA: Computers and Structures, Inc.

Cooke, G. (1988). An Introduction to the Mechanical Properties of Structural Steel at Elevated Temperatures. *Fire Safety Journal*, 45-54.

Dehaan, J. D., & Icove, D. J. (2012). *Kirk's Fire Investigation* (7th ed.). Upper Saddle River, NJ: Pearson.

Drysdale, D. (1998). *An Introduction to Fire Dynamics* (2nd Edition ed.). West Sussex: John Wiley and Sons.

El-Rimawi, J. A., Burgess, I. W., & Plank, R. J. (1996). The treatment of strain reversal in structural members during the cooling phase of a fire. *Journal of Constructional Steel Research, 37*(2), 115-135.

Federal Emergency Management Association (FEMA). (2002). *World Trade Center Building Performance Study.* FEMA Publication 403.

Franssen, J. M. (1990). The unloading of building materials submitted to fire. *Fire Safety Journal, 16*, 213-227.

Franssen, J.-M., & Zaharia, R. (2006). *Design of Steel Structures Subjected to Fire* (2nd ed.). Liege: Les Editions de l'Universite de Liege.

Gorbett, G. E., Hopkins, R., & Kennedy, P. M. (2008). The Current Knowledge & Training Regarding Backdraft, Flashover, and other Rapid Fire Progression Phenomena. *Advanced Fire, Arson, & Explosion Investigation Training Program.* Sarasota: NAFI.

Gorbett, G. E., Meacham, B., & Wood, C. (2010). Development and Assessment of a Decistion Support Framework for Enhancing the Forensic Analysis and Interpretation of Fire Patterns. *Proceedings ISFI 2010* (pp. 39-55). Sarasota: National Association of Fire Investigators.

Harmathy, T. Z. (1993). *Fire Safety Design and Concrete.* UK: Longman Scientific and Technical.

Icove, D. J., Dehaan, J. D., & Haynes, G. A. (2013). *Forensic Fire Scene Reconstruction* (3rd ed.). Upper Saddle River, NJ: Pearson.

Jowsey, A. (2006). *Fire Imposed Heat Fluxes for Structural Analysis (Doctoral Dissertation, The Univeristy of Edinburgh).* Retrieved from www.era.lib.ed.ac.uk

Kirby, B. L. (2000). *The Temperatures Attained by Unprotected Steelwork in Building Fires.* Moorgate: Corus Research.

Kirby, B. R., & Preston, R. R. (1988). High temperature properties of hot-rolled structural steels for use in fire engineering design studies. *Fire Safety Journal, 13*, pp. 27-37.

Lentini, J. J. (2006). *Scientific Protocolsfor Fire Investigation.* Boca Raton, FL: CRC.

Lentini, J. J. (2008). Toward a More Scientific Determination: Minimizing Expectation Bias in Fire Investigations. *Proceedings ISFI 2008* (pp. 15-21). Sarasota: National Association of Fire Investigators.

Mamlouk, M. S., & Zaniewski, J. P. (1999). *Materials for Civil and Construction Engineers.* Menlo Park, CA: Addison Wesley Longman, Inc.

NFPA. (2002). Recommendations of the Research Advisory Council on Post-fire Analysis.

NFPA. (2006). *NFPA 251: standard methods of tests of fire resistance of building construction and materials.* Quincy: NFPA.

NFPA. (2011). *NFPA 921: Guide for Fire and Explosion Investigation.* Quincy, MA: NFPA.

NIST. (2010). *Fire Dynamics Simulator Technical Reference Guide.* Gaithersburg, MD: NIST.

Papadopoulos, P. G., Papadopoulou, A. K., & Papaioannou, K. K. (2008). Simple nonlinear static analysis of steel portal frame with pitched roof exposed to fire. *Structural Engineering and Mechanics, 29*(1), pp. 37-53.

Ramberg, W., & Osgood, W. (1943). Description of stress-strain curves by three parameters. *National Advisory Committee for Aeronautics, Technical Note 902*.

Rein, G., Empis, C. A., & Carvel, R. (2007). *The Dalmarnock Fire Tests: Experiments and Modeling.* Edinburgh: School of Engineering and Electronics, University of Edinburugh.

Society of Fire Protection Engineers. (2008). *Handbook of Fire Protection Engineering* (4th ed.). Quincy: NFPA.

Tao, Z., Wang, X., & Uy, B. (2013). Stress-strain curves of structural and reinforcing steels after exposure to elevated temperatures. *Journal of Materials in Civil Engineering, 25*(9), 1306-1316.

Tinsley, A. T., & Gorbett, G. E. (2013). Fire Investigation Origin Determination Survey. *Fire and Arson Investigator, 63*(4), 24-40.

Wang, P., Li, G., & Guo, S. (2007). Effects of the cooling phase of a fire on steel structures. *Fire Safety Journal*(43), 451-458.

Wang, Y. C., & Kodur, V. R. (2000). Research toward the use of unprotected steel structures. *Journal of Structural Engineering, 126(12)*, pp. 1442-1450.

Wong, S. (2001). *The stuructural response of industrial portal frame structures in fire.* (Doctoral Dissertation) University of Sheffield.

Zalosh, R. G. (2003). *Industrial Fire Protection Engineering.* Hoboken, NJ.: John Wiley and Sons.

Vita

Andrew Tinsley was born in 1983 to Tom and Denice Tinsley in Knoxville, TN. He lived in several locations after being born, but wound up back in Knoxville at the age of four. His father, who was a large inspiration to his academic career, met his untimely death in 1994. His mother remarried to Willis Freeman a few years later. He attended Karns from kindergarten through 12th grade and graduated high school in December of 2001. At this point, he began his college career at Pellissippi State Technical Community College with the intent of transferring to the University of Tennessee to obtain his B.S. in Civil Engineering. After obtaining his B.S. and M.S. (both in Civil Engineering) from the University of Tennessee, he began the pursuit of his Ph.D. He is a registered professional engineer and presently teaches as an Associate Professor in Eastern Kentucky University's Fire Protection and Safety Engineering Technology Program. In addition, he is Co-Owner of ARC Fire Engineering operating out of Nicholasville, KY providing a variety of fire protection and safety consulting services.

Andrew has been active in his community for a number of years. He began in the cub scouts which eventually led to the Boy Scouts where he received the rank of Eagle Scout. Once in college, he became active with the local volunteer fire department eventually obtaining the rank of captain and served as the department's training officer. In the meantime, Andrew worked as a graduate research assistant at the University of Tennessee helping to research a cost effective, high durability concrete mix for use on bridge decks. Also during graduate school, he worked as an associate engineer with Construction Engineering Consultants, based in Knoxville, TN. After leaving this job, Andrew worked as a design engineer with Professional Project Services in Oak Ridge, TN assisting with large scale government infrastructure projects.

He married in 2006 to Amanda and they currently reside in Richmond, KY. In 2012, the couple had their first child, Abigail Sue and Alton Thomas was born in 2014. In his free time, he enjoys politics, golf, fishing, hunting, boating, and the fire service.